Università degli Studi di Padova

Department of Information Engineering

Master Thesis in Automation Engineering

Bearing Rigidity Theory: characterization and control of mixed formations and localization

Supervisor
prof. Angelo Cenedese
Università di Padova

Co-supervisor
Dott.ssa Giulia Michieletto
Università di Padova

Master Candidate
Beniamino Pozzan

Abstract

In this thesis the applications of the bearing rigidity theory to the control of multiagent *mixed* formations embedded in the three dimensional special Euclidean group $SE(3)$ are investigated. The concept of mixed framework is introduced and it is used to characterize the dynamical bearing rigidity properties. It is shown how non-mixed and mixed formations are strictly connected and how the major results from the former category can be applied to the latter. The problem of distributed formation stabilization and coordinated agent motion is presented, along with the current solutions designed for non mixed formations. The results of the characterization of mixed frameworks are then exploited to prove how those controllers can be perfectly applied to the mixed cases too. In conclusion it is proposed a solution to the location estimation problem of non-mixed formations embedded in $SE(3)$.

Contents

Listing of figures

Listing of tables

Listing of Symbols

$\mathbb{R}$	Real numbers set
$\mathbb{S}^d$	d-sphere
$SO(d)$	d-dimensional Special Orthogonal group
$SE(d)$	d-dimensional Special Euclidean group
$\mathfrak{so}(3)$	3-dimensional Special Orthogonal algebra
$\mathbf{I}_d$	Identity matrix of dimension d
$\mathbf{0}_{m\times n}$	$(m \times n)$ matrix with all entries equal to 0
$\mathbf{1}_{m\times n}$	$(m \times n)$ matrix with all entries equal to 1
$\mathbf{e}_i$	i-th canonical vector
$\mathcal{G}$	Graph
$\mathcal{K}$	Complete graph associated the the graph $\mathcal{G}$
$\mathcal{V}$	Vertex set for a graph
$\mathcal{E}$	Edge set for a graph
$\mathcal{E}_\mathcal{K}$	Complete edge set for a graph
$\mathbf{E}$	Incidence matrix associated to a graph
$\mathcal{D}_i$	metric space in which the i-th agent of the formation is embedded
$\mathcal{M}$	domain of a bearing measurement
$\mathbf{b}_\mathcal{G}(\mathbf{x})$	bearing vector stacking all the bearing measurements $\mathbf{b}_i \in \mathcal{M}$ associated to the framework $(\mathcal{G}, \mathbf{x})$
$\bar{\mathcal{I}}$	instantaneous variation domain, Cartesian product of the command spaces $\mathcal{I}_i$ of each agent
$\mathcal{H}$	collection of command spaces
$\boldsymbol{\delta}$	instantaneous variation vector stacking all the agent commands $\boldsymbol{\delta}_i \in \mathcal{I}_i$
$\mathbf{B}_\mathcal{G}(\mathbf{x}(t))$	bearing rigidity matrix associated to the framework $(\mathcal{G}, \mathbf{x}(t))$
$\mathcal{S}_t$	trivial variation set
$\mathcal{R}_\mathcal{O}$	coordinated rotation set
$\mathcal{F}_i$	frame attached to the i-th agent
$\mathcal{F}_W$	common inertial frame
$\mathbf{p}_i$	position of the i-th agent
$\mathbf{q}_i$	quaternion indicating the orientation of $\mathcal{F}_i$ w.r.t. $\mathcal{F}_W$
$\mathbf{x}_i$	configuration of the i-th agent

d_{ij}	inverse distance between agent i and j
$\boldsymbol{\omega}_i$	angular velocity of the i-th agent expressed in $\mathcal{F}_i$. If the world frame $\mathcal{F}_W$ is considered, then subscript w is added.
$\mathbf{v}_i$	linear velocity of the i-th agent center of mass expressed in $\mathcal{F}_i$. If the world frame $\mathcal{F}_W$ is considered, then subscript w is added.
$\mathbf{S}_{p,i}$	matrix mapping the translational agent command $\boldsymbol{\delta}_{p,i}$ into the linear velocity $\mathbf{v}_{w,i}$ of the i-th agent
$\mathbf{S}_{o,i}$	matrix mapping the orientation agent command $\boldsymbol{\delta}_{o,i}$ into the angular velocity $\boldsymbol{\omega}_{w,i}$ of the i-th agent
$\mathbf{u}_i$	vector stacking the linear velocity and angular velocity of the i-th agent

Acknowledgments

Desidero ringraziare la mia famiglia, che mi ha supportato, ma soprattutto sopportato, in questi mesi: siete stati fondamentali per permettermi di arrivare fin qui. Ringrazio tutti i DarkAce: ragazzi siete fantastici, mi avete accompagnato dalla triennale fino alla fine dalla magistrale facendomi passare domeniche magnifiche. Ringrazio i miei coinquilini, Alessandro e Francesco: la tranquillità del nostro appartamento dovrebbe venire presa a modello. Ringrazio Giulio e Nicola: avete trasformato la realizzazione di un progetto in un divertimento memorabile. Ringrazio il Professor Cenedese e la dottoressa Michieletto per l'aiuto che mi hanno dato nella realizzazione di questo lavoro e per il tempo che mi hanno dedicato. In particolare, ringrazio il professor Cenedese per i colloqui improvvisi dopo lezione.

1 Introduction

Distributed control and location estimation of multiagent systems have received tremendous research attention in recent years because of their potential across many application domains [1, 2]. The term *agent* refers to a general dynamical system, characterized by its actuation, sensing and communication capabilities. Distributed strategies are preferred because they have lots of advantages with respect to centralized ones, for example they allow to increase the robustness against failure of the agents, to extend the flexibility of the global system and they can result less expensive. On the other hand, distributed strategies require more complex algorithms to be implemented.

Multiagent systems are treated as formations if the fulfilment of the desired task involves the knowledge of the pose, intended as position and orientation (if present), of each agent. Instead, if only the collective behaviour is of interest, we talk about swarms. Formation control is required when a certain geometric pattern is aimed to form with or without a group reference. The mathematical formulation of the geometric pattern is strictly related with the sensing capabilities of the agents and, as shown in [2], the latter is strictly related with the interaction topology of the formation. In particular, the more informative the sensing capability is, the simpler the interaction topology results.

If the agents are able to acquire their own position (e.g. through the use of the GPS), then the geometric pattern can be expressed as the set of desired positions and it is not even required an interaction topology. Nevertheless it is important to develop solutions that do not require GPS or other information coming from outside the formation. A few motiva-

tions for this topic are:

- the need of multiagent system capable to operate in GPS-denied environments, such as inside buildings, underwater and in deep space;
- security reasons;
- accuracy reasons, for example the absolute accuracy of the the GPS may not meet the requirements of high-accuracy formation control tasks.

Employing inter-agents measurements, namely using onboard sensors to acquire information about the neighbour agents and avoiding to depend on not-always-trustable data from outside the formation, resulted a valid answer to this need. Inter-agents measurements can be divided in two groups: *range measurements* and *bearing measurements*.

Range measurements give information about the distance between two agents while bearing measurements provide data about the displacement of an agent with respect to another. The latter possibility is nowadays very interesting thanks to the improvements on optical cameras.

Optical camera can be easily installed on aerial and ground vehicles, they are inherently bearing-only sensors [3, sec 5.4.3] and have very appreciable properties such as low-cost, lightweight, and low-power characteristics.

If now the geometric pattern is expressed as a set of desired inter-agents bearing measurements, which characteristics is the interaction topology required to have? The answer lays on the concept of *rigidity*, which can be roughly stated as the property of a formation to exhibit a variation on the measurements whenever a deformation occurs. The related mathematical tool is the *bearing rigidity theory*.

«According to the most general definition, rigidity theory aims at studying the *stiffness* of a given system, understood as a reaction to an induced deformation» [4]. Rigidity analysis started considering geometric systems but nowadays it affects several practical research areas (see [5]) and formation control is only one of them. One of the major contributions to the development of the rigidity theory was provided by Asimow and Roth which characterized the rigidity of systems composed by bars and joints through the concept of *framework* [6]. The authors used a graph-based representation of the systems, where each node represents a joint and each edge represents a bar, together with a set of elements in $\mathbb{R}^d$, $d \geqslant 2$ that represents the position of the joints.

Recently, in order to answer the need of autonomous multiagent systems wherein the connections among the elements of the formation are virtual, representing the sensing relations

among the devices, the rigidity theory has enlarged its focus. The concept of framework has thus been redefined by considering also manifolds more complex than the (n-dimensional) Euclidean space.

As the inter-agents measurements can be divided into range measurements and bearing measurements, the same applies to the rigidity theory, with the *distance rigidity theory* and the more recent *bearing rigidity theory*. Distance rigidity theory is employed when range measurements are gathered; therefore, distance constraints can be imposed to preserve the formation shape. A survey on the distance rigidity and its applications on the control and localization of multiagent systems can be found in [7, 8, 9, 10, 11, 12]. All these works share the same fundamental aspect: the distance constraints for a framework can be characterized by a properly defined matrix whose rank determines the rigidity properties of the system.

Bearing rigidity theory began to develop for frameworks defined in $\mathbb{R}^2$ and in that scenario it is also called *parallel* rigidity. There, the constraints are imposed over the directions of the interacting agents (the edges of the graph associated to the framework). In this way is possible to preserve the angles between pairs of interconnected agents and the lines joining them [13, 14, 15, 16]. The first natural extension regards frameworks embedded in $\mathbb{R}^d$, $d > 2$, where the bearing between two agents is represented by the normalized vector connecting the two [17, 18, 19, 20]. In both cases the necessary and sufficient condition to guarantee the rigidity properties of a framework rests upon the rank of a matrix summarizing the involved constraints; in a similar way of what has been stated for the distance rigidity.

Up until now the agents have been modeled as particle points in $\mathbb{R}^d$, $d \geqslant 2$; this in not a realistic scenario. Indeed, the measurements are almost always expressed in the local frame of each agent and therefore each device should be modeled as a rigid body with a certain position and orientation w.r.t. a common inertial frame which is supposed to be unavailable to the group. This new situation is studied in [21] and in [22]; in these works agents acting on the plane are considered. The extension to the 3D space, with the limitation of having agents that can rotate along only one common axis, is performed in [23, 24, 25]. The most complete scenario, where fully-actuated agents having six degrees of freedom are considered, is analysed in [26]. Analogously to the former cases, the rigidity properties of the aforementioned multiagent systems can be established through the definition of a matrix accounting for the inter-agents sensing interplay.

This thesis aims to extend the current bearing rigidity theory toward *mixed* formation, namely formation composed by agents characterized by different actuation capabilities, and to provide a solution to the location estimation problem for formation with fully-actuated

agents. In order to do so, the chapters are organized in the following way.

- Chapter 2 is dedicated to present the concepts and results about the bearing rigidity theory, formal definition are provided in accordance to the existing literature, in particular [4].
- In chapter 3 the mixed formations are introduced and characterized.
- After the presentation of the main results about formation control for homogeneous frameworks, chapter 4 deals with the generalization toward the mixed case. Simulations are provided to validate the reasoning.
- Chapter 5 deals with the problem of location estimation for formations composed by fully-actuated agents.
- Finally, in chapter 6 all the main results are summarized and suggestions for future works are given.

2

Bearing Rigidity Theory

This chapter is dedicated to the introduction to the bearing rigidity theory and it is based on [4]. Rigidity theory aims at studying the stiffness of a given system, understood as a reaction to an induced deformation. Central is the concept of framework, a mathematical descriptor that employs graphs to model the interactions between the elements of the system and manifolds to characterize its configuration. Bearing rigidity is particularly suited to be applied to mobile robot formations that use bearing-based inter-agents measurements. The reason is that it gives the requirements under which the preservation of constraints on the measurements is necessary and sufficient condition to the preservation of the shape of the formation.

2.1 Notations and required concepts

This section is dedicated to the introduction of the needed mathematical tools for the rest of this thesis. *Graphs* play a main role in the rigidity theory, therefore it is reasonable to start from them. For a deeper discussion, see [27].

A Graph is an ordered pair $\mathcal{G} = (\mathcal{V}, \mathcal{E})$ consisting of the vertex set $\mathcal{V} = \{ v_1 \dots v_n \}$ and the edge set $\mathcal{E} = \{ e_1 \dots e_m \} \subseteq \mathcal{V} \times \mathcal{V}$, having cardinality $|\mathcal{V}| = n$ and $|\mathcal{E}| = m$, respectively. Graph can be characterized by the presence or not of orientation associated to the edges. If the edges have no orientation, namely $e_k = (v_i, v_j) \in \mathcal{E}$ is identical to $e_h = (v_j, v_i) \in \mathcal{E}$, then the graph is *undirected*. Instead, a graph is called *directed* if its

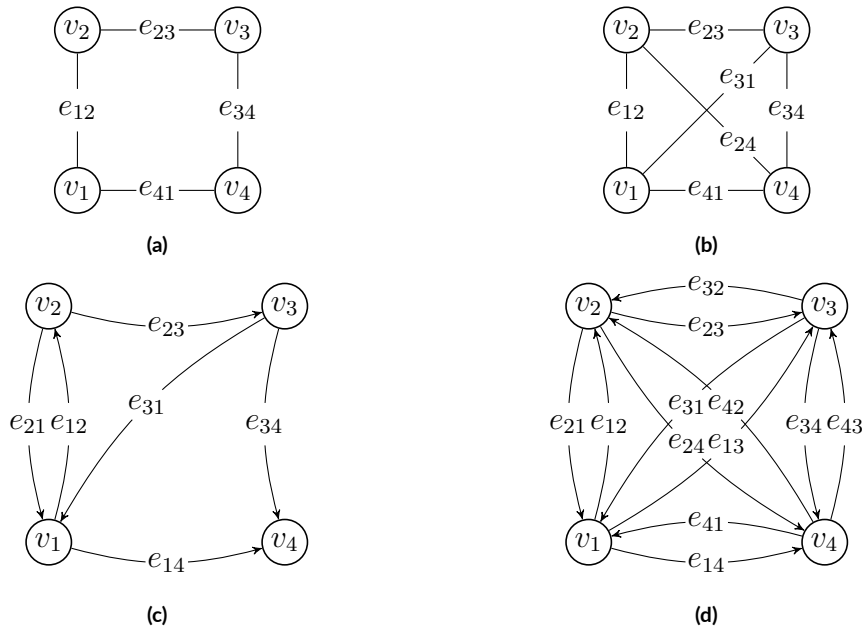

Figure 2.1: Example of an undirected graph (a) and of its corresponding complete graph (b), of an directed graph (c) and of its corresponding complete graph (d).

edges have orientation, thus the edge $e_k = (v_i, v_j) \in \mathcal{E}$ is directed from $v_i \in \mathcal{V}$ to $v_j \in \mathcal{V}$. $v_i, v_j \in \mathcal{V}$ are also called *head* and *tail* of the edge, respectively. For any graph $\mathcal{G} = (\mathcal{V}, \mathcal{E})$, the corresponding *complete graph* $\mathcal{K} = (\mathcal{V}, \mathcal{E}_\mathcal{K})$ is the graph characterized by the same vertex set $\mathcal{V}$, while the edge set is completed so that each pair of distinct vertices is joined by an edge if $\mathcal{G}$ is undirected and by a pair of edges (one in each direction) if $\mathcal{G}$ is directed. Examples of an undirected graph and a directed graph, together with their corresponding complete graphs are reported in figure 2.1.

For a directed graph, the *incidence matrix* $\mathbf{E} \in \mathbb{R}^{n \times m}$, is the $\{0, \pm 1\}$-matrix defined as

$$[\mathbf{E}]_{ik} = \begin{cases} -1 & \text{if } e_k = (v_i, v_j) \in \mathcal{E} \text{ (\textit{outgoing edge})} \\ 1 & \text{if } e_k = (v_j, v_i) \in \mathcal{E} \text{ (\textit{ingoing edge})} \\ 0 & \text{otherwise,} \end{cases}$$

and, in a similar way, the matrix $\mathbf{E}_o \in \mathbb{R}^{n \times m}$, is given by

$$[\mathbf{E}_o]_{ik} = \begin{cases} -1 & \text{if } e_k = (v_i, v_j) \in \mathcal{E} \text{ (\textit{outgoing edge})} \\ 0 & \text{otherwise.} \end{cases}$$

$\mathbf{E} \in \mathbb{R}^{n \times m}$ completely summarize the structure of the graph; reading it column wise it provides the head and the tail of each edge, while reading it row wise it is possible to quantify the interconnection of each vertex. On the other hand, $\mathbf{E}_o \in \mathbb{R}^{n \times m}$ provides only information about the number of edges exiting from a given vertex.

The matrices $\bar{\mathbf{E}} = \mathbf{E} \otimes \mathbf{I}_d \in \mathbb{R}^{dn \times dm}$ and $\bar{\mathbf{E}}_o = \mathbf{E}_o \otimes \mathbf{I}_d \in \mathbb{R}^{dn \times dm}$ are defined; where $\otimes$ is the Kronecker product

$$\mathbf{A} \otimes \mathbf{B} = \begin{bmatrix} a_{11}\mathbf{B} & \dots & a_{1n}\mathbf{B} \\ \vdots & \ddots & \vdots \\ a_{m1}\mathbf{B} & \dots & a_{mn}\mathbf{B} \end{bmatrix} \in \mathbb{R}^{mp \times nq}; \quad \mathbf{A} \in \mathbb{R}^{m \times n}, \quad \mathbf{B} \in \mathbb{R}^{p \times q};$$

$\mathbf{I}_d$ is the d-dimensional identity matrix and $d \geqslant 2$ is the dimension of the considered space.

The d-sphere embedded in $\mathbb{R}^{d+1}$ is denoted as $\mathbb{S}^d$,

$$\mathbb{S}^d = \left\{ \mathbf{x} \in \mathbb{R}^{d+1} \;\middle|\; \|\mathbf{x}\| = 1 \right\};$$

with $\|\cdot\|$ the Euclidean norm operator. The vectors of the canonical basis of $\mathbb{R}^d$ are indicated as $\mathbf{e}_i$, $i \in \{ 1 \dots d \}$, and they have a one in the i-th entry and zeros elsewhere.

Massive use will be made of $\mathbf{P} \colon \mathbb{R}^d \backslash \{ \mathbf{0}_d \} \to \mathbb{R}^{d \times d}$,

$$\mathbf{P}(\mathbf{x}) = \mathbf{I}_d - \frac{\mathbf{x}}{\|\mathbf{x}\|} \frac{\mathbf{x}^\top}{\|\mathbf{x}\|},$$

that maps any non-zero vector to the orthogonal complement of the vector $\mathbf{x}$ (*orthogonal projection operator*). Hence, $\mathbf{P}(\mathbf{x})\mathbf{y}$ indicates the projection of $\mathbf{y} \in \mathbb{R}^d$ onto the orthogonal complement of $\mathbf{x} \in \mathbb{R}^d$. Given two vectors $\mathbf{x}, \mathbf{y} \in \mathbb{R}^3$, their cross product is denoted as $\mathbf{x} \times \mathbf{y} = [\mathbf{x}]_\times \mathbf{y} = -[\mathbf{y}]_\times \mathbf{x}$, where the map $[\cdot]_\times \colon \mathbb{R}^3 \to \mathfrak{so}(3)$ associates each vector $\mathbf{x} = \begin{bmatrix} a & b & c \end{bmatrix}^\top \in \mathbb{R}^3$ to the corresponding skew-symmetrical matrix belonging to the Special Orthogonal algebra $\mathfrak{so}(3)$,

$$[\mathbf{x}]_\times = \begin{bmatrix} 0 & -c & b \\ c & 0 & -a \\ -b & a & 0 \end{bmatrix}$$

Given a matrix $\mathbf{A} \in \mathbb{R}^{p \times q}$, its *null space* and *image space* are denoted as $\ker(\mathbf{A})$ and $\mathrm{Im}(\mathbf{A})$, respectively. The dimension of $\mathrm{Im}(\mathbf{A})$ is indicated as $\mathrm{rk}(\mathbf{A})$, whereas $\mathrm{null}(\mathbf{A})$

stands for the nullity of the matrix, namely $\mathrm{null}(\mathbf{A}) = \dim(\ker(\mathbf{A}))$. Finally, the notation $\mathrm{diag}(\mathbf{A}_k) \in \mathbb{R}^{rp \times rq}$ is used to indicate the block diagonal matrix associated to the set $\{ \mathbf{A}_k \in \mathbb{R}^{p \times q} \}_{k=1}^{r}$.

2.2 Framework for bearing rigidity

Here the main concept related to the bearing rigidity theory are provided. Consider a generic formation of $n \geqslant 3$ agents; each agent is associated to an element of the *metric space* $\mathcal{D}_i$ describing its configuration.[1] In addition, each agent is provided with bearing sensing capabilities, i.e., it is able to recover relative direction measurements w.r.t. some neighbours. Such n-agents formation can be modeled as a framework embedded in the product metric space $\bar{\mathcal{D}} := \prod_{i=1}^{n} \mathcal{D}_i$.

Definition 2.1 (Framework in $\bar{\mathcal{D}}$)**.** A framework in $\bar{\mathcal{D}}$ is an ordered pair $(\mathcal{G}, \mathbf{x})$ consisting of a connected (directed or undirected) graph $\mathcal{G} = (\mathcal{V}, \mathcal{E})$ with $|\mathcal{V}| = n$, and a configuration $\mathbf{x} \in \bar{\mathcal{D}}$.

The two components of the framework characterize a formation in terms of both agents configuration and interaction capabilities. $\mathcal{G}$ describes the available bearing measurements associating each agent to a vertex. It can be directed or undirected reflecting the possibility of the agents interactions to be either unidirectional or bidirectional. Anyway, in rigidity theory it is normally assumed to be time invariant. The formation configuration $\mathbf{x} \in \bar{\mathcal{D}}$ is associated with the set $\{ \mathbf{x}_i \in \mathcal{D}_i \}_{i=1}^{n}$ describing the agent configurations so that $\mathbf{x}_i \in \mathcal{D}_i$ coincides with the i-th agent position when it is modeled as a particle point, and with the pair of its position and (partial/full) attitude when the rigid body model is assumed. Two major assumptions are now stated:

- For the rest of this thesis, non-degenerate formations are considered.
- For the rest of this thesis, homogeneous formations are considered.

Definition 2.2 (Non-Degenerate Formation)**.** A n-agents formation modeled as a framework $(\mathcal{G}, \mathbf{x})$ in $\bar{\mathcal{D}}$ is *non-degenerate* if the agents are univocally placed, i.e., two agents can

[1] The term *configuration* is used instead of *state* because the latter depends on the dynamical system used to model the agent. The two usually coincide if the single integrator model is adopted.

not have the same position, and not all collinear, namely the matrix of the coordinates describing their positions is of rank greater than 1.

Definition 2.3 (Homogeneous Formation)**.** A n-agents formation modeled as a framework $(\mathcal{G}, \mathbf{x})$ in $\bar{\mathcal{D}}$ is *homogeneous* if all the agents are characterized by the same configuration space, i.e., $\mathcal{D}_i = \mathcal{D}$ for all $i \in \{1 \dots n\}$, hence $\bar{\mathcal{D}} \coloneqq \mathcal{D}^n$.

The sensing capability and the configuration of a formation characterize its bearing rigidity properties. According to the framework model, any edge $e_k = e_{ij} = (v_i, v_j) \in \mathcal{E}$ ($|\mathcal{E}| = m$) represents a bearing measurement $\mathbf{b}_k = \mathbf{b}_{ij} \in \mathcal{M}$ recovered by the i-th agent which is able to sense the j-th agent, $i, j \in \{1 \dots n\}, i \neq j$. The *bearing measurement domain* can thus be defined as $\bar{\mathcal{M}} \coloneqq \mathcal{M}^m$.[2] Depending on the chosen model, the available measurements can be expressed in a common frame or according for local frames attached to each agent; however, in both cases, these are related to the framework configuration as stated in the following definition where an arbitrary edge labelling is introduced.

Definition 2.4 (Bearing Rigidity Function)**.** Given a n-agents formation modeled as a framework $(\mathcal{G}, \mathbf{x})$ in $\bar{\mathcal{D}}$, the *bearing rigidity function* is the map associating the configuration $\mathbf{x} \in \bar{\mathcal{D}}$ to the vector $\mathbf{b}_{\mathcal{G}}(\mathbf{x}) = \left[\mathbf{b}_1^\top \dots \mathbf{b}_m^\top\right]^\top \in \bar{\mathcal{M}}$ stacking all the available bearing measurements.

Starting form definition 2.4 it is possible to introduce the first notion related to the bearing rigidity theory, namely the equivalence and congruence of different frameworks.

Definition 2.5 (Bearing Equivalence)**.** Two frameworks $(\mathcal{G}, \mathbf{x})$ and $(\mathcal{G}, \mathbf{x}')$ are *bearing equivalent (BE)* if $\mathbf{b}_{\mathcal{G}}(\mathbf{x}) = \mathbf{b}_{\mathcal{G}}(\mathbf{x}')$.

Definition 2.6 (Bearing Congruence)**.** Two frameworks $(\mathcal{G}, \mathbf{x})$ and $(\mathcal{G}, \mathbf{x}')$ are *bearing congruent (BC)* if $\mathbf{b}_{\mathcal{K}}(\mathbf{x}) = \mathbf{b}_{\mathcal{K}}(\mathbf{x}')$, where $\mathcal{K}$ is the complete graph associated to $\mathcal{G}$.

Using the preimage under the bearing rigidity function, the set

$$\mathcal{Q}(\mathbf{x}) = \mathbf{b}_{\mathcal{G}}^{-1}(\mathbf{b}_{\mathcal{G}}(\mathbf{x})) \subseteq \bar{\mathcal{D}}$$

includes all the configurations $\mathbf{x}' \in \bar{\mathcal{D}}$ such that $(\mathcal{G}, \mathbf{x}')$ is BE to $(\mathcal{G}, \mathbf{x})$, while the set

$$\mathcal{C}(\mathbf{x}) = \mathbf{b}_{\mathcal{K}}^{-1}(\mathbf{b}_{\mathcal{K}}(\mathbf{x})) \subseteq \bar{\mathcal{D}}$$

[2] It is assumed that all the agents have the same sensing apparatus. Otherwise each agent would have had a different bearing measurement domain $\mathcal{M}_i$ $i \in \{1 \dots n\}$.

contains all the configurations $\mathbf{x}' \in \bar{\mathcal{D}}$ such that $(\mathcal{G}, \mathbf{x}')$ is BC to $(\mathcal{G}, \mathbf{x})$.

Proposition 2.1. *It holds that* $\mathcal{C}(\mathbf{x}) \subseteq \mathcal{Q}(\mathbf{x})$.

Proof. Assume that the $|\mathcal{E}_{\mathcal{K}}|$ edges of $\mathcal{K}$ are labelled such that the the first m are also the edges of $\mathcal{G}$. Suppose that $\mathbf{x}' \in \mathcal{C}(\mathbf{x})$; then from definitions 2.4 and 2.6, $\mathbf{b}'_k = \mathbf{b}_k$ for $k \in \{\, 1 \dots |\mathcal{E}_{\mathcal{K}}| \,\}$, where $\mathbf{b}'_k, \mathbf{b}_k \in \mathcal{M}$ are the bearing measurements associated to the k-th edge of $(\mathcal{K}, \mathbf{x}')$, $(\mathcal{K}, \mathbf{x})$, respectively. This implies that also $\mathbf{b}'_k = \mathbf{b}_k$ for $k \in \{\, 1 \dots m \,\}$, hence $\mathbf{b}_{\mathcal{G}}(\mathbf{x}) = \mathbf{b}_{\mathcal{G}}(\mathbf{x}')$, which is exactly definition 2.5 and $\mathbf{x}' \in \mathcal{Q}(\mathbf{x})$. □

The definition of these sets allows to introduce the (local and global) properties of bearing rigidity.

Definition 2.7 (Bearing Rigidity in $\bar{\mathcal{D}}$)**.** A framework $(\mathcal{G}, \mathbf{x})$ is (locally) *bearing rigid (BR)* in $\bar{\mathcal{D}}$ if there exists a neighbourhood $\mathcal{U}(\mathbf{x}) \subseteq \bar{\mathcal{D}}$ of $\mathbf{x}$ such that

$$\mathcal{Q}(\mathbf{x}) \cup \mathcal{U}(\mathbf{x}) = \mathcal{C}(\mathbf{x}) \cup \mathcal{U}(\mathbf{x}). \tag{2.1}$$

Definition 2.8 (Global Bearing Rigidity in $\bar{\mathcal{D}}$)**.** A framework $(\mathcal{G}, \mathbf{x})$ is *globally bearing rigid (GBR)* in $\bar{\mathcal{D}}$ if every framework which is BE to $(\mathcal{G}, \mathbf{x})$ is also BC to $(\mathcal{G}, \mathbf{x})$, or equivalently if $\mathcal{Q}(\mathbf{x}) = \mathcal{C}(\mathbf{x})$.

The meaning of the sets $\mathcal{U}(\mathbf{x}), \mathcal{C}(\mathbf{x}), \mathcal{Q}(\mathbf{x}) \subset \bar{\mathcal{D}}$ is graphically represented in figure 2.2 on the facing page. The requirement of "closeness" in the configurations space is missed in definition 2.8 of global bearing rigidity. As a consequence, this property results to be stronger than the previous one as proved in the next theorem.

Theorem 2.2. *A GBR framework* $(\mathcal{G}, \mathbf{x})$ *is also BR.*

Proof. For a GBR framework $(\mathcal{G}, \mathbf{x})$, it holds that $\mathcal{Q}(\mathbf{x}) = \mathcal{C}(\mathbf{x})$. Consequently, condition (2.1) is valid for $\mathcal{U}(\mathbf{x}) = \bar{\mathcal{D}}$ demonstrating that the framework is BR. □

All the properties previously defined concern rigidity for *static* frameworks. Nevertheless, in real-world scenarios agents belonging to a formation are generally able to move. For this reason, the analysis of bearing rigidity for *dynamic* agents formations is performed. Dynamic agents formations can be modeled as frameworks $(\mathcal{G}, \mathbf{x})$ where the configuration can change over time, namely $\mathbf{x} = \mathbf{x}(t) \in \bar{\mathcal{D}}$, while the graph $\mathcal{G}$ is fixed. The goal for the rest of this section is to identify the constraints under which a given dynamic formation can deform while maintaining its rigidity, i.e., preserving the existing bearings among the agents.

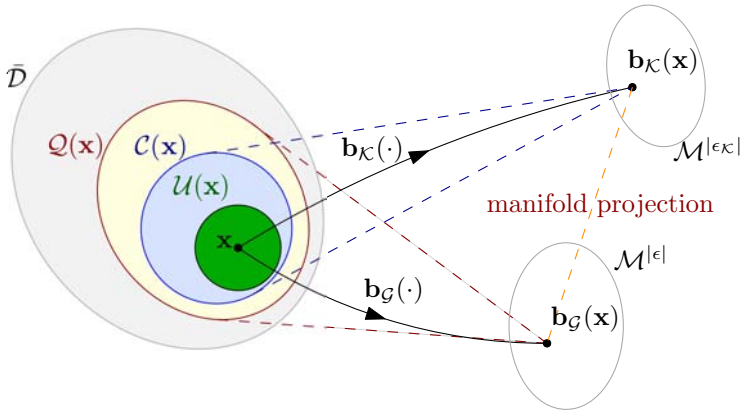

Figure 2.2: Graphical representation of the sets $\mathcal{Q}(\mathbf{x}), \mathcal{C}(\mathbf{x}), \mathcal{U}(\mathbf{x}) \subseteq \bar{\mathcal{D}}$ involved in the definition of bearing rigidity and global bearing rigidity.

For a given formation the *instantaneous variation vector* $\boldsymbol{\delta}(t) \in \bar{\mathcal{I}}$ represents a deformation of $\mathbf{x}(t)$ taking place in an infinitesimal time interval. This vector belongs to the *instantaneous variation domain* $\bar{\mathcal{I}} := \prod_{i=1}^{n} \mathcal{I}_i$ whose identity depends on the space of agent controllable variables through the agent command space $\mathcal{I}_i$. The characterization of $\mathcal{I}_i$ is made by the adopted dynamic model and the same applies for the function that relate $\frac{d}{dt}\mathbf{x}(t)$ to $\boldsymbol{\delta}(t)$.

Remark. Normally, it holds that $\frac{d}{dt}\mathbf{x}(t) \neq \boldsymbol{\delta}(t)$, namely, the time derivative of the configuration do not coincide with the instantaneous variation vector.

For now, it is assumed that all agents have the same command spaces, that is $\mathcal{I}_i = \mathcal{I}$, and thus $\bar{\mathcal{I}} = \mathcal{I}^n$. The introduction of $\boldsymbol{\delta}(t)$ allows to describe the bearing measurement dynamics in terms of configuration deformations. The relation between $\boldsymbol{\delta}(t)$ and the time derivative of the bearing rigidity function, clarified in the next definition, constitutes the starting point for the study of the rigidity properties of dynamic formations.

Definition 2.9 (Bearing Rigidity Matrix)**.** For a given (dynamic) framework $(\mathcal{G}, \mathbf{x})$, the *bearing rigidity matrix* is the matrix $\mathbf{B}_{\mathcal{G}}(\mathbf{x}(t))$ that satisfies the relation

$$\dot{\mathbf{b}}_{\mathcal{G}}\big(\mathbf{x}(t)\big) = \frac{d}{dt}\mathbf{b}_{\mathcal{G}}\big(\mathbf{x}(t)\big) = \mathbf{B}_{\mathcal{G}}\big(\mathbf{x}(t)\big)\boldsymbol{\delta}(t). \tag{2.2}$$

The dimension of the bearing rigidity matrix typically depends on the spaces $\bar{\mathcal{M}}$ and $\bar{\mathcal{I}}$. Nevertheless, one can observe that the null space of $\mathbf{B}_{\mathcal{G}}(\mathbf{x}(t))$ always identifies the (first-order) deformations of the configuration $\mathbf{x}(t)$ that maintain the bearing measurements un-

changed. From a physical perspective, such variations of $(\mathcal{G}, \mathbf{x})$ can be considered as sets of command inputs to provide to the agents to instantaneously drive the formation from the initial configuration $\mathbf{x} = \mathbf{x}(t)$ to a final configuration $\mathbf{x}'$ belonging to $\mathcal{Q}(\mathbf{x})$.

Definition 2.10 (Infinitesimal Variation)**.** For a given (dynamic) framework $(\mathcal{G}, \mathbf{x})$, an *infinitesimal variation* is an instantaneous variation $\boldsymbol{\delta}(t) \in \bar{\mathcal{I}}$ that allows to preserve the relative direction among the interacting agents.

Lemma 2.3. *For a given (dynamic) framework $(\mathcal{G}, \mathbf{x})$, an infinitesimal variation in an instantaneous variation $\boldsymbol{\delta}(t) \in \bar{\mathcal{I}}$ such that $\boldsymbol{\delta}(t) \in \ker\big(\mathbf{B}_{\mathcal{G}}\big(\mathbf{x}(t)\big)\big)$.*

For a given $(\mathcal{G}, \mathbf{x})$, there are many infinitesimal variations. However, there exists infinitesimal variations that hold for *any* graphs. This follows from the next results.

Theorem 2.4. *Given a (dynamic) framework $(\mathcal{G}, \mathbf{x})$ and denoting as $\mathcal{K}$ the complete graph associated to $\mathcal{G}$, it holds that $\ker\big(\mathbf{B}_{\mathcal{K}}\big(\mathbf{x}(t)\big)\big) \subseteq \ker\big(\mathbf{B}_{\mathcal{G}}\big(\mathbf{x}(t)\big)\big)$.*

Proof. Since each edge of the graph $\mathcal{G}$ belongs to the graph $\mathcal{K}$, the equation set defined by $\mathbf{B}_{\mathcal{G}}\big(\mathbf{x}(t)\big)\boldsymbol{\delta}(t) = \mathbf{0}$ constitutes a subset of the equations set defined by $\mathbf{B}_{\mathcal{K}}\big(\mathbf{x}(t)\big)\boldsymbol{\delta}(t) = \mathbf{0}$. Then $\boldsymbol{\delta}(t) \in \ker\big(\mathbf{B}_{\mathcal{K}}\big(\mathbf{x}(t)\big)\big)$ implies $\boldsymbol{\delta}(t) \in \ker\big(\mathbf{B}_{\mathcal{G}}\big(\mathbf{x}(t)\big)\big)$. □

In the light of theorem 2.4, the notion of *trivial variations* is introduced by considering the infinitesimal variations related to the complete graph $\mathcal{K}$ associated to $\mathcal{G}$. These ensure the measurements preservations for each pair of node in the formation $(\mathbf{x}' \in \mathcal{C}(\mathbf{x}))$, i.e., the formation shape preservation.

Definition 2.11 (Trivial Variation)**.** For a given (dynamic) framework $(\mathcal{G}, \mathbf{x})$, a *trivial variation* in an instantaneous variation $\boldsymbol{\delta}(t) \in \bar{\mathcal{I}}$ such that shape uniqueness is preserved.

Lemma 2.5. *For a given (dynamic) framework $(\mathcal{G}, \mathbf{x})$, a trivial variation in an instantaneous variation $\boldsymbol{\delta}(t) \in \bar{\mathcal{I}}$ such that $\boldsymbol{\delta}(t) \in \ker\big(\mathbf{B}_{\mathcal{K}}\big(\mathbf{x}(t)\big)\big)$, where $\mathbf{B}_{\mathcal{K}}\big(\mathbf{x}(t)\big)$ is the bearing rigidity matrix computed for the complete graph $\mathcal{K}$ associated to $\mathcal{G}$.*

Theorem 2.4 is fundamental for the next definition that constitutes the core of the rigidity theory.

Definition 2.12 (Infinitesimal Bearing Rigidity in $\bar{\mathcal{D}}$)**.** A (dynamic) framework $(\mathcal{G}, \mathbf{x})$ is *infinitesimally bearing rigid (IBR)* in $\bar{\mathcal{D}}$ if

$$\ker\left(\mathbf{B}_{\mathcal{K}}\big(\mathbf{x}(t)\big)\right) = \ker\left(\mathbf{B}_{\mathcal{G}}\big(\mathbf{x}(t)\big)\right)$$

Otherwise, it is *infinitesimally bearing flexible (IBF)*.

A framework $(\mathcal{G}, \mathbf{x})$ is IBR if all its infinitesimal variation are also trivial. Contrarily a framework is IBF it there exists at least an infinitesimal variation that wraps the configuration $\mathbf{x} = \mathbf{x}(t)$ in $\mathbf{x}' \in \mathcal{Q}(\mathbf{x}) \backslash \mathcal{C}(\mathbf{x})$.

Remark 2.1. Trivial variations assume a specific physical meaning for non-degenerate formations cases, as detailed in the following section, leading to a characterization of the dimension of $\ker\left(\mathbf{B}_{\mathcal{K}}\big(\mathbf{x}(t)\big)\right)$ that implies a (necessary and sufficient) condition to check whether a given framework is IBR.

For now on, the time dependency is dropped out to simplify the notation.

2.3 Metric space realizations

In this section the theory presented so far is applied to multiagent systems embedded in specific domains. As previously stated, all the formations are homogeneous and, moreover, all the agents in the same formation are modeled with the same command space $\mathcal{I}$.

2.3.1 Bearing rigidity theory in $\mathbb{R}^d$

Here, formations of $n \geqslant 3$ agents wherein each element is modeled as a *particle point* whose configuration coincides with its position $\mathbf{p}_i \in \mathbb{R}^d$, $d \in \{\, 2, 3 \,\}$ and $i \in \{\, 1 \dots n \,\}$ are considered. A common inertial frame $\mathcal{F}_W$ is assumed to be known by all the agents.

Adopting the framework model, the formation can be described by the pair $(\mathcal{G}, \mathbf{x})$, where the configuration $\mathbf{x} \in \bar{\mathcal{D}}$ with $\bar{\mathcal{D}} = \mathbb{R}^{dn}$ is associated to the *position vector*

$$\mathbf{p} = \left[\mathbf{p}_1^\top \dots \mathbf{p}_n^\top\right]^\top \in \mathbb{R}^{dn},$$

and the graph $\mathcal{G} = (\mathcal{V}, \mathcal{E})$ is *undirected* since the particle point choice allows to assume bidirectional agent interations. In particular, considering an arbitrary orientation for $\mathcal{G}$, the

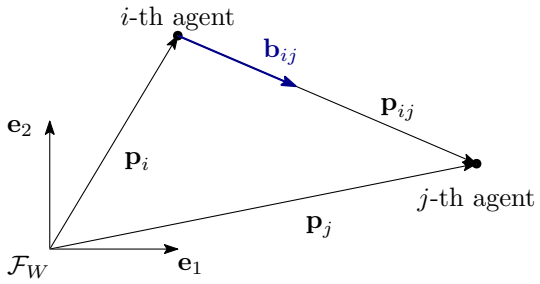

Figure 2.3: Example of two agents of a formation embedded in $\mathbb{R}^{2n}$, there is no local frame, the bearing measurements are directly expressed in the inertial frame $\mathcal{F}_W$.

bearing measurement associated to the (directed) edge $e_k = e_{ij} \in \mathcal{E}$ results to be

$$\mathbf{b}_k = \mathbf{b}_{ij} = \frac{\mathbf{p}_j - \mathbf{p}_i}{\|\mathbf{p}_j - \mathbf{p}_i\|} = d_{ij}\mathbf{p}_{ij} = \bar{\mathbf{p}}_{ij} \in \mathbb{S}^{d-1}, \tag{2.3}$$

where $\mathbf{p}_{ij} = \mathbf{p}_j - \mathbf{p}_i \in \mathbb{R}^d$, and $d_{ij} = \|\mathbf{p}_j - \mathbf{p}_i\|^{-1} \in \mathbb{R}$. Note that $\mathbf{b}_{ij} = -\mathbf{b}_{ji}$, namely, any orientation of $\mathcal{G}$ entails the same amount of bearing information, and that $\mathcal{M} = \mathbb{S}^{d-1}$. An example of the interaction of two agent belonging to a formation embedded in $\mathbb{R}^{2n}$ is reported in figure 2.3.

Exploiting equation (2.3), the bearing rigidity function for this type of frameworks can be expressed as

$$\mathbf{b}_{\mathcal{G}}(\mathbf{x}) = \operatorname{diag}(d_{ij}\mathbf{I}_d)\bar{\mathbf{E}}^\top \mathbf{p} \in \mathbb{S}^{(d-1)m}, \tag{2.4}$$

where $\bar{\mathbf{E}} \in \mathbb{R}^{dn \times dm}$ is obtained from the incidence matrix of the (oriented) graph $\mathcal{G}$.[3] Each agent belonging to a formation $(\mathcal{G}, \mathbf{x})$ in $\mathbb{R}^{dn}$ is characterized by d translational degrees of freedom (tdofs) as its position can vary over time in a controllable manner.[4] Hence the instantaneous variation vector can be selected as

$$\boldsymbol{\delta} = \boldsymbol{\delta}_p = \left[\dot{\mathbf{p}}_1^\top \dots \dot{\mathbf{p}}_n^\top\right]^\top \in \mathbb{R}^{dn} \tag{2.5}$$

and the variation domain $\bar{\mathcal{I}}$ coincides with $\mathbb{R}^{dn}$. Using equation (2.4) it can be observed that the dynamics of the measurements depends on the position variation of the interacting agents. Indeed, it hold that

[3] The bearing vector $\mathbf{b}_{\mathcal{G}}(\mathbf{x})$ does not belong to $\mathbb{S}^{(d-1)m}$. Instead, it belongs to $\left(\mathbb{S}^{d-1}\right)^m$; nevertheless, this little abuse of notation will be maintained for the rest of the thesis.

[4] This is due by the choice of single integrator model.

Proposition 2.6.

$$\dot{\mathbf{b}}_{ij} = d_{ij}\mathbf{P}(\bar{\mathbf{p}}_{ij})(\dot{\mathbf{p}}_j - \dot{\mathbf{p}}_i), \quad \forall (v_i, v_j) \in \mathcal{E}. \tag{2.6}$$

See proof on page 91.

Combining equations (2.2), (2.5) and (2.6) the bearing rigidity matrix can be written as

$$\mathbf{B}_{\mathcal{G}}(\mathbf{x}) = \operatorname{diag}(d_{ij}\mathbf{P}(\bar{\mathbf{p}}_{ij}))\bar{\mathbf{E}}^{\top} \in \mathbb{R}^{dm \times dn}. \tag{2.7}$$

This coincides with the gradient of the bearing rigidity function along the position vector $\mathbf{p}$, i.e., $\mathbf{B}_{\mathcal{G}}(\mathbf{x}) = \nabla_{\mathbf{p}}\mathbf{b}_{\mathcal{G}}(\mathbf{x})$.

According to lemma 2.3, the infinitesimal variation of $(\mathcal{G}, \mathbf{x})$ are identified by the null space of the matrix (2.7). However, to check the infinitesimal rigidity of the framework is necessary to retrieve its trivial variations (lemma 2.5 and definition 2.12).

Proposition 2.7. *Given a (non-degenerate) n-agents formation $(\mathcal{G}, \mathbf{x})$ embedded in $\bar{\mathcal{D}} = \mathbb{R}^{dn}$, its trivial variation set coincides with the $(d+1)$-dimensional set*

$$\mathcal{S}_t = \operatorname{span}\{\, \mathbf{1}_n \otimes \mathbf{I}_d, \mathbf{p} \,\}, \tag{2.8}$$

See proof on page 91.

The set (2.8) has a very precise physical meaning: it represents the translation and uniform scaling of the configuration $\mathbf{x}$. Then, it is possible to state the following theorem.

Theorem 2.8 (Condition for IBR)**.** *A non-degenerate framework $(\mathcal{G}, \mathbf{x})$ in $\mathbb{R}^{dn}$ is IBR if and only if* $\ker(\mathbf{B}_{\mathcal{G}}(\mathbf{x})) = \mathcal{S}_t$*, or equivalently,* $\operatorname{rk}(\mathbf{B}_{\mathcal{G}}(\mathbf{x})) = dn - d - 1$.

Proof. Proposition 2.7 proves that $\ker(\mathbf{B}_{\mathcal{K}}(\mathbf{x})) = \mathcal{S}_t$, then recalling definition 2.12 the first conclusion trivially follows. For the second part, the framework is IBR if and only if $\operatorname{null}(\mathbf{B}_{\mathcal{G}}(\mathbf{x})) = \operatorname{null}(\mathbf{B}_{\mathcal{K}}(\mathbf{x}))$. Then, notice that

$$\operatorname{rk}(\mathbf{B}_{\mathcal{G}}(\mathbf{x})) = dn - d - 1 \Leftrightarrow \operatorname{null}(\mathbf{B}_{\mathcal{G}}(\mathbf{x})) = d + 1$$

which is exactly the dimension of $\mathcal{S}_t$. □

Figure 2.4 on the next page shows some frameworks embedded in $\mathbb{R}^{dn}$, $d \in \{\, 2, 3 \,\}$ that are IBF and IBR. For example, figures 2.4b to 2.4d are IBF because they can be dilated horizontally without affecting the bearing measurements.

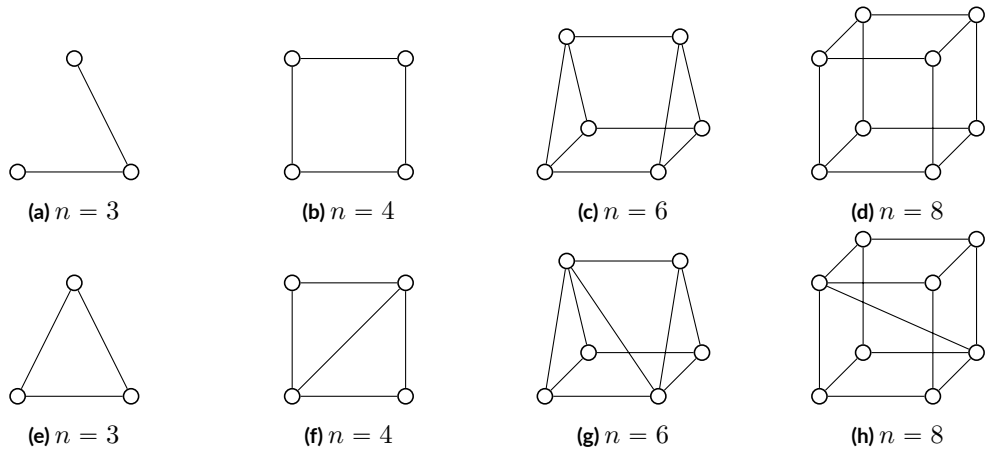

(a) $n = 3$ **(b)** $n = 4$ **(c)** $n = 6$ **(d)** $n = 8$

(e) $n = 3$ **(f)** $n = 4$ **(g)** $n = 6$ **(h)** $n = 8$

Figure 2.4: Example of IBF frameworks (a-b) and infinitesimally bearing rigid (IBR) frameworks (e-f) in $\mathbb{R}^{2n}$; IBF frameworks (c-d) and infinitesimally bearing rigid (IBR) frameworks (g-h) in $\mathbb{R}^{3n}$.

2.3.2 Bearing rigidity theory in $\mathbb{R}^d \times \mathbb{S}^1$

In this section (non-degenerate) formations composed by $n \geqslant 3$ agents whose configuration is defined in the Cartesian product $\mathbb{R}^d \times \mathbb{S}^1$, $d \in \{ 2, 3 \}$ are considered. Each agent is modeled as a *rigid body* associated to a *local reference frame* $\mathcal{F}_i$ whose origin O_i coincides with its center of mass (COM). Thus, its configuration $\mathbf{x}_i$ corresponds to the vector $\mathbf{p}_i \in \mathbb{R}^d$, that indicates the position of O_i in the global reference frame $\mathcal{F}_W$, and the angle $\alpha_i \in [0, 2\pi)$, that specifies the orientation of $\mathcal{F}_i$ w.r.t. $\mathcal{F}_W$.

Remark 2.2. The space $\mathbb{S}^1$ is isomorphic to the interval $[0, 2\pi)$ and it is also isomorphic to the two-dimensional Special Orthogonal group

$$SO(2) = \left\{ \mathbf{R} \in \mathbb{R}^{2\times 2} \;\middle|\; \mathbf{R}\mathbf{R}^\top = \mathbf{I}_2, \quad \det(\mathbf{R}) = +1 \right\}.$$

Hence, when a formation on a plane is considered, i.e., for $d = 2$, the orientation of each i-th agent, $i \in \{ 1 \dots n \}$, is (completely) specified by an angle $\alpha_i \in [0, 2\pi)$ that is univocally associated to a rotation matrix $\mathbf{R}_i = \mathbf{R}(\alpha_i) \in SO(2)$. When the $3D$ case is accounted ($d = 3$), instead, the matrix $\mathbf{R}_i = \mathbf{R}(\alpha_i) \in SO(3)$, belonging to the three-dimensional Spacial Orthogonal group

$$SO(3) = \left\{ \mathbf{R} \in \mathbb{R}^{3\times 3} \;\middle|\; \mathbf{R}\mathbf{R}^\top = \mathbf{I}_3, \quad \det(\mathbf{R}) = +1 \right\},$$

denotes a rotation of angle $\alpha_i \in [0, 2\pi)$ around the arbitrary (unit) vector $\mathbf{n} \in \mathbb{S}^2$.

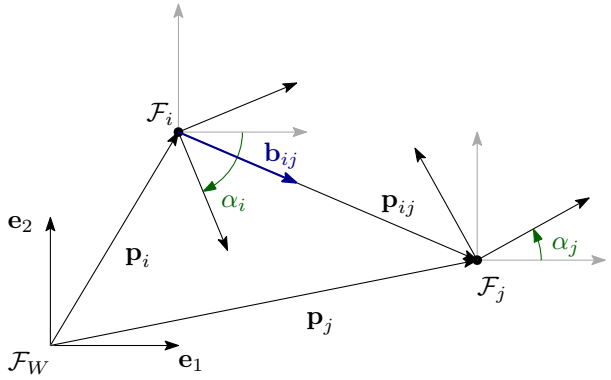

Figure 2.5: Example of two agents of a formation embedded in $(\mathbb{R}^n \times \mathbb{S}^1)^n$; each agent has its own local frame.

The described formation can be modeled as a framework $(\mathcal{G}, \mathbf{x})$ embedded in

$$\bar{\mathcal{D}} = \left(\mathbb{R}^d \times [0, 2\pi)\right)^n.$$

In this case the configuration $\mathbf{x} = \{ (\mathbf{p}_1, \alpha_1) \dots (\mathbf{p}_n, \alpha_n) \}$ is associated to the *position vector* $\mathbf{p} = \left[\mathbf{p}_1^\top \dots \mathbf{p}_n^\top\right]^\top \in \mathbb{R}^{dn}$ and the *orientation vector* $\boldsymbol{\alpha} = [\alpha_1 \dots \alpha_n]^\top \in [0, 2\pi)^n$. The graph is *directed*, since it is assumed that agents do not have access to the inertial frame so the gathered measurements are inherently expressed in the local frames and the sensing capabilities are not necessarily reciprocal between pairs of agents. Thus, the directed edge $e_k = (v_i, v_j) \in \mathcal{E}$ refers to the bearing measurement of the j-th agent obtained by the i-th agent. However, this can be expressed in terms of the relative position and orientation of the agents in $\mathcal{F}_W$, namely

$$\mathbf{b}_k = \mathbf{b}_{ij} = \mathbf{R}_i^\top \bar{\mathbf{p}}_{ij} \in \mathbb{S}^{d-1}, \tag{2.9}$$

where $\bar{\mathbf{p}}_{ij} \in \mathbb{S}^{d-1}$ is the normalized relative position vector introduced in equation (2.3), and $\mathbf{R}_i = \mathbf{R}(\alpha_i) \in SO(d)$ is the rotation matrix that describes the orientation of $\mathcal{F}_i$ w.r.t. $\mathcal{F}_W$. Note that $\mathcal{M} = \mathbb{S}^{d-1}$ as in the previous case and that, from equation (2.9) and according to definition 2.4, the bearing rigidity function can be compactly expressed as

$$\mathbf{b}_{\mathcal{G}}(\mathbf{x}) = \operatorname{diag}(d_{ij}\mathbf{R}_i^\top)\bar{\mathbf{E}}^\top \mathbf{p} \in \mathbb{S}^{(d-1)m}.$$

An example of two interacting agents embedded in $\mathbb{R}^2 \times \mathbb{S}^1$ is reported in figure 2.5.

Each agent belonging to a framework in $\left(\mathbb{R}^d \times \mathbb{S}^1\right)^n$ is characterized by d tdofs and only one rotational dof (rdof) that are assumed to be independently controllable. Hence, the instantaneous variation vector $\boldsymbol{\delta}$ belonging to $\bar{\mathcal{I}} = \mathbb{R}^{(d+1)n}$ results from the contribution of

two components related to the (first-order) variation of the position and of the orientation vectors, namely $\boldsymbol{\delta} = \begin{bmatrix}\boldsymbol{\delta}_p^\top & \boldsymbol{\delta}_o^\top\end{bmatrix}^\top \in \mathbb{R}^{(d+1)n}$ where

$$\boldsymbol{\delta}_p = \begin{bmatrix}\dot{\mathbf{p}}_1^\top \dots \dot{\mathbf{p}}_n^\top\end{bmatrix}^\top \in \mathbb{R}^{dn}, \quad \boldsymbol{\delta}_o = \begin{bmatrix}\dot{\alpha}_1 \dots \dot{\alpha}_n\end{bmatrix}^\top \in \mathbb{R}^n.$$

Remark 2.3. For $d = 2$, $\dot{\alpha}_i$ corresponds to the variation of the i-th agent orientation on the plane. For $d = 3$, it identifies a variation only along the direction determined by $\mathbf{n} \in \mathbb{S}^2$.

Proposition 2.9. *The time derivative of a generic bearing measurement* $\mathbf{b}_{ij} \in \mathbb{S}^{d-1}$ *in* (2.9) *results to be*

$$\dot{\mathbf{b}}_{ij} = \begin{cases} d_{ij}\mathbf{R}_i^\top \mathbf{P}(\bar{\mathbf{p}}_{ij})(\dot{\mathbf{p}}_j - \dot{\mathbf{p}}_i) + \mathbf{R}_i^\top \bar{\mathbf{p}}_{ij}^\perp \dot{\alpha}_i, & \text{if } d = 2 \\ d_{ij}\mathbf{R}_i^\top \mathbf{P}(\bar{\mathbf{p}}_{ij})(\dot{\mathbf{p}}_j - \dot{\mathbf{p}}_i) + \mathbf{R}_i^\top [\bar{\mathbf{p}}_{ij}]_\times \mathbf{n}\dot{\alpha}_i. & \text{if } d = 3 \end{cases}$$

where $\bar{\mathbf{p}}_{ij}^\perp = \mathbf{R}(-\pi/2)\bar{\mathbf{p}}_{ij} \in \mathbb{R}^2$ *with* $\mathbf{R}(-\pi/2) \in SO(2)$ *the (unit) vector perpendicular to* $\bar{\mathbf{p}}_{ij}$ *on the plane.*

See proof on page 93.

As a consequence, according to definition 2.9, the bearing rigidity matrix can be written as

$$\mathbf{B}_{\mathcal{G}}(\mathbf{x}) = \begin{bmatrix}\mathbf{D}_1 \bar{\mathbf{E}}^\top & \mathbf{D}_2 \mathbf{E}_o^\top\end{bmatrix} \in \mathbb{R}^{dm \times (d+1)n}, \tag{2.10}$$

where $\bar{\mathbf{E}} \in \mathbb{R}^{dn \times dm}$, $\mathbf{E}_o \in \mathbb{R}^{n \times m}$ are derived from $\mathcal{G}$ and

$$\mathbf{D}_1 = \operatorname{diag}(d_{ij}\mathbf{R}_i^\top \mathbf{P}(\bar{\mathbf{p}}_{ij})) \in \mathbb{R}^{dm \times dm}, \tag{2.11}$$

$$\mathbf{D}_2 = \begin{cases} -\operatorname{diag}(\mathbf{R}_i^\top \bar{\mathbf{p}}_{ij}^\perp) \in \mathbb{R}^{2m \times m} & \text{if } d = 2 \\ -\operatorname{diag}(\mathbf{R}_i^\top [\bar{\mathbf{p}}_{ij}]_\times \mathbf{n}) \in \mathbb{R}^{3m \times m} & \text{if } d = 3 \end{cases}. \tag{2.12}$$

Accounting for the null space of the bearing rigidity matrix in correspondence of $\mathcal{K}$, it results that when $\boldsymbol{\delta}_o = \mathbf{0}$, the trivial motions coincide with the translation and uniform scaling of the entire configuration, and when $\boldsymbol{\delta}_o \neq \mathbf{0}$, with the *coordinated rotation*, namely the equal rotation of all the agents jointly with the equal rotation of the whole formation.[5]

[5] The center of rotation of the formation can be arbitrary, but the axis of rotation must be parallel to the ones of the agents. If the center is the barycentre of the formation, then the rotation is called *pure coordinated rotation*.

Proposition 2.10. *Given a (non-degenerate) n-agents formation $(\mathcal{G}, \mathbf{x})$ embedded in $\bar{\mathcal{D}} = (\mathbb{R}^d \times \mathbb{S}^1)^n$, $d \in \{2, 3\}$ its coordinated rotation set $\mathcal{R}_{\circlearrowleft}$ results*

$$\mathcal{R}_{\circlearrowleft} = \begin{cases} \operatorname{span}\left\{ \begin{bmatrix} (\mathbf{I}_n \otimes \mathbf{R}(\pi/2))\mathbf{p} \\ \mathbf{1}_n \end{bmatrix} \right\}, & \text{if } d = 2 \\ \operatorname{span}\left\{ \begin{bmatrix} (\mathbf{I}_n \otimes [\mathbf{n}]_\times)\mathbf{p} \\ \mathbf{1}_n \end{bmatrix} \right\}, & \text{if } d = 3 \end{cases}, \tag{2.13}$$

where the vector $\mathbf{1}_n \in \mathbb{R}^n$ has all entries equal to one.

See proof on page 94.

Since $\dim(\mathcal{R}_{\circlearrowleft}) = 1$ for $d \in \{2, 3\}$, the set including all the trivial variation vectors related to translations, scaling and coordinated rotations of a framework, namely

$$\mathcal{S}_t = \operatorname{span}\left\{ \begin{bmatrix} \mathbf{1}_n \otimes \mathbf{I}_d \\ \mathbf{0}_n \end{bmatrix}, \begin{bmatrix} \mathbf{p} \\ \mathbf{0}_n \end{bmatrix}, \mathcal{R}_{\circlearrowleft} \right\}, \tag{2.14}$$

has dimension $\dim(\mathcal{S}_t) = d + 2$. Similarly to the case investigated in section 2.3.1, the determination of the space (2.14) is fundamental for the statement of the next theorem.

Theorem 2.11 (Condition for IBR)**.** *A non-degenerate framework $(\mathcal{G}, \mathbf{x})$ in $(\mathbb{R}^d \times \mathbb{S}^1)^n$ with $d \in \{2, 3\}$ is IBR if and only if*

$$\ker(\mathbf{B}_{\mathcal{G}}(\mathbf{x})) = \mathcal{S}_t,$$

or equivalently,

$$\operatorname{rk}(\mathbf{B}_{\mathcal{G}}(\mathbf{x})) = (d+1)n - d - 2.$$

Proof. The first conclusion trivially follows from definition 2.12. For the second part, the framework is IBR if and only if $\operatorname{null}(\mathbf{B}_{\mathcal{G}}(\mathbf{x})) = \operatorname{null}(\mathbf{B}_{\mathcal{K}}(\mathbf{x}))$. Then, notice that

$$\operatorname{rk}(\mathbf{B}_{\mathcal{G}}(\mathbf{x})) = (d+1)n - d - 2 \Leftrightarrow \operatorname{null}(\mathbf{B}_{\mathcal{G}}(\mathbf{x})) = d + 2$$

which is exactly the dimension of $\mathcal{S}_t$. □

Figure 2.6 on the next page shows some IBF and IBR formations embedded in $(\mathbb{R}^d \times \mathbb{S}^1)^n$; the blue edges represent mono directional measurements while the red edges represent

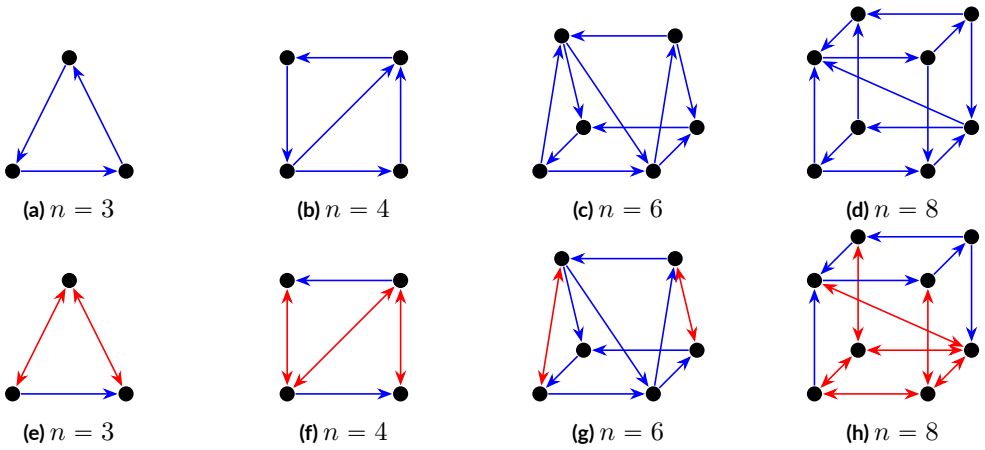

Figure 2.6: Example of IBF frameworks (a-b) and IBR frameworks (e-f) in $(\mathbb{R}^2 \times \mathbb{S}^1)^n$; IBF frameworks (c-d) and IBR frameworks (g-h) in $(\mathbb{R}^3 \times \mathbb{S}^1)^n$. The red edges represent bi-directional measurements while the blue ones represent mono-directional measurements.

bidirectional measurements.

2.3.3 Bearing rigidity theory in $SE(3)$

The last and most complete scenario is here presented, namely, the case of n-agents ($n \geqslant 3$) formations whose configuration is embedded on $SE(3)$, i.e., on the Cartesian product $\mathbb{R}^3 \times SO(3)$.

Analogously to the previous section, each agent is modeled as a *rigid body* with a *local reference frame* $\mathcal{F}_i$ and its configuration $\mathbf{x}_i$ corresponds to the pair $(\mathbf{p}_i, \mathbf{R}_i)$ where the vector $\mathbf{p}_i \in \mathbb{R}^3$ identifies the position of O_i in the world frame $\mathcal{F}_W$ and the matrix $\mathbf{R}_i \in SO(3)$ defines the orientation of $\mathcal{F}_i$ w.r.t $\mathcal{F}_W$.

This kind of formations can be modeled as a framework $(\mathcal{G}, \mathbf{x})$ in $\bar{\mathcal{D}} = SE(3)^n$, where $\mathcal{G}$ is a *directed* graph according to the same motivations presented in section 2.3.2. The configuration $\mathbf{x}$ is composed by the *position vector* $\mathbf{p} = \left[\mathbf{p}_1^\top \dots \mathbf{p}_n^\top\right]^\top \in \mathbb{R}^{3n}$, and the $(3n \times 3)$ *orientation matrix* $\mathbf{R}_a = \left[\mathbf{R}_1^\top \dots \mathbf{R}_n^\top\right]^\top \in SO(3)^n$, stacking all the agent positions and orientations, respectively. In the same way of the $\mathbb{R}^d \times \mathbb{S}^1$ case, the bearing measurement of the j-th agent computed by the i-th one can be expressed as

$$\mathbf{b}_k = \mathbf{b}_{ij} = \mathbf{R}_i^\top \bar{\mathbf{p}}_{ij} \in \mathbb{S}^2, \tag{2.15}$$

where $\bar{\mathbf{p}}_{ij} \in \mathbb{S}^2$, $\mathbf{R}_i \in SO(3)$ have the same meaning provided in section 2.3.2 and it results

$\mathcal{M} = \mathbb{S}^2$. According to definition 2.4, the bearing rigidity function results to be

$$\mathbf{b}_{\mathcal{G}}(\mathbf{x}) = \operatorname{diag}(d_{ij}\mathbf{R}_i^\top)\bar{\mathbf{E}}^\top \mathbf{p} \in \mathbb{S}^{2m}.$$

The agents are assumed to be *fully-actuated*, namely they are characterized by six independent dofs: 3tdofs and 3 rdofs controllable in a decoupled manner.

Remark 2.4. The time derivative of a matrix $\mathbf{R}_i \in SO(3)$ results to be $\dot{\mathbf{R}}_i = [\boldsymbol{\omega}_{w,i}]_\times \mathbf{R}_i$, where $\boldsymbol{\omega}_{w,i} \in \mathbb{R}^3$ is the angular velocity of th i-th agent expressed in the global inertial frame $\mathcal{F}_W$ (see section A.1 on page 87). As a consequence, note that the command space $\mathcal{I}$ of each i-th agent includes its linear velocity $\dot{\mathbf{p}}_i \in \mathbb{R}^3$ and its angular velocity $\boldsymbol{\omega}_{w,i} \in \mathbb{R}^3$, both expressed in $\mathcal{F}_W$.

Given this premises, the instantaneous variation vector can be identify as

$$\boldsymbol{\delta} = \begin{bmatrix} \boldsymbol{\delta}_p^\top & \boldsymbol{\delta}_o^\top \end{bmatrix}^\top \in \bar{\mathcal{I}}$$

with $\bar{\mathcal{I}} = \mathbb{R}^{6n}$, where

$$\boldsymbol{\delta}_p = \begin{bmatrix} \dot{\mathbf{p}}_1^\top \dots \dot{\mathbf{p}}_n^\top \end{bmatrix}^\top \in \mathbb{R}^{3n}, \quad \boldsymbol{\delta}_o = \begin{bmatrix} \boldsymbol{\omega}_{w,1}^\top \dots \boldsymbol{\omega}_{w,n}^\top \end{bmatrix}^\top \in \mathbb{R}^{3n}.$$

Proposition 2.12. *The time derivative of a generic bearing measurement* $\mathbf{b}_{ij} \in \mathbb{S}^2$ *in* (2.15) *results to be*

$$\dot{\mathbf{b}}_{ij} = d_{ij}\mathbf{R}_i^\top \mathbf{P}(\bar{\mathbf{p}}_{ij})(\dot{\mathbf{p}}_j - \dot{\mathbf{p}}_i) + \mathbf{R}_i^\top [\bar{\mathbf{p}}_{ij}]_\times \boldsymbol{\omega}_{w,i} \tag{2.16}$$

See proof on page 95.

Therefore, the $(3m \times 6n)$ bearing rigidity matrix can be written in a compact form as

$$\mathbf{B}_{\mathcal{G}}(\mathbf{x}) = \begin{bmatrix} \operatorname{diag}(d_{ij}\mathbf{R}_i^\top \mathbf{P}(\bar{\mathbf{p}}_{ij}))\bar{\mathbf{E}}^\top & -\operatorname{diag}(\mathbf{R}_i^\top [\bar{\mathbf{p}}_{ij}]_\times)\bar{\mathbf{E}}_o^\top \end{bmatrix}. \tag{2.17}$$

Comparing equation (2.17) with equation (2.10) it is possible to observe that the translation, uniform scaling and coordinated rotation are trivial variations also for a framework in $SE(3)^n$, however the concept of coordinated rotation has to be redefined since the agents orientation is no longer controllable via a single angle.

First, note that the angular velocity of each agent can be an arbitrary vector in $\mathbb{R}^3$, resulting from the linear combination of the (unit) vectors $\mathbf{e}_h \in \mathbb{S}^2$, $h = 1, 2, 3$ that identifies the axes of the frame $\mathcal{F}_W$. Hence, three basic coordinate rotations can be distinguished such that

all the agents are rotated in the same way of the whole formation around $\mathbf{e}_h$, $h = 1, 2, 3$. Each coordinated rotation can thus be expressed as a suitable sequence of basic coordinated rotations, hence $\dim(\mathcal{R}_{\circlearrowleft}) = 3$ where $\mathcal{R}_{\circlearrowleft}$ is the coordinated rotation set. In a more formal way

Proposition 2.13. *Given a (non-degenerate) n-agents formation $(\mathcal{G}, \mathbf{x})$ embedded in $\bar{\mathcal{D}} = SE(3)^n$ its coordinated rotation set $\mathcal{R}_{\circlearrowleft}$ results*

$$\mathcal{R}_{\circlearrowleft} = \operatorname{span}\left\{ \left\{ \begin{bmatrix} (\mathbf{I}_n \otimes [\mathbf{e}_h]_\times)\mathbf{p} \\ \mathbf{1}_n \otimes \mathbf{e}_h \end{bmatrix} \right\}_{h=1,2,3} \right\}. \tag{2.18}$$

See proof on page 96.

Therefore, the trivial variation set $\mathcal{S}_t$ has dimension $\dim(\mathcal{S}_t) = 7$ and it results,

$$\mathcal{S}_t = \operatorname{span}\left\{ \begin{bmatrix} \mathbf{1}_n \otimes \mathbf{I}_3 \\ \mathbf{0}_{3n} \end{bmatrix}, \begin{bmatrix} \mathbf{p} \\ \mathbf{0}_{3n} \end{bmatrix}, \mathcal{R}_{\circlearrowleft} \right\}. \tag{2.19}$$

It is finally possible to state the last theorem

Theorem 2.14 (Condition for IBR)**.** *A non-degenerate framework $(\mathcal{G}, \mathbf{x})$ in $SE(3)^n$ is IBR if and only if*

$$\ker(\mathbf{B}_{\mathcal{G}}(\mathbf{x})) = \mathcal{S}_t,$$

or equivalently,

$$\operatorname{rk}(\mathbf{B}_{\mathcal{G}}(\mathbf{x})) = 6n - 7.$$

Proof. The first conclusion trivially follows from definition 2.12. For the second part, the framework is IBR if and only if $\operatorname{null}(\mathbf{B}_{\mathcal{G}}(\mathbf{x})) = \operatorname{null}(\mathbf{B}_{\mathcal{K}}(\mathbf{x}))$. Then, notice that

$$\operatorname{rk}(\mathbf{B}_{\mathcal{G}}(\mathbf{x})) = 6n - 7 \Leftrightarrow \operatorname{null}(\mathbf{B}_{\mathcal{G}}(\mathbf{x})) = 7$$

which is exactly the dimension of $\mathcal{S}_t$. □

Figure 2.7 on the next page shows some IBF and IBR formations embedded in $SE(3)^n$; the blue edges represent mono directional measurements while the red edges represent bidirectional measurements.

Before moving to the next section it is interesting to associate the five different configuration domains $\mathcal{D}$ to the real devices that they are required to model.

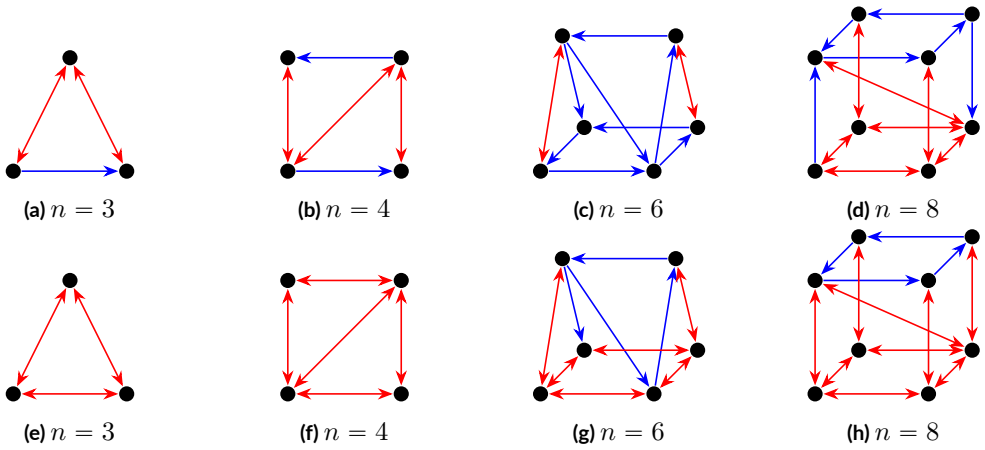

Figure 2.7: Example of IBF frameworks (a-d) and IBR frameworks (e-h) in $SE(3)^n$. The red edges represent bi-directional measurements while the blue ones represent mono-directional measurements.

- Frameworks embedded in $\mathcal{D} = \mathbb{R}^{dn}$, $d = 2, 3$, are suitable to model teams of mobile sensors interacting in a certain (two-dimensional or three-dimensional) area of interest.

- The agent configuration domain $(\mathbb{R}^2 \times \mathbb{S}^1)$ is suitable to model unmanned ground vehicles (UGV). But, it is crucial to realize that the choice performed in section 2.3.2 of having *decoupled* tdofs and rdof heavily constrains the characteristic of the agents. A possible valid solution is to use robot equipped with omnidirectional wheels.

- The agent configuration domain $(\mathbb{R}^3 \times \mathbb{S}^1)$ is usually chosen to model standard under-actuated unmanned aerial vehicles (UAV), in particular 4dofs-UAV (quadrotors), with the axis of rotation $\mathbf{n}$ perpendicular to the ground. If it is true that $(\mathbb{R}^3 \times \mathbb{S}^1)$ is sufficient to characterize the *static* configuration of a quadrotor, problems arise when the dynamics has to be taken into account. In fact 4dofs-UAV requires to tilt around different axes than $\mathbf{n}$ to perform all the possible translations. This shows that not only the agent commands can not be decouples but also that the configuration domain is not rich enough to correctly model such kind of agents. A possible solution is to resolve to fully-actuated UAV, that are introduced in the following, and reduce (through software) their actuation capability.

- $SE(3)$ is indeed the only agent configuration domain that can model any real agent. An example of agent with $\mathcal{I} = \mathbb{R}^6$ is the *tilted-propellers exacopter*, a type of fully-actuated (and decoupled) UAV.

3

Characterization of Mixed Formations

In the previous chapter the bearing rigidity theory has been studied for formations composed by *identical* elements. Identical elements stands for agents that have the same relevant characteristics for the bearing rigidity theory, namely, bearing sensing apparatus $\mathcal{M}_i$, configuration domain $\mathcal{D}_i$ and command space $\mathcal{I}_i$. This chapter, instead, is dedicated to the characterization of the dynamic rigidity properties of *mixed formations*. A general structure will be given along with properties that hold for any mixed framework; then, specific results will be proven for particular cases of study. But, in order to do so, it is first necessary to formalize the concept of mixed formation.

3.1 Mixed formations

Mixed formations are formations composed by agents that do not have the same actuation capability and that can be naturally modeled with different configuration domains. Therefore, a reasonable solution is to call a formation *mixed* if it is not homogeneous.

Example 3.1 (Mixed Formation)**.** A team of autonomous robot composed by four UGVs and two 6dofs-UAVs that has to accomplish surveillance tasks can be modeled as a mixed formation. The four UGV are embedded in $(\mathbb{R}^2 \times \mathbb{S}^1)$ while the two UAV are embedded in $SE(3)$.

Taking inspiration for example 3.1, the requirement of *connectivity* of $\mathcal{G}$ in definition 2.1

on page 8 imposes that the interaction graph $\mathcal{G}$ of a mixed formation must have at least an edge connecting two agents of different typology.

Therefore, suppose that an UGV agent, modeled as in section 2.3.2, has to measure the bearing of an UAV modeled as in section 2.3.3. With just this consideration two major problems arise:

- the bearing measurement device that is mounted on the UGV can no longer take measures in $\mathcal{M} = \mathbb{S}^1$. It is instead required to acquire measures in the 3D space, $\mathcal{M} = \mathbb{S}^2$, as it is done by the UAVs. This is a simple consequence of the fact about having no more all agent laying on a plane.
- It is not clear how the two different configuration domains ($\mathbb{R}^2 \times \mathbb{S}^1$) and $SE(3)$ should interact. Trivially, the vector $\mathbf{p}_{ij} = \mathbf{p}_j - \mathbf{p}_i$ is not even defined if the type of agent i and agent j is different.

The source of these problems is the fact that the real agents are rigid bodies belonging to the 3D space and as such they have to be modeled. Therefore the correct configuration domain for all the agents, independently from their type, is $SE(3)$ and the different actuation capabilities have to be modeled through different command spaces $\mathcal{I}_i$ $i \in \{ 1 \dots n \}$.

Definition 3.1 (Mixed Framework in $SE(3)^n$)**.** A mixed framework in $\bar{\mathcal{D}} = SE(3)^n$ is an ordered triple $(\mathcal{G}, \mathbf{x}, \mathcal{H})$ consisting of a connected graph $\mathcal{G} = (\mathcal{V}, \mathcal{E})$ with $|\mathcal{V}| = n$, a configuration $\mathbf{x} \in SE(3)$, and a collection of command spaces $\mathcal{H} = \{ \mathcal{I}_1 \dots \mathcal{I}_n \}$.

A (unconstrained) rigid body in the 3D space with configuration $\mathbf{x} \in SE(3)$ has six degrees of freedom, related to its capability to translate and rotate. The first one is associated to the linear velocity of its COM, $\mathbf{v}_w \in \mathbb{R}^3$, while the second is associated to the angular velocity $\boldsymbol{\omega}_w \in \mathbb{R}^3$, both expressed in the inertial frame $\mathcal{F}_W$. The resulting kinematic (or dynamics, if a single integrator model is used) is

$$\begin{cases} \dot{\mathbf{p}} = \mathbf{v}_w \\ \dot{\mathbf{R}} = [\boldsymbol{\omega}_w]_\times \mathbf{R} \end{cases}$$

The case of fully-actuated agents, that has already been studied, can be related to the reasoning above. In particular, if the i-th agent, $i \in \{ 1 \dots n \}$ has command space $\mathcal{I}_i = \mathbb{R}^6$ as in section 2.3.3, then it has 3 tdofs and 3 rdofs. Its command vector can be written as $\boldsymbol{\delta}_i = \begin{bmatrix} \boldsymbol{\delta}_{p,i}^\top & \boldsymbol{\delta}_{o,i}^\top \end{bmatrix}^\top$, where $\boldsymbol{\delta}_{p,i} \in \mathbb{R}^3$ and $\boldsymbol{\delta}_{o,i} \in \mathbb{R}^3$ are the commands responsible to the

variation of the position and orientation, respectively. Namely,

$$\begin{aligned} \mathbf{v}_{w,i} &= \boldsymbol{\delta}_{p,i} \\ \boldsymbol{\omega}_{w,i} &= \boldsymbol{\delta}_{o,i} \end{aligned} \tag{3.1}$$

Observation. It does not make sense to consider mixed formation in $\mathbb{R}^n$ characterized by agents having all 6 dofs. Therefore at least an agent $i \in \{ 1 \dots n \}$ must be under-actuated, $\mathcal{I}_i \subset \mathbb{R}^6$.

For each under-actuated agent the map $S_i : \mathcal{I}_i \to \mathbb{R}^6$ defines the actuation capability as a function of the command vector $\boldsymbol{\delta}_i \in \mathcal{I}_i$:

$$\begin{bmatrix} \mathbf{v}_{w,i} \\ \boldsymbol{\omega}_{w,i} \end{bmatrix} = S_i(\boldsymbol{\delta}_i). \tag{3.2}$$

Moreover, if the translational degrees of freedom and the rotational ones can be decoupled, then S_i can be decoupled too into

$$S_{p,i} : \mathcal{I}_{p,i} \to \mathbb{R}^3 \qquad \mathbf{v}_{w,i} = S_{p,i}(\boldsymbol{\delta}_{p,i}) \tag{3.3}$$

$$S_{o,i} : \mathcal{I}_{o,i} \to \mathbb{R}^3 \qquad \boldsymbol{\omega}_{w,i} = S_{o,i}(\boldsymbol{\delta}_{o,i}) \tag{3.4}$$

where $\mathcal{I}_{p,i}, \mathcal{I}_{o,i} \subseteq \mathbb{R}^3$ are the command spaces that account for variations of position and orientation of agent $i \in \{ 1 \dots n \}$, respectively. Upon this definition, it results $\mathcal{I}_i = \mathcal{I}_{p,i} \times \mathcal{I}_{o,i}$. The terms $c_{p,i}, c_{o,i}$ are used to indicate the dimension of $\mathcal{I}_{p,i}, \mathcal{I}_{o,i}$, respectively; namely the tdofs and rdofs of agent i. Moreover $c_i = c_{p,i} + c_{o,i}$ corresponds to the total number of degree of freedom associated to agent i while $c_t = \sum_{i=1}^{n} c_{t,i}, c_o = \sum_{i=1}^{n} c_{o,i}, c = \sum_{i=1}^{n} c_i$ are the number of translational, rotational and total degrees of freedom of the whole formation.

Observation. Equations (3.3) and (3.4) are valid also for full-actuated agents. In these cases $S_{p,i}$ and $S_{o,i}$ are the identity maps. For this reason it is no more necessary to distinguish between full-actuated and under-actuated agents.

Table 3.1 on the next page summarizes the relevant quantities for the three major types of agent: UGV, 4dof-UAV and 6dof-UAV.

Table 3.1: Summary of the relevant quantities for the three agent types of interest.

type	$c_{t,i}$	$c_{r,i}$	$\mathcal{I}_{p,i}$	$\mathcal{I}_{o,i}$	$\mathbf{S}_{p,i}$	$\mathbf{S}_{o,i}$
UGV	2	1	$\mathbb{R}^2$	$\mathbb{R}$	$\begin{bmatrix} 1 & 0 \\ 0 & 1 \\ 0 & 0 \end{bmatrix}$	$\begin{bmatrix} 0 \\ 0 \\ 1 \end{bmatrix}$
4dofs-UAV	3	1	$\mathbb{R}^3$	$\mathbb{R}$	$\mathbf{I}_3$	$\mathbf{n}$
6dofs-UAV	3	3	$\mathbb{R}^3$	$\mathbb{R}^3$	$\mathbf{I}_3$	$\mathbf{I}_3$

3.2 Bearing rigidity theory for mixed formations

It is now possible to present the similarities and differences between the bearing rigidity properties defined in chapter 2 and the ones regarding mixed agents formations.

Definitions 2.4 to 2.6 on page 9 about bearing rigidity function, bearing equivalence and bearing congruence are valid also for mixed frameworks. Nevertheless, the definitions of bearing rigidity and global bearing rigidity (definitions 2.7 and 2.8) do not make sense because, being related to the *static* properties of the framework, they do not take into account the differences between the agents. Instead, all the concepts regarding *dynamic rigidity* apply for mixed frameworks, first of all the property of infinitesimal bearing rigidity. In particular, after noticing that, regardless the characteristics of the agents, the bearing measurement related to $e_k = (v_i, v_j) \in \mathcal{E}$ is exactly the same presented in section 2.3.3:

$$\mathbf{b}_k = \mathbf{b}_{ij} = \mathbf{R}_i^\top \bar{\mathbf{p}}_{ij} \in \mathbb{S}^2,$$

it is possible to embed equations (3.1), (3.3) and (3.4) in the expression of its time derivative (proposition 2.12) obtaining

Proposition 3.1. *The time derivative of a generic bearing measurement $\mathbf{b}_{ij} \in \mathbb{S}^2$ for a mixed framework $(\mathcal{G}, \mathbf{x}, \mathcal{H})$ result to be*

$$\dot{\mathbf{b}}_{ij} = d_{ij}\mathbf{R}_i^\top \mathbf{P}(\bar{\mathbf{p}}_{ij})\big(S_{p,j}(\boldsymbol{\delta}_{p,j}) - S_{p,i}(\boldsymbol{\delta}_{p,i})\big) + \mathbf{R}_i^\top [\bar{\mathbf{p}}_{ij}]_\times S_{o,i}(\boldsymbol{\delta}_{o,i}). \tag{3.5}$$

Great importance is reserved for special cases where the expression of equations (3.3) and (3.4)

are linear because this allows to use a matrix representation:

$$\mathbf{v}_{w,i} = S_{p,i}(\boldsymbol{\delta}_{p,i}) = \mathbf{S}_{p,i}\boldsymbol{\delta}_{p,i} \qquad \mathbf{S}_{p,i} \in \mathbb{R}^{3\times c_{p,i}}, \tag{3.6a}$$

$$\boldsymbol{\omega}_{w,i} = S_{o,i}(\boldsymbol{\delta}_{o,i}) = \mathbf{S}_{o,i}\boldsymbol{\delta}_{o,i} \qquad \mathbf{S}_{o,i} \in \mathbb{R}^{3\times c_{o,i}}, \tag{3.6b}$$

and in this situation equation (3.5) can be rewritten as

$$\dot{\mathbf{b}}_{ij} = d_{ij}\mathbf{R}_i^\top \mathbf{P}(\bar{\mathbf{p}}_{ij})(\mathbf{S}_{p,j}\boldsymbol{\delta}_{p,j} - \mathbf{S}_{o,i}\boldsymbol{\delta}_{o,i}) + \mathbf{R}_i^\top [\bar{\mathbf{p}}_{ij}]_\times \mathbf{S}_{o,i}\boldsymbol{\delta}_{o,i}.$$

This last equation allows a very compact expression for the bearing rigidity matrix $\mathbf{B}_{\mathcal{G}}(\mathbf{x}) \in \mathbb{R}^{3m\times c}$:

$$\mathbf{B}_{\mathcal{G}}(\mathbf{x}) = \begin{bmatrix} \operatorname{diag}(d_{ij}\mathbf{R}_i^\top \mathbf{P}(\bar{\mathbf{p}}_{ij}))\bar{\mathbf{E}}^\top \mathbf{S}_p & -\operatorname{diag}(\mathbf{R}_i^\top [\bar{\mathbf{p}}_{ij}]_\times)\bar{\mathbf{E}}_o^\top \mathbf{S}_o \end{bmatrix} \tag{3.7}$$

where $\mathbf{S}_p = \operatorname{diag}(\mathbf{S}_{p,i}) \in \mathbb{R}^{3n\times c_t}$ and $\mathbf{S}_o = \operatorname{diag}(\mathbf{S}_{o,i}) \in \mathbb{R}^{3n\times c_o}$.

It is therefore possible to verify whether a mixed framework is IBR or not with the same procedure explained in chapter 2. The trivial variation set has once again capital importance and, for mixed frameworks embedded in $SE(3)$ its general structure can be characterized.

3.2.1 The trivial variation set

Mixed formations embedded in $SE(3)$ are fundamentally formations composed by agents having configuration $\mathbf{x}_i \in SE(3)$ and (eventually) reduced actuation capability. Therefore, the trivial variation set for such formations is strictly related to the one presented in equation (2.19) on page 22. For such formations, it has been proven that the trivial variation set has always dimension 7 and it accounts for three translations, a scaling and three coordinated rotations. Rearranging the terms in (3.7) it is possible to highlight the effects of the reduced actuation capability. In fact,

$$\mathbf{B}_{\mathcal{G}}(\mathbf{x}) = \underbrace{\begin{bmatrix} \operatorname{diag}(d_{ij}\mathbf{R}_i^\top \mathbf{P}(\bar{\mathbf{p}}_{ij}))\bar{\mathbf{E}}^\top & -\operatorname{diag}(\mathbf{R}_i^\top [\bar{\mathbf{p}}_{ij}]_\times)\bar{\mathbf{E}}_o^\top \end{bmatrix}}_{=:\mathbf{A}} \underbrace{\begin{bmatrix} \mathbf{S}_p & \mathbf{0} \\ \mathbf{0} & \mathbf{S}_o \end{bmatrix}}_{=:\mathbf{S}}, \tag{3.8}$$

expresses the bearing rigidity matrix as the product of two matrices: $\mathbf{A} \in \mathbb{R}^{3m\times 6n}$ is the bearing rigidity matrix for the fully-actuated formation modeled as a framework $(\mathcal{G}, \mathbf{x})$ embedded in $SE(3)^n$ having the same graph $\mathcal{G}$ and the same configuration $\mathbf{x} \in SE(3)^n$ and

for such reason is called the fully-actuated *twin* of $(\mathcal{G}, \mathbf{x}, \mathcal{H})$. While $\mathbf{S} \in \mathbb{R}^{6n \times c}$ accounts for the reduced actuation capability.

The trivial variation set $\mathcal{S}_t$ corresponds to the null space of the bearing rigidity matrix evaluated on the complete graph $\mathcal{K}$, therefore, when $\mathcal{G}$ is complete,

$$\mathcal{S}_t = \ker\left(\mathbf{AS}\right).$$

Observation 3.1. For an agent i of a mixed formation it is always possible to choose $\mathcal{I}_i$ and S_i such that

$$\ker(S_i) = \{\, \mathbf{0} \,\}$$

and, if they are defined

$$\ker(\mathbf{S}_{p,i}) = \{\, \mathbf{0} \,\}, \quad \ker(\mathbf{S}_{o,i}) = \{\, \mathbf{0} \,\}$$

In light of observation 3.1, the trivial variation set can be written as

$$\mathcal{S}_t = \left\{\, \boldsymbol{\delta} \in \bar{\mathcal{I}} \;\middle|\; \mathbf{S}\boldsymbol{\delta} \in \ker(\mathbf{A}) \,\right\} \subseteq \bar{\mathcal{I}}, \tag{3.9}$$

namely, an infinitesimal variation $\boldsymbol{\delta} \in \bar{\mathcal{I}}$ is a trivial variation if the result of its embedding into $\mathbb{R}^{6n}$ through the matrix $\mathbf{S} \in \mathbb{R}^{6n \times c}$ is a trivial variation for the equivalent fully-actuated formation. It is not possible to directly compare the trivial variation set of a mixed formation with the one of the fully-actuated twin because they are not subsets of the same space. Nevertheless, it is possible to compare $\ker(\mathbf{A}) \subseteq \mathbb{R}^{6n}$ with

$$\mathcal{T} = \{\, \mathbf{S}\boldsymbol{\delta} \mid \boldsymbol{\delta} \in \mathcal{S}_t \,\} \subseteq \mathbb{R}^{6n},$$

which represents the trivial variations *embedded* by the matrix $\mathbf{S}$ into $\mathbb{R}^{6n}$. In particular, it holds that

$$\mathcal{T} \subseteq \ker(\mathbf{A})$$

which implies that constraining the actuation capability of the agents results in a reduction of the trivial variations. Indeed, $\dim(\mathcal{S}_t) = \dim(\mathcal{T}) \leqslant \mathrm{null}(\mathbf{A}) = 7$, the number of *independent* trivial variation is lower (with the equality only if there is no constraint) than seven.

3.3 Characterization of noticeable mixed formations

This section is dedicated to the characterization of two particular mixed formations. In the first case, a formation composed by UGVs and 6dof-UAVs is considered, while in the second one the UGV are substituted by 4dof-UAVs.

3.3.1 UGVs and 6dof-UAVs case

Assume, that $0 < n_a < n$ agents are 6dof-UAVs and the others $n_b = n - n_a$ are UGVs. W.l.o.g. the agents can be labelled such that the first n_a are the 6dof-UAVs while the others are the UGVs. To simplify the notation, for now on the first type of agent is called type A, while the second is called type B. In this way type A agents have $c_{p,a} = 3$ tdofs, $c_{o,a} = 3$ rdofs and obviously $c_a = 6$ dofs while type B agents have $c_{p,b} = 2$, $c_{o,b} = 1$, $c_b = 3$ dofs.

Embedding *all* the instantaneous variations into $\mathbb{R}^{6n}$, it results

$$\mathrm{Im}(\mathbf{S}) = \mathrm{span}\left\{ \begin{bmatrix} \mathbf{I}_{n_a} \otimes \mathbf{I}_3 & \mathbf{0}_{3n_a \times 2n_b} & \mathbf{0}_{3n_a \times 3n_a} & \mathbf{0}_{3n_a \times n_b} \\ \mathbf{0}_{3n_b \times 3n_a} & \mathbf{I}_{n_b} \otimes \begin{bmatrix} 1 & 0 \\ 0 & 1 \\ 0 & 0 \end{bmatrix} & \mathbf{0}_{3n_a \times 3n_a} & \mathbf{0}_{3n_a \times n_b} \\ \mathbf{0}_{3n_a \times 3n_a} & \mathbf{0}_{3n_a \times 2n_b} & \mathbf{I}_{n_a} \otimes \mathbf{I}_3 & \mathbf{0}_{3n_a \times n_b} \\ \mathbf{0}_{3n_b \times 3n_a} & \mathbf{0}_{3n_b \times 2n_b} & \mathbf{0}_{3n_b \times 3n_a} & \mathbf{I}_{n_b} \otimes \begin{bmatrix} 0 \\ 0 \\ 1 \end{bmatrix} \end{bmatrix} \right\} \subseteq \mathbb{R}^{6n},$$

and recalling equation (3.6) it is possible to notice that, for $i \in \{ (n_a + 1) \dots n \}$,

$$\mathbf{v}_{w,i} = \mathrm{span}\left\{ \begin{bmatrix} 1 & 0 \\ 0 & 1 \\ 0 & 0 \end{bmatrix} \right\}, \quad \boldsymbol{\omega}_{w,i} = \mathrm{span}\left\{ \begin{bmatrix} 1 \\ 0 \\ 0 \end{bmatrix} \right\},$$

which correctly reflects the property of type B agents to be able to move only on the horizontal plane and rotate around the vertical axis. Therefore, the intersection $\mathrm{Im}(\mathbf{S}) \cap \mathrm{null}(\mathbf{A}) =$

$\mathcal{T}$ results

$$\mathcal{T} = \operatorname{span}\left\{ \begin{bmatrix} \mathbf{1}_n \otimes \begin{bmatrix} 1 \\ 0 \\ 0 \end{bmatrix} \\ \mathbf{0}_{3n\times 1} \end{bmatrix}, \begin{bmatrix} \mathbf{1}_n \otimes \begin{bmatrix} 0 \\ 1 \\ 0 \end{bmatrix} \\ \mathbf{0}_{3n\times 1} \end{bmatrix}, \mathbf{s}, \begin{bmatrix} (\mathbf{I}_n \otimes [\mathbf{e}_3]_\times)\mathbf{p} \\ \mathbf{1}_n \otimes \begin{bmatrix} 0 \\ 0 \\ 1 \end{bmatrix} \end{bmatrix} \right\} \subseteq \mathbb{R}^{6n}, \quad (3.10)$$

where the first two components represent the translation of the COM of the formation along $\mathbf{e}_1, \mathbf{e}_2 \in \mathbb{R}^3$; while the last component is the coordinated rotation around $\mathbf{e}_3 \in \mathbb{R}^3$. When all the type B agents have the same altitude, namely

$$\langle \mathbf{e}_3, \mathbf{p}_i \rangle = z_b \quad \forall i \in \{ (n_a + 1) \dots n \}, \quad (3.11)$$

$\mathbf{s}$ represents the scaling of the formation together with the appropriate vertical translation of the COM that ensure the type B agents to satisfy their constraints.[1] Therefore,

$$\mathbf{s} = \begin{cases} \begin{bmatrix} \mathbf{p} - z_b(\mathbf{1}_n \otimes \mathbf{e}_3) \\ \mathbf{0}_{3n\times 1} \end{bmatrix} & \text{if equation (3.11) holds,} \\ \mathbf{0}_{6n\times 1} & \text{otherwise.} \end{cases} \quad (3.12)$$

The trivial variations set has dimension $\dim(\mathcal{S}_t) = \dim(\mathcal{T}) = k \in \{ 3, 4 \}$, and it accounts for two translations along the axes $\mathbf{e}_1, \mathbf{e}_2$ of $\mathcal{F}_W$, a coordinated rotation around the axis $\mathbf{e}_3$ of $\mathcal{F}_W$ and an optional scaling that maintains unchanged the altitude of the type B agents. Mathematically, it results,

$$\begin{aligned} \mathcal{S}_t &= \{ \boldsymbol{\delta} \in \bar{\mathcal{I}} \mid \mathbf{S}\boldsymbol{\delta} \in \mathcal{T} \} \\ &= \operatorname{span}\left\{ \begin{bmatrix} \mathbf{1}_{n_a} \otimes \begin{bmatrix} 1 \\ 0 \\ 0 \end{bmatrix} \\ \mathbf{1}_{n_b} \otimes \begin{bmatrix} 1 \\ 0 \end{bmatrix} \\ \mathbf{0}_{3n_a\times 1} \\ \mathbf{0}_{n_b\times 1} \end{bmatrix}, \begin{bmatrix} \mathbf{1}_{n_a} \otimes \begin{bmatrix} 0 \\ 1 \\ 0 \end{bmatrix} \\ \mathbf{1}_{n_b} \otimes \begin{bmatrix} 0 \\ 1 \end{bmatrix} \\ \mathbf{0}_{3n_a\times 1} \\ \mathbf{0}_{n_b\times 1} \end{bmatrix}, \check{\mathbf{s}} \right\} \cup \mathcal{R}_{\circlearrowleft} \end{aligned}$$

[1] $\langle \mathbf{x}, \mathbf{y} \rangle = \mathbf{x}^\top \mathbf{y} \in \mathbb{R}$ is the usual inner product.

where $\check{\mathbf{s}} \in \mathbb{R}^c$ is the generator for the (possible) scaling, while $\mathcal{R}_{\circlearrowleft} \subseteq \mathbb{R}^c$ is the coordinated rotation set. Their expression, differently from the ones in (3.10) and (3.12) is not immediate to write and require some additional definitions.

Be $\check{\mathbf{p}}_i = {\mathbf{S}_{o,i}}^\top \mathbf{p}_i \in \mathbb{R}^{c_{p,i}}$ and $\check{\mathbf{p}}_a = \begin{bmatrix}\check{\mathbf{p}}_1^\top \dots \check{\mathbf{p}}_{n_a}^\top\end{bmatrix}^\top \in \mathbb{R}^{3n_a}$, $\check{\mathbf{p}}_b = \begin{bmatrix}\check{\mathbf{p}}_{n_a+1}^\top \dots \check{\mathbf{p}}_n^\top\end{bmatrix}^\top \in \mathbb{R}^{2n_b}$, $\check{\mathbf{p}} = \begin{bmatrix}\check{\mathbf{p}}_a^\top & \check{\mathbf{p}}_b^\top\end{bmatrix}^\top$; then,

$$\check{\mathbf{s}} = \begin{cases} \begin{bmatrix} \check{\mathbf{p}}_a - z_b(\mathbf{1}_{n_a} \otimes \mathbf{e}_3) \\ \check{\mathbf{p}}_b \\ \mathbf{0}_{3n_a \times 1} \\ \mathbf{0}_{n_b \times 1} \end{bmatrix} & \text{if equation (3.11) holds,} \\ \mathbf{0}_{c \times 1} & \text{otherwise;} \end{cases}$$

and

$$\mathcal{R}_{\circlearrowleft} = \operatorname{span}\left\{ \begin{bmatrix} \begin{bmatrix} \mathbf{I}_{n_a} \otimes [\mathbf{e}_3]_\times & \mathbf{0}_{3n_a \times 2n_b} \\ \mathbf{0}_{2n_b \times 3n_a} & \mathbf{I}_{n_b} \otimes \begin{bmatrix} 0 & -1 \\ 1 & 0 \end{bmatrix} \end{bmatrix} \check{\mathbf{p}} \\ \mathbf{1}_{n_a} \otimes \mathbf{e}_3 \\ \mathbf{1}_{n_b} \end{bmatrix} \right\} \subseteq \mathbb{R}^c.$$

Example 3.2 (UGVs-6dofsUAVs IBR formation)**.** Consider a UGVs-6dofsUAVs mixed formation composed by 4 UGVs laying on the vertex of a square in the plane ${\mathbf{e}_3}^\top \mathbf{p}_i = 0$ and a 6dofsUAV in the middle of the square, vertically translated about the same length of the sides of the square, figure 3.1 on the following page. This formation is IBR with just 4 bidirectional measurements connecting the aerial vehicle to the ground ones and has four independent trivial variations. If the UGVs are substituted by 4dofs-UAVs the formation becomes IBF: the nullity of the bearing rigidity matrix increases to eight, namely there are three independent infinitesimal variation that are not trivial variations.

In this section it has been implicitly assumed that all the UGVs share the same rotation axis $\mathbf{n} \in \mathbb{S}^2$ which also defines (up to a translation) their plane of operation. Moreover it has been assumed that $\mathbf{n} = \mathbf{e}_3$. Even if the first assumption can not be discarded, it is possible to consider frameworks in which the axis of rotation is any (unit) vector $\mathbf{n}' \in \mathbb{S}^2$. The simplest way to extend the reasoning above to this new situation is to introduce the rotation matrix $\mathbf{R}_{n,n'} \in SO(3)$ such that

$$\mathbf{n}' = \mathbf{R}_{n',n}\mathbf{n}.$$

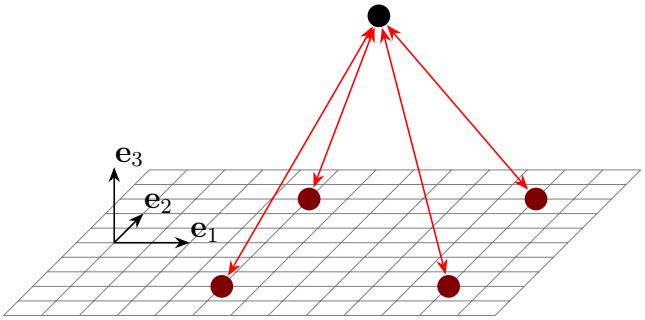

Figure 3.1: Example of IBR mixed formation composed by four UGVs, denoted by the maroon circles, laying on the plane $\mathbf{e}_3^\top \mathbf{p} = 0$ and a 6dofs-UAV, denoted by the black circle. Only 8 of 20 directed edges are sufficient to ensure the instantaneous bearing rigidity.

Then the rotated inertial frame $\mathcal{F}_{w'}$ can be defined as the rotation of $\mathcal{F}_W$ through $\mathbf{R}_{n',n}$. Representing the configuration $\mathbf{x} \in SE(3)^3$ w.r.t. $\mathcal{F}_{w'}$ leads to a new framework for which the rotation axis of the UGVs is exactly $\mathbf{n}$.

3.3.2 4DOF-UAVS AND 6DOF-UAVS CASE

This case is quite similar to the precedent with the only difference that the type B agent is now a 4dofs-UAV with $c_{p,b} = 3$, $c_{o,b} = 1$, $c_b = 4$ dofs. Embedding again all the instantaneous variations into $\mathbb{R}^{6n}$, it results

$$\mathrm{Im}(\mathbf{S}) = \mathrm{span}\left\{ \begin{bmatrix} \mathbf{I}_{n_a} \otimes \mathbf{I}_3 & \mathbf{0}_{3n_a \times 3n_b} & \mathbf{0}_{3n_a \times 3n_a} & \mathbf{0}_{3n_a \times n_b} \\ \mathbf{0}_{3n_b \times 3n_a} & \mathbf{I}_{n_b} \otimes \mathbf{I}_3 & \mathbf{0}_{3n_a \times 3n_a} & \mathbf{0}_{3n_a \times n_b} \\ \mathbf{0}_{3n_a \times 3n_a} & \mathbf{0}_{3n_a \times 3n_b} & \mathbf{I}_{n_a} \otimes \mathbf{I}_3 & \mathbf{0}_{3n_a \times n_b} \\ \mathbf{0}_{3n_b \times 3n_a} & \mathbf{0}_{3n_b \times 3n_b} & \mathbf{0}_{3n_b \times 3n_a} & \mathbf{I}_{n_b} \otimes \mathbf{n} \end{bmatrix} \right\} \subseteq \mathbb{R}^{6n},$$

where it is possible to observe that the only constraint is imposed on the rotation capabilities of type B agents:

$$\boldsymbol{\omega}_{w,i} = \mathrm{span}\{\, \mathbf{n} \,\} \quad \forall i \in \{\, (n_a + 1) \dots n \,\}.$$

Performing the same reasoning presented in section 3.3.1, the intersection $\mathrm{Im}(\mathbf{S}) \cap \mathrm{null}(\mathbf{A}) = \mathcal{T}$ results

$$\mathcal{T} = \mathrm{span}\left\{ \begin{bmatrix} \mathbf{1}_n \otimes \mathbf{I}_3 \\ \mathbf{0}_{3n \times 1} \end{bmatrix}, \begin{bmatrix} \mathbf{p} \\ \mathbf{0}_{3n \times 1} \end{bmatrix}, \begin{bmatrix} (\mathbf{I}_n \otimes [\mathbf{n}]_\times)\mathbf{p} \\ \mathbf{1}_n \otimes \mathbf{n} \end{bmatrix} \right\} \subseteq \mathbb{R}^{6n},$$

namely, three translations, a scaling and a coordinated rotation around the (unit) vector $\mathbf{n} \in$

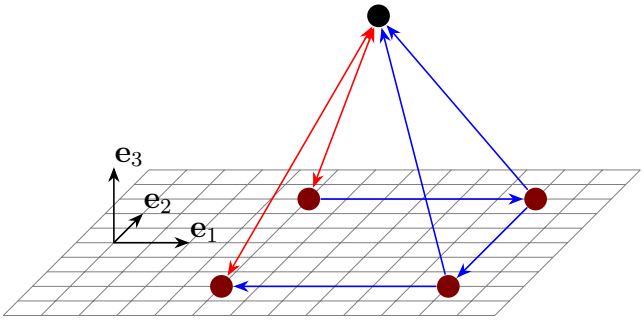

Figure 3.2: Example of IBR mixed formation composed by four 4dofs-UAVs, denoted by the maroon circles, capable of rotating around $\mathbf{e}_3$ and a 6dofs-UAV, denoted by the black circle. Only 9 of 20 directed edges are sufficient to ensure the instantaneous bearing rigidity.

$\mathbb{S}^2$. Finally, the trivial variation set has expression

$$\begin{aligned}\mathcal{S}_t &= \left\{ \boldsymbol{\delta} \in \bar{\mathcal{I}} \;\middle|\; \mathbf{S}\boldsymbol{\delta} \in \mathcal{T} \right\} \\ &= \operatorname{span}\left\{ \begin{bmatrix} \mathbf{1}_n \otimes \mathbf{I}_3 \\ \mathbf{0}_{3n_a \times 1} \\ \mathbf{0}_{n_b \times 1} \end{bmatrix}, \begin{bmatrix} \mathbf{p} \\ \mathbf{0}_{3n_a \times 1} \\ \mathbf{0}_{n_b \times 1} \end{bmatrix}, \begin{bmatrix} (\mathbf{I}_n \otimes [\mathbf{n}]_\times)\mathbf{p} \\ \mathbf{1}_{n_a} \otimes \mathbf{n} \\ \mathbf{1}_{n_b} \end{bmatrix} \right\}.\end{aligned}$$

Example 3.3 (4dofsUAVs-6dofsUAVs IBR formation)**.** Consider the formation presented in example 3.2 having 4dofsUAVs instead of UGVs, figure 3.2. This formation is IBR with only 9 directed edges and it has five independent trivial variations. If the 4dofsUAVs are substituted by 6dofs-UAVs the formation becomes IBF: the nullity of the bearing rigidity matrix increases to twelve, namely there are five independent infinitesimal variation that are not trivial variations.

4

Control of Mixed Formations

In the previous chapters it has been shown as, given a formation modeled as framework $(\mathcal{G}, \mathbf{x})$, it is possible to determine if it is infinitesimally bearing rigid inspecting the null space of the bearing rigidity matrix. Moreover, it has been proven how the same procedure can be applied for mixed frameworks. This chapter moves forward the analysis of bearing rigidity theory addressing the problem of *bearing-based* mixed formation control.

In control theory controlling a dynamical system can be performed in two ways, in open loop and in close loop; close loop controllers use measurements as *feedback* in order to improve their performances. In bearing-based formation control such feedback is provided by the bearing measurements.

Real-world mixed formations are accurately modeled as formations composed by rigid bodies with (eventually) limited actuation capability; therefore, their rigidity properties can be inferred from the ones of their equivalent fully-actuated twins. It will be shown that this reasoning can be perfectly applied to the problem of formation control. To do so, the major results about the control of fully-actuated formations, which have been provided by [28], are reported, and then extended.

Control people are happier working with linear systems. Therefore, using the pair $(\mathbf{p}_i, \mathbf{R}_i) \in SE(3)$ to represent the configuration of a rigid body in the 3D world, as it has been done until now, makes them sad. The reason lays on the kinematic equation governing the time derivative of $\mathbf{R}_i \in SO(3)$, $\dot{\mathbf{R}}_i = [\boldsymbol{\omega}_{w,i}]_\times \mathbf{R}_i$ which is highly non-linear w.r.t. the input vector $\boldsymbol{\omega}_{w,i} \in \mathbb{R}^3$. This motivates the choice to migrate toward a quaternion-based representation of the orientation of the agents.

The body frame $\mathcal{F}_i$ is again associated to agent i; its origin O_i coincides with the COM. $\mathbf{p}_i \in \mathbb{R}^3$ denotes the position of O_i w.r.t. the inertial frame $\mathcal{F}_W$. However, now the orientation of $\mathcal{F}_i$ w.r.t. $\mathcal{F}_W$ is indicated using the unit quaternion $\mathbf{q}_i = \begin{bmatrix} \eta_i & \boldsymbol{\varepsilon}_i^\top \end{bmatrix}^\top \in \mathbb{S}^3$, where $\eta_i = \cos(\alpha_i/2)$, $\boldsymbol{\varepsilon}_i = \mathbf{n}_i \sin(\alpha_i/2)$, with the pair $(\mathbf{n}_i, \alpha_i) \in \mathbb{S}^2 \times [0, \pi)$ the (axis-angle) representation of the orientation. Namely, $\mathcal{F}_i$ is obtained rotating $\mathcal{F}_W$ around $\mathbf{n}_i$ by the angle α_i. The configuration of each agent is represented by the vector $\mathbf{x}_i = \begin{bmatrix} \mathbf{p}_i^\top & \mathbf{q}_i^\top \end{bmatrix}^\top \in \mathbb{R}^3 \times \mathbb{S}^3$ and, given a framework embedded in $\mathbb{R}^{3n} \times \mathbb{S}^{3n}$, $\mathbf{p} = \begin{bmatrix} \mathbf{p}_1^\top \dots \mathbf{p}_n^\top \end{bmatrix}^\top \in \mathbb{R}^{3n}$, $\mathbf{q} = \begin{bmatrix} \mathbf{q}_1^\top \dots \mathbf{q}_n^\top \end{bmatrix}^\top \in \mathbb{S}^{3n}$, $\mathbf{x} = \begin{bmatrix} \mathbf{p}^\top & \mathbf{q}^\top \end{bmatrix}^\top \in \mathbb{R}^{3n} \times \mathbb{S}^{3n}$ are introduced to represent the position, orientation and configuration of the whole formation.

In this way, the kinematic of a single agent is controlled by the equations

$$\dot{\mathbf{p}}_i = \mathbf{R}(\mathbf{q}_i)\mathbf{v}_i, \tag{4.1a}$$

$$\dot{\mathbf{q}}_i = \frac{1}{2}\mathbf{q}_i \circ \boldsymbol{\omega}_i^+, \tag{4.1b}$$

which require many explanations.

- The matrix $\mathbf{R}(\mathbf{q}_i) \in SO(3)$ is the rotation matrix associated to the quaternion $\mathbf{q}_i \in \mathbb{S}^3$ and it can be obtained through Rodrigues' formula

$$\mathbf{R}(\mathbf{q}_i) = \mathbf{I}_3 + 2\eta_i[\boldsymbol{\varepsilon}_i]_\times + 2\boldsymbol{\varepsilon}_i\boldsymbol{\varepsilon}_i^\top - 2\boldsymbol{\varepsilon}_i^\top\boldsymbol{\varepsilon}_i\mathbf{I}_3.$$

- The operator $\circ$ denotes the quaternions composition rule

$$\begin{aligned} \mathbf{q}_1 \circ \mathbf{q}_2 &= \begin{bmatrix} \eta_1 \\ \boldsymbol{\varepsilon}_1 \end{bmatrix} \circ \begin{bmatrix} \eta_2 \\ \boldsymbol{\varepsilon}_2 \end{bmatrix}, \\ &= \begin{bmatrix} \eta_1\eta_2 - \boldsymbol{\varepsilon}_1^\top\boldsymbol{\varepsilon}_2 \\ \eta_1\boldsymbol{\varepsilon}_2 + \eta_2\boldsymbol{\varepsilon}_1 + \boldsymbol{\varepsilon}_1 \times \boldsymbol{\varepsilon}_2 \end{bmatrix}, \end{aligned} \tag{4.2}$$

$$\begin{aligned}\mathbf{q}_1 \circ \mathbf{q}_2 &= \begin{bmatrix} \eta_1 & -\boldsymbol{\varepsilon}_1^\top \\ \boldsymbol{\varepsilon}_1 & \eta_1 \mathbf{I}_3 + [\boldsymbol{\varepsilon}_1]_\times \end{bmatrix} \begin{bmatrix} \eta_2 \\ \boldsymbol{\varepsilon}_2 \end{bmatrix} = \mathbf{M}(\mathbf{q}_1)\mathbf{q}_2, \\ &= \begin{bmatrix} \eta_2 & -\boldsymbol{\varepsilon}_2^\top \\ \boldsymbol{\varepsilon}_2 & \eta_2 \mathbf{I}_3 - [\boldsymbol{\varepsilon}_2]_\times \end{bmatrix} \begin{bmatrix} \eta_1 \\ \boldsymbol{\varepsilon}_1 \end{bmatrix} = \mathbf{N}(\mathbf{q}_2)\mathbf{q}_1.\end{aligned}$$

- $\boldsymbol{\omega}_i^+ = \begin{bmatrix} 0 & \boldsymbol{\omega}_i^\top \end{bmatrix}^\top \in \mathbb{R}^4$ is the *pure* quaternion associated to $\boldsymbol{\omega}_i \in \mathbb{R}^3$. Moreover, the linear velocity $\mathbf{v}_i \in \mathbb{R}^3$ and the angular velocity $\boldsymbol{\omega}_i \in \mathbb{R}^3$ of the agent are both expressed in the *local* frame $\mathcal{F}_i$. This choice is motivated by the fact that the actuators responsible of the generation of $\mathbf{v}_i$ and $\boldsymbol{\omega}_i$ are rigidly attached to the body of the agent and therefore the two vectors are naturally expressed in $\mathcal{F}_i$.
- Finally, the partial proof of the relation $\dot{\mathbf{q}}_i = 1/2\, \mathbf{q}_i \circ \boldsymbol{\omega}_i^+$ is available in section A.1.2.

Observation 4.1. In equation (4.1b) the pure quaternion $\boldsymbol{\omega}_i^+ \in \mathbb{R}^4$ is used. Nevertheless, exploiting the fact the its first component is always zero and equation (4.2), the formula can be simplified into

$$\dot{\mathbf{q}}_i = \frac{1}{2} \begin{bmatrix} -\boldsymbol{\varepsilon}_i^\top \\ \eta_i \mathbf{I}_3 + [\boldsymbol{\varepsilon}_i]_\times \end{bmatrix} \boldsymbol{\omega}_i = \bar{\mathbf{M}}(\mathbf{q}_i)\boldsymbol{\omega}_i. \tag{4.3}$$

Remark 4.2. The rotation of a vector $\mathbf{x} \in \mathbb{R}^3$ can be equally performed using rotation matrices or quaternions. Be $\mathbf{R} \in SO(3)$ and $\mathbf{q} = \begin{bmatrix} \eta & \boldsymbol{\varepsilon}^\top \end{bmatrix}^\top \in \mathbb{S}^3$ the representation of the same rotation. Then the rotated vector $\mathbf{y} \in \mathbb{R}^3$ has expressions

$$\mathbf{y} = \mathbf{R}\mathbf{x} \quad \text{and}$$
$$\mathbf{y}^+ = \begin{bmatrix} 0 \\ \mathbf{y} \end{bmatrix} = \mathbf{q} \circ \begin{bmatrix} 0 \\ \mathbf{x} \end{bmatrix} \circ \mathbf{q}^{-1} = \mathbf{M}(\mathbf{q})\mathbf{N}(\mathbf{q}^{-1}) \begin{bmatrix} 0 \\ \mathbf{x} \end{bmatrix},$$

where $\mathbf{q}^{-1} = \begin{bmatrix} \eta & -\boldsymbol{\varepsilon}^\top \end{bmatrix}^\top \in \mathbb{S}^3$ is the quaternion conjugate.

Exploiting remark 4.2 it is possible to characterize the time derivative a quaternion when the angular velocity is expressed in the inertial frame $\mathcal{F}_W$.

Observation 4.3. Given the angular velocity $\boldsymbol{\omega}_i \in \mathbb{R}^3$ expressed in the body frame, its representation on the inertial frame is given by the relation

$$\boldsymbol{\omega}_{w,i}^+ = \begin{bmatrix} 0 \\ \boldsymbol{\omega}_{w,i} \end{bmatrix} = \mathbf{q}_i \circ \begin{bmatrix} 0 \\ \boldsymbol{\omega}_i \end{bmatrix} \circ \mathbf{q}_i^{-1}.$$

Therefore, equation (4.1b) can be rewritten as

$$\dot{\mathbf{q}}_i = \frac{1}{2}\mathbf{q}_i \circ \boldsymbol{\omega}_i^+ = \frac{1}{2}\mathbf{q}_i \circ \mathbf{q}_i^{-1} \circ \boldsymbol{\omega}_{w,i}^+ \circ \mathbf{q}_i = \frac{1}{2}\boldsymbol{\omega}_{w,i}^+ \circ \mathbf{q}_i.$$

It is still possible to obtain a reduced expression as in observation 4.1, in fact

$$\dot{\mathbf{q}}_i = \frac{1}{2}\begin{bmatrix} -\boldsymbol{\varepsilon}_i^\top \\ \eta_i \mathbf{I}_3 - [\boldsymbol{\varepsilon}_i]_\times \end{bmatrix} \boldsymbol{\omega}_{w,i} = \bar{\mathbf{N}}(\mathbf{q}_i)\boldsymbol{\omega}_{w,i}.$$

Stacking all the linear velocities of the agents of the formation into $\mathbf{v} = \begin{bmatrix}\mathbf{v}_1^\top \dots \mathbf{v}_n^\top\end{bmatrix}^\top \in \mathbb{R}^{3n}$ and all the angular velocities into $\boldsymbol{\omega} = \begin{bmatrix}\boldsymbol{\omega}_1^\top \dots \boldsymbol{\omega}_n^\top\end{bmatrix}^\top \in \mathbb{R}^{3n}$, the formation input vector can be defined as $\mathbf{u} = \begin{bmatrix}\mathbf{v}^\top & \boldsymbol{\omega}^\top\end{bmatrix}^\top \in \mathbb{R}^{6n}$. Therefore, the formation kinematic results

$$\dot{\mathbf{x}} = \begin{bmatrix} \mathbf{D}_1(\mathbf{q}) & \mathbf{0}_{3n\times 3n} \\ \mathbf{0}_{4n\times 3n} & \mathbf{D}_2(\mathbf{q}) \end{bmatrix} \mathbf{u} = \mathbf{D}(\mathbf{q})\mathbf{u}, \tag{4.4}$$

where $\mathbf{D}_1(\mathbf{q}) = \operatorname{diag}(\mathbf{R}(\mathbf{q}_i)) \in \mathbb{R}^{3n\times 3n}$ and $\mathbf{D}_2(\mathbf{q}) = \operatorname{diag}(\frac{1}{2}\bar{\mathbf{M}}(\mathbf{q}_i)) \in \mathbb{R}^{4n\times 3n}$. A fully-actuated formation is being considered, therefore it make sense to associate the instantaneous variations $\boldsymbol{\delta} \in \bar{\mathcal{I}}$ to the whole input vector, namely, $\mathbf{u} = \boldsymbol{\delta}$, and $\bar{\mathcal{I}} = \mathbb{R}^{6n}$.

The bearing measurement associated to the edge $e_k = (v_i, v_j) \in \mathcal{E}$ results, using the quaternions,

$$\mathbf{b}_{ij}^+ = \mathbf{q}_i^{-1} \circ \bar{\mathbf{p}}_{ij}^+ \circ \mathbf{q}_i \in \mathbb{S}^3,$$

where $\bar{\mathbf{p}}_{ij}^+ = \begin{bmatrix}0 & \bar{\mathbf{p}}_{ij}^\top\end{bmatrix}^\top \in \mathbb{S}^3$. Anyway, notice that

$$\mathbf{b}_{ij}^+ = \begin{bmatrix} 0 \\ \mathbf{b}_{ij} \end{bmatrix} = \begin{bmatrix} 0 \\ \mathbf{R}(\mathbf{q}_i)^\top \bar{\mathbf{p}}_{ij} \end{bmatrix}.$$

The two equations carries the same information.

Now that the kinematic and bearing measurements of a framework $(\mathcal{G}, \mathbf{x})$ embedded in $\mathbb{R}^{3n} \times \mathbb{S}^{3n}$ have been characterized, the dynamic bearing rigidity properties can be studied. Recall that the multiagent systems that are being considered are exactly the same of the ones used in section 2.3.3, therefore it is expected that this analysis will provide the same results regarding the characterization of the infinitesimal bearing rigidity. For example, the dimension of the trivial variation set should remain the same. Its generators, instead, are expected to be different because the agent commands are now expressed in the local frames:

$\mathbf{v}_i = \boldsymbol{\delta}_{p,i}$ and $\boldsymbol{\omega}_i = \boldsymbol{\delta}_{o,i}$. The time derivative of the bearing measurement $\mathbf{b}_{ij} \in \mathbb{S}^2$ can be computed from equation (2.16) on page 21, exploiting equation (4.1a) and the relation $\boldsymbol{\omega}_{w,i} = \mathbf{R}(\mathbf{q}_i)\boldsymbol{\omega}_i$ which leads to

$$\dot{\mathbf{b}}_{ij} = d_{ij}\mathbf{P}(\mathbf{b}_{ij})\big(\mathbf{R}(\mathbf{q}_i)^\top\mathbf{R}(\mathbf{q}_j)\mathbf{v}_j - \mathbf{v}_i\big) + [\mathbf{b}_{ij}]_\times\boldsymbol{\omega}_i, \tag{4.5}$$

where the first addend comes from

$$\begin{aligned} d_{ij}\mathbf{R}(\mathbf{q}_i)^\top\mathbf{P}(\bar{\mathbf{p}}_{ij})\big(\dot{\mathbf{p}}_{w,j} - \dot{\mathbf{p}}_{w,i}\big) &= d_{ij}\mathbf{R}(\mathbf{q}_i)^\top\mathbf{P}(\bar{\mathbf{p}}_{ij})\mathbf{R}(\mathbf{q}_i)\mathbf{R}(\mathbf{q}_i)^\top\big(\dot{\mathbf{p}}_{w,j} - \dot{\mathbf{p}}_{w,i}\big) \\ &= d_{ij}\mathbf{P}(\mathbf{b}_{ij})\mathbf{R}(\mathbf{q}_i)^\top\big(\dot{\mathbf{p}}_{w,j} - \dot{\mathbf{p}}_{w,i}\big) \\ &= d_{ij}\mathbf{P}(\mathbf{b}_{ij})\mathbf{R}(\mathbf{q}_i)^\top\big(\mathbf{R}(\mathbf{q}_j)\dot{\mathbf{p}}_j - \mathbf{R}(\mathbf{q}_i)\dot{\mathbf{p}}_i\big) \\ &= d_{ij}\mathbf{P}(\mathbf{b}_{ij})\big(\mathbf{R}(\mathbf{q}_i)^\top\mathbf{R}(\mathbf{q}_j)\mathbf{v}_j - \mathbf{v}_i\big), \end{aligned}$$

and the second comes from section A.1.1 on page 87. From equation (4.5), the expression of the k-th row block, associated to the edge $(v_i, v_j) \in \mathcal{E}$, of the $(3m \times 6n)$ bearing rigidity matrix $\mathbf{B}_\mathcal{G}(\mathbf{x})$ can be derived and it results

$$\begin{cases} \begin{bmatrix} \mathbf{0}_{3\times3(i-1)} & -d_{ij}\mathbf{P}(\mathbf{b}_{ij}) & \mathbf{0}_{3\times3(j-i-1)} & d_{ij}\mathbf{P}(\mathbf{b}_{ij})\mathbf{R}(\mathbf{q}_i)^\top\mathbf{R}(\mathbf{q}_j) \\ \mathbf{0}_{3\times(3(n-j)+3(i-1))} & [\mathbf{b}_{ij}]_\times & \mathbf{0}_{3\times3(n-i)} & \end{bmatrix} & \text{if } i < j, \\ \begin{bmatrix} \mathbf{0}_{3\times3(j-1)} & d_{ij}\mathbf{P}(\mathbf{b}_{ij})\mathbf{R}(\mathbf{q}_i)^\top\mathbf{R}(\mathbf{q}_j) & \mathbf{0}_{3\times3(i-j-1)} & -d_{ij}\mathbf{P}(\mathbf{b}_{ij}) \\ \mathbf{0}_{3\times(3(n-i)+3(i-1))} & [\mathbf{b}_{ij}]_\times & \mathbf{0}_{3\times3(n-i)} & \end{bmatrix} & \text{if } i < j. \end{cases} \tag{4.6}$$

The following theorem characterizes the infinitesimal rigidity properties for frameworks embedded in $\mathbb{R}^{3n} \times \mathbb{S}^{3n}$.

Theorem 4.1 (Theorem III.3 in [28]). *Given a formation modeled as a framework $(\mathcal{G}, \mathbf{x})$ in $\mathbb{R}^{3n} \times \mathbb{S}^{3n}$ subject to (4.4); it is IBR if and only if*

$$\begin{aligned} &\ker(\mathbf{B}_\mathcal{G}(\mathbf{x})) = \ker(\mathbf{B}_\mathcal{K}(\mathbf{x})), \textit{ or equivalently} \\ &\operatorname{null}(\mathbf{B}_\mathcal{G}(\mathbf{x})) = 7. \end{aligned}$$

Proof. The first conclusion correspond to definition 2.12. The second follows from the fact that the framework models the same multiagent system described in section 2.3.3 and there-

fore it has a trivial variation set with the same dimension. □

Proposition 4.2. *Given a formation modeled as a framework* $(\mathcal{G}, \mathbf{x})$ *in* $\mathbb{R}^{3n} \times \mathbb{S}^{3n}$ *subjected to* (4.4)*; it has trivial variation set* $\mathcal{S}_t$ *corresponding to*

$$\mathcal{S}_t = \operatorname{span}\{\, \mathbf{u}_1^*, \mathbf{u}_2^*, \mathbf{u}_3^* \,\}$$

with

$$\mathbf{u}_1^* = \begin{bmatrix} \mathbf{D}_1(\mathbf{q})^\top (\mathbf{1}_n \otimes \mathbf{I}_3) \\ \mathbf{0}_{3n\times 3} \end{bmatrix} \in \mathbb{R}^{6n\times 3}$$
$$\mathbf{u}_2^* = \begin{bmatrix} \mathbf{D}_1(\mathbf{q})^\top \tilde{\mathbf{p}} \\ \mathbf{0}_{3n\times 3} \end{bmatrix} \in \mathbb{R}^{6n\times 1}$$
$$\mathbf{u}_3^* = \begin{bmatrix} \mathbf{D}_1(\mathbf{q})^\top \begin{bmatrix} \mathbf{E}_1\tilde{\mathbf{p}} & \mathbf{E}_2\tilde{\mathbf{p}} & \mathbf{E}_3\tilde{\mathbf{p}} \end{bmatrix} \\ \operatorname{diag}(\{\, \mathbf{R}(\mathbf{q}_i) \,\})\,(\mathbf{1}_n \otimes \mathbf{I}_3) \end{bmatrix} \in \mathbb{R}^{6n\times 3}$$

where $\mathbf{E}_i \in \mathbb{R}^{3n\times 3n}$ *is defined as* $\mathbf{E}_i = \mathbf{I}_n \otimes [\mathbf{e}_i]_\times$, $\mathbf{e}_i \in \mathbb{R}^3$ *with* $i \in \{\, 1, 2, 3 \,\}$. $\bar{p} = 1/n(\mathbf{1}_n \otimes \mathbf{I}_3)^\top \mathbf{p} \in \mathbb{R}^3$ *is the barycentre of the formation and* $\tilde{\mathbf{p}} \in \mathbb{R}^{3n}$ *is such that* $\tilde{\mathbf{p}} = \mathbf{p} - (\mathbf{1}_3 \otimes \mathbf{I}_n)\bar{\mathbf{p}}$.

Proof. The trivial variation set $\mathcal{S}_t$ of the proposition and the one defined in equation (2.19) on page 22 represent the same deformations. They only differ in which frames are used to encode them; the latter exploits the inertial frame $\mathcal{F}_W$ while in the former each infinitesimal variation is expressed in the local frames $\mathcal{F}_i$. Moreover, $\mathbf{u}_2^*, \mathbf{u}_3^*$ represent *pure* scaling and coordinated rotations, respectively. □

The migration toward the quaternion based representation of the orientation of the agents for a fully-actuated formation is complete and it is possible to introduce the bearing-based control problem.

4.2 Bearing-based formation control for fully-actuated multiagent systems

Controlling a formation can be thought as two dual tasks. The first one is the *distributed formation stabilization* which consists in the generation and maintenance of a given geometric pattern while the second is the *distributed agent motion coordination* which aims is to move

the formation without deforming it. A solution for both tasks have been proposed in [28] and is here reported along with some reasoning about the stability of the controllers.

4.2.1 Distributed formation stabilization

The problem of distributed formation stabilization consists on driving the formation configuration $\mathbf{x} \in \mathbb{R}^{3n} \times \mathbb{S}^{3n}$ toward a *desired* configuration $\mathbf{x}_d \in \mathbb{R}^{3n} \times \mathbb{S}^{3n}$. However, being a bearing-based control, the controller is only able to resort to the bearing measurement, therefore it is more accurate to define this task as the problem of driving the formation configuration toward a new one having bearing measurement equal to $\mathbf{b}^*_{\mathcal{G}} := \mathbf{b}_{\mathcal{G}}(\mathbf{x}_d) \in \mathbb{S}^{2n}$, the *desired bearing vector*. Under the assumption that the considered framework $(\mathcal{G}, \mathbf{x})$ is IBR, this is equivalent to driving the formation toward a final configuration $\mathbf{x}_f \in \mathbb{R}^{3n} \times \mathbb{S}^{3n}$ that is BC to the desired one. The task can also be stated as a minimization problem.

Problem 4.1 (Distributed Formation Stabilization)**.** Given a framework $(\mathcal{G}, \mathbf{x})$ and the desired bearing vector $\mathbf{b}^*_{\mathcal{G}} \in \mathbb{S}^{2n}$, associated to the desired configuration $\mathbf{x}_d \in \mathbb{R}^{3n} \times \mathbb{S}^{3n}$, the distributed formation stabilization problem consists on the *minimization* of the cost function

$$J(\mathbf{x}) := \frac{1}{2}\|\mathbf{b}_{\mathcal{G}}(\mathbf{x}) - \mathbf{b}^*_{\mathcal{G}}\|^2$$

in a distributed fashion.

The authors in [22] solved this problem for frameworks embedded in $(\mathbb{R}^2 \times \mathbb{S}^1)^n$ using a gradient descent procedure, namely they chose the input vector $\mathbf{u}$ of the formations such that the time derivative of the configuration was equal to minus the gradient of the cost function,

$$\dot{\mathbf{x}} = -\nabla_{\mathbf{x}} J(\mathbf{x}) \tag{4.7}$$

and they proved the validity of this approach through numerical simulations.[1] However, the same solution can not be exploited for framework embedded in $\mathbb{R}^{3n} \times \mathbb{S}^{3n}$. The reason lays on the different metric spaces that are used to represent the orientation of the agents. In $(\mathbb{R}^2 \times \mathbb{S}^1)^n$ each agent orientation is associated to a single angle and there is a one to one correspondence between all the possible time derivative of such angle and the agent command responsible to the changes of the orientation ($\boldsymbol{\delta}_{o,i}$). This is no more true if the agent are fully-actuated rigid bodies with orientation characterized by quaternions (or rotation matrices, it

[1] The authors used a *scale-free* version of equation (4.7), which is discussed later.

is the same). Indeed, given a unit quaternion $\mathbf{q} \in \mathbb{S}^3$ its tangent space is given by

$$\left\{ \bar{\mathbf{M}}(\mathbf{q})\boldsymbol{\omega} \;\middle|\; \boldsymbol{\omega} \in \mathbb{R}^3 \right\} \subsetneq \mathbb{R}^4,$$

which has not dimension four. Then, given $\mathbf{x} \in \mathbb{R}^{3n} \times \mathbb{S}^{3n}$, there is no proof that it exists $\mathbf{u} \in \mathbb{R}^{6n}$ such that $\dot{\mathbf{x}} = \mathbf{D}(\mathbf{q})\mathbf{u}$ satisfies equation (4.7). Putting it in different words, equation (4.7) solves problem 4.1 in a *unconstrained* way, treating the configuration $\mathbf{x}$ as an element of $\mathbb{R}^{7n}$.

An other solution is to employ the control law

$$\mathbf{u} = k_c \left(\mathbf{B}_{\mathcal{G}}(\mathbf{x})\right)^{\top} \mathbf{b}^*_{\mathcal{G}}, \tag{4.8}$$

where $k_c > 0$ is a tunable gain controlling the convergence rate, which actually drives the *bearing error*

$$\mathbf{e}(\mathbf{x}, \mathbf{x}_d) \coloneqq \mathbf{b}_{\mathcal{G}}(\mathbf{x}) - \mathbf{b}_{\mathcal{G}}(\mathbf{x}_d) \tag{4.9}$$

to zero, as proven in the following proposition.

Proposition 4.3. *Given a framework $(\mathcal{G}, \mathbf{x})$ embedded in $\mathbb{R}^{3n} \times \mathbb{S}^{3n}$ and subjected to equation (4.4), and a desired configuration $\mathbf{x}_d \in \mathbb{R}^3 \times \mathbb{S}^3$, the dynamical system modelling the dynamics of the bearing error (4.9) when the control law (4.8) is employed presents an equilibrium point in $\mathbf{0}_{3m}$ which is asymptotically stable.*

Proof. This first part of the proof will shows that the equilibrium is simply stable using the direct Lyapunov method. The bearing error dynamics results

$$\begin{aligned}
\dot{\mathbf{e}}(\mathbf{x}, \mathbf{x}_d) &= \dot{\mathbf{b}}_{\mathcal{G}}(\mathbf{x}) - \dot{\mathbf{b}}_{\mathcal{G}}(\mathbf{x}_d) \\
&= \mathbf{B}_{\mathcal{G}}(\mathbf{x})\mathbf{u} \\
&= k_c \mathbf{B}_{\mathcal{G}}(\mathbf{x}) \big(\mathbf{B}_{\mathcal{G}}(\mathbf{x})\big)^{\top} \mathbf{b}_{\mathcal{G}}(\mathbf{x}_d) \\
&= -k_c \mathbf{B}_{\mathcal{G}}(\mathbf{x}) \big(\mathbf{B}_{\mathcal{G}}(\mathbf{x})\big)^{\top} \mathbf{e}(\mathbf{x}, \mathbf{x}_d),
\end{aligned}$$

where the last equality derives from $\big(\mathbf{B}_{\mathcal{G}}(\mathbf{x})\big)^{\top} \mathbf{b}_{\mathcal{G}}(\mathbf{x}) = \mathbf{0}$. The proposed Lyapunov function is

$$\mathrm{V}(\mathbf{e}) = \frac{1}{2k_c} \mathbf{e}(\mathbf{x}, \mathbf{x}_d)^{\top} \mathbf{e}(\mathbf{x}, \mathbf{x}_d)$$

which is positive definite and it has time derivative

$$\dot{\mathrm{V}}(\mathbf{e}) = -\mathbf{e}(\mathbf{x}, \mathbf{x}_d)^\top \underbrace{\mathbf{B}_{\mathcal{G}}(\mathbf{x})\big(\mathbf{B}_{\mathcal{G}}(\mathbf{x})\big)^\top}_{=:\mathbf{Q}(\mathbf{x})} \mathbf{e}(\mathbf{x}, \mathbf{x}_d). \tag{4.10}$$

$\mathbf{Q}(\mathbf{x}) \in \mathbb{R}^{3m\times 3m}$ in equation (4.10) is positive semi-definite for every value of $\mathbf{x} \in \mathbb{R}^3 \times \mathbb{S}^3$, therefore $\dot{\mathrm{V}}(\mathbf{e})$ is negative semi-definite and the equilibrium point $\mathbf{e}(\mathbf{x}, \mathbf{x}_d) = \mathbf{0}_{3m}$ is simply stable. □

See full proof on page 96.

However, the control law equation (4.8) carries an heavy drawback: it requires the knowledge about the inter-agents *distances* d_{ij} which goes against every reasoning about the bearing-based structure. A working solution has been proposed in [28] where the authors used the *scale-free* version of equation (4.8), namely

$$\mathbf{u} = k_c \left(\bar{\mathbf{B}}_{\mathcal{G}}(\mathbf{x})\right)^\top \mathbf{b}^*_{\mathcal{G}}, \tag{4.11}$$

where $\bar{\mathbf{B}}_{\mathcal{G}}(\mathbf{x})$ is the scale-free version of the bearing rigidity matrix in which in every row block of equation (4.6) on page 41 the inter-agents distance d_{ij} has been removed. This approach turns out to be bearing-based, but not *only* bearing based, and decentralized; in fact, the commands of each agent in the formations are,

$$\begin{cases} \mathbf{v}_i = -k_c \displaystyle\sum_{j\,:\, v_j\in\mathcal{N}_i} \mathbf{P}(\mathbf{b}_{ij})^\top \mathbf{b}^*_{ij} + k_c \sum_{\substack{j \text{ s.t.} \\ v_i\in\mathcal{N}_j}} \mathbf{R}(\mathbf{q}_{ij})\mathbf{P}(\mathbf{b}_{ji})^\top \mathbf{b}^*_{ji} \\ \boldsymbol{\omega}_i = k_c \displaystyle\sum_{j\,:\, v_j\in\mathcal{N}_i} [\mathbf{b}_{ij}]_\times^\top \mathbf{b}^*_{ij} \end{cases}, \tag{4.12}$$

where $\mathcal{N}_i = \{\, v_j \in \mathcal{V} \mid (v_i, v_j) \in \mathcal{E} \,\} \subset \mathcal{V}$ identifies the agents that are sensed by the i-th agent. $\mathbf{q}_{ij} = \mathbf{q}_i^{-1} \circ \mathbf{q}_j \in \mathbb{S}^3$ is the relative orientation between i-th and j-th agents, while $\mathbf{b}^*_{ij} \in \mathbb{S}^2$ and $\mathbf{b}^*_{ji} \in \mathbb{S}^2$ denote the desired bearing measurement from agent i to j and vice-versa. Analysing (4.12), the i-th agent requires knowledge about

- its own bearing measurements $\mathbf{b}_{ij} \in \mathbb{S}^2$ and the desired values $\mathbf{b}^*_{ij} \in \mathbb{S}^2$ that they should match, $j : v_j \in \mathcal{N}_i$. Trivially these values are available onboard.
- its orientation $\mathbf{q}_i \in \mathbb{S}^3$, which is not directly measured but can be recovered through location estimation algorithms, as it will be explained in chapter 5.

- the orientation $\mathbf{q}_j \in \mathbb{S}^3$, the bearing measurement $\mathbf{b}_{ji} \in \mathbb{S}^2$ and the desired bearing measurement $\mathbf{b}^*_{ji} \in \mathbb{S}^2$, j s.t. $v_i \in \mathcal{N}_j$ of all the agents that sense it. This implies *communication* between the agents.

The need to know the orientations and the need to communication are the reason this control law is not a «bearing only» solution. However, it does not require data from outside the formation and the communication is necessary only between neighbour agents, namely, agents interconnected by and edge; therefore it perfectly met the requirements stated in chapter 1.

4.2.2 Distributed agent motion coordination

Distributed agent motion coordination consists on driving the formation, again, in a distributed fashion, to new configurations such that the shape is preserved and no deformations occurs. Indeed, this is a dual task w.r.t. the one discussed in the previous section because here it is looked for control inputs $\mathbf{u} \in \mathbb{R}^{6n}$ such that the bearing vector remains unchanged. It should be clear by now that the solution lays on the elements of the trivial variation set which, by definition, satisfies the requirements. Recalling proposition 4.2 on page 42, the formation shape is preserved by any input belonging to the set

$$\left\{ \mathbf{u} \in \mathbb{R}^{6n} \;\middle|\; \mathbf{u} = \mathbf{u}^*_1 \mathbf{s} + \mathbf{u}^*_2 c + \mathbf{u}^*_3 \mathbf{r}, \quad \mathbf{s}, \mathbf{r} \in \mathbb{R}^3, \quad c \in \mathbb{R} \right\},$$

where $\mathbf{s} \in \mathbb{R}^3$ represents a common linear velocity, $c \in \mathbb{R}$ an expansion rate and $\mathbf{r} \in \mathbb{R}^3$ a common angular velocity, all expressed in the inertial frame.

Assigned a suitable triplet $(\mathbf{s}^*, c^*, \mathbf{c}^*) \in \mathbb{R}^3 \times \mathbb{R} \times \mathbb{R}^3$, each i-th agent can thus implement the following commands to fulfil the distributed coordination task

$$\begin{cases} \mathbf{v}_i = \mathbf{R}(\mathbf{q}_i)^\top \left(\mathbf{s}^* + c^* (\mathbf{p}_i - \bar{\mathbf{p}}) + [\mathbf{r}^*]_\times (\mathbf{p}_i - \bar{\mathbf{p}}) \right) \\ \boldsymbol{\omega}_i = \mathbf{R}(\mathbf{q}_i)^\top \mathbf{r}^* \end{cases}. \tag{4.13}$$

Equation (4.13) requires each i-th agent to know not only its orientation, but also it position, but again this problem will be addressed in chapter 5; moreover, it is still necessary to have communication between agents, in order to compute the barycentre $\bar{\mathbf{p}} \in \mathbb{R}^3$.

The advantage of having characterized the mixed formation in the 3D space as mixed frameworks $(\mathcal{G}, \mathbf{x}, \mathcal{H})$ embedded in $SE(3)^n$ is now made clear. In fact, it will be shown that even for mixed formations, the control law expressed by equation (4.11) on page 45 is able to drive the the formation toward the desired shape and that the elements of the trivial variation set are the right candidates to perform distributed agents motion coordination.

The migration from the rotation matrices to the quaternions to represents the orientations is straightforward and therefore mixed frameworks embedded in $\mathbb{R}^{3n} \times \mathbb{S}^{3n}$ are considered. More delicate is the question about the agent commands, characterized by the set $\mathcal{H}$, which are expressed in the inertial frame in chapter 3 while now they are required to be expressed in the local frames. Recalling equation (3.2),

$$\begin{bmatrix} \mathbf{v}_{w,i} \\ \boldsymbol{\omega}_{w,i} \end{bmatrix} = S_i(\boldsymbol{\delta}_i), \tag{3.2 revisited}$$

each agent command $\boldsymbol{\delta}_i \in \mathcal{I}_i, \mathcal{I}_i \in \mathcal{H}, i \in \{\, 1 \dots n \,\}$ is mapped into the linear and angular velocities expressed in the inertial frame $\mathcal{F}_W$. Thus, the maps

$$\begin{aligned} S_i &: \mathcal{I}_i \to \mathbb{R}^6 \\ S_{p,i} &: \mathcal{I}_{p,i} \to \mathbb{R}^3 && \text{(3.3 revisited)} \\ S_{o,i} &: \mathcal{I}_{o,i} \to \mathbb{R}^3 && \text{(3.4 revisited)} \end{aligned}$$

and the matrices

$$\begin{aligned} \mathbf{S}_{p,i} &\in \mathbb{R}^{3 \times c_{p,i}}, && \text{(3.6a revisited)} \\ \mathbf{S}_{o,i} &\in \mathbb{R}^{3 \times c_{o,i}}, && \text{(3.6b revisited)} \end{aligned}$$

have to be redefined. They now express the reduced actuation capability in the local frames $\mathcal{F}_i$, the first one, for example, becomes

$$\begin{bmatrix} \mathbf{v}_i \\ \boldsymbol{\omega}_i \end{bmatrix} = S_i(\boldsymbol{\delta}_i),$$

Table 4.1: Summary of the relevant quantities for the three agent types of interest when the reduced actuation constraints are expressed in the local frames.

type	$c_{t,i}$	$c_{r,i}$	$\mathcal{I}_{p,i}$	$\mathcal{I}_{o,i}$	$\mathbf{S}_{p,i}$	$\mathbf{S}_{o,i}$
UGV	2	1	$\mathbb{R}^2$	$\mathbb{R}$	$\begin{bmatrix} 1 & 0 \\ 0 & 1 \\ 0 & 0 \end{bmatrix}$	$\begin{bmatrix} 0 \\ 0 \\ 1 \end{bmatrix}$
4dofs-UAV	3	1	$\mathbb{R}^3$	$\mathbb{R}$	$\mathbf{I}_3$	$\begin{bmatrix} 0 \\ 0 \\ 1 \end{bmatrix}$
6dofs-UAV	3	3	$\mathbb{R}^3$	$\mathbb{R}^3$	$\mathbf{I}_3$	$\mathbf{I}_3$

and the others follow in the same way,

$$\begin{aligned} \mathbf{v}_i &= S_{p,i}(\boldsymbol{\delta}_{p,i}) = \mathbf{S}_{p,i}\boldsymbol{\delta}_{p,i}, \\ \boldsymbol{\omega}_i &= S_{o,i}(\boldsymbol{\delta}_{o,i}) = \mathbf{S}_{o,i}\boldsymbol{\delta}_{o,i}. \end{aligned} \tag{4.14}$$

Table 4.1 reports the relevant data for the three types of agent of interest. Notice that the only difference from table 3.1 on page 28 consists on the expression of matrix $\mathbf{S}_{o,i} \in \mathbb{R}^{3\times 1}$ relative to 4dofs-UAVs; these agents can only rotate around their *local* vertical axes, which coordinates, expressed in the inertial frame $\mathcal{F}_W$ compose the vector $\mathbf{n} \in \mathbb{S}^2$.

The i-th agent kinematic equations, which in their most general expression are given by equation (4.1), are now represented by

$$\begin{aligned} \dot{\mathbf{p}}_i &= \mathbf{R}(\mathbf{q}_i) S_{p,i}(\boldsymbol{\delta}_{p,i}), \\ \dot{\mathbf{q}}_i &= \frac{1}{2}\mathbf{q}_i \circ \begin{bmatrix} 0 \\ S_{o,i}(\boldsymbol{\delta}_{o,i}) \end{bmatrix}, \end{aligned}$$

and assuming that the constraining maps $S_{p,i}$, $S_{o,i}$ are linear and time invariant, the formation kinematic equation (4.4) results

$$\dot{\mathbf{x}} = \begin{bmatrix} \mathbf{D}_1(\mathbf{q})\mathbf{S}_p & \mathbf{0}_{3n\times 3n} \\ \mathbf{0}_{4n\times 3n} & \mathbf{D}_2(\mathbf{q})\mathbf{S}_o \end{bmatrix} \boldsymbol{\delta} = \mathbf{D}(\mathbf{q})\mathbf{S}\boldsymbol{\delta}, \tag{4.15}$$

where $\mathbf{S}_p = \operatorname{diag}(\mathbf{S}_{p,i}) \in \mathbb{R}^{3n\times c_t}$, $\mathbf{S}_o = \operatorname{diag}(\mathbf{S}_{o,i}) \in \mathbb{R}^{3n\times c_o}$ and $\mathbf{S} = \operatorname{diag}(\{\, \mathbf{S}_p, \mathbf{S}_o \,\})$.

The time derivative of the bearing measurement associated to the edge $(v_i, v_j) \in \mathcal{E}$ is

$$\dot{\mathbf{b}}_{ij} = d_{ij}\mathbf{P}(\mathbf{b}_{ij})\big(\mathbf{R}(\mathbf{q}_i)^\top \mathbf{R}(\mathbf{q}_j)\mathbf{S}_{p,j}\boldsymbol{\delta}_{p,j} - \mathbf{S}_{p,i}\boldsymbol{\delta}_{p,i}\big) + [\mathbf{b}_{ij}]_\times \mathbf{S}_{o,i}\boldsymbol{\delta}_{o,i},$$

and the bearing rigidity matrix $\mathbf{B}_\mathcal{G}(\mathbf{x}) \in \mathbb{R}^{3m\times c}$, that satisfies equation $\dot{\mathbf{b}}_\mathcal{G}(\mathbf{x}) = \mathbf{B}_\mathcal{G}(\mathbf{x})\boldsymbol{\delta}$, results

$$\mathbf{B}_\mathcal{G}(\mathbf{x}) = \mathbf{A}\mathbf{S}$$

as in equation (3.8) on page 29 with the difference that here $\mathbf{A} \in \mathbb{R}^{3m\times 6n}$ is the bearing rigidity matrix for the fully-actuated twin embedded in $\mathbb{R}^{3n} \times \mathbb{S}^{3n}$, whose row blocks are reported in equation (4.6) on page 41.

4.3.1 Distributed formation stabilization

A mixed framework $(\mathcal{G}, \mathbf{x}, \mathcal{H})$ embedded in $\mathbb{R}^{3n} \times \mathbb{S}^{3n}$ is by all means equivalent to a framework $(\mathcal{G}, \mathbf{x})$ embedded in $\mathbb{R}^{3n} \times \mathbb{S}^{3n}$ but with a different bearing rigidity matrix $\mathbf{B}_\mathcal{G}(\mathbf{x})$. Therefore, the same reasoning that applies in section 4.2.1 can be repeated here. In particular,

- the gradient based control law expressed by equation (4.7) on page 43 is even more unusable, because not only it does not consider that $\mathbf{x} \in \mathbb{R}^{3n} \times \mathbb{S}^3$, but also it does not take into account the reduced actuation capability. Indeed, $\nabla_\mathbf{x} J(\mathbf{x})$ has the same expression for both mixed and non-mixed formations.

- Control law based on the bearing rigidity matrix in its non-scale-free version (form now on called *scaled* version) expressed by equation (4.8) on page 44, where $\mathbf{u} \in \mathbb{R}^{6n}$, is substituted by $\boldsymbol{\delta} \in \mathbb{R}^c$ namely,

  $$\boldsymbol{\delta} = k_c \left(\mathbf{B}_\mathcal{G}(\mathbf{x})\right)^\top \mathbf{b}^*_\mathcal{G}, \tag{4.16}$$

  can be perfectly applied and proposition 4.3 about the stability still applies even for mixed frameworks. Consequently,

- the scale-free version of equation (4.16),

  $$\boldsymbol{\delta} = k_c \left(\bar{\mathbf{B}}_\mathcal{G}(\mathbf{x})\right)^\top \mathbf{b}^*_\mathcal{G} \tag{4.17}$$

  is expected to perform as well as the one given by equation (4.11) on page 45 in the case of non-mixed formations, which has been proven by simulations in [28]. This conjecture will be proven in section 4.4.

The control law based on the scale-free version of the bearing rigidity matrix, equation (4.17) has the property of being *distributed* as the one for the fully-actuated formations, indeed, analogously to equation (4.12) the agent commands have expressions

$$\begin{cases} \boldsymbol{\delta}_{p,i} = -k_c \, \mathbf{S}_{p,i}{}^{\top} \sum\limits_{j\colon v_j \in \mathcal{N}_i} \mathbf{P}(\mathbf{b}_{ij})^{\top} \mathbf{b}^*_{ij} + k_c \, \mathbf{S}_{p,i}{}^{\top} \sum\limits_{\substack{j \text{ s.t.} \\ v_i \in \mathcal{N}_j}} \mathbf{R}(\mathbf{q}_{ij}) \mathbf{P}(\mathbf{b}_{ji})^{\top} \mathbf{b}^*_{ji} \\ \\ \boldsymbol{\delta}_{o,i} = k_c \, \mathbf{S}_{o,i}{}^{\top} \sum\limits_{j\colon v_j \in \mathcal{N}_i} [\mathbf{b}_{ij}]_{\times}^{\top} \mathbf{b}^*_{ij} \end{cases},$$

and again (local) communication and the knowledge of the orientations are required.

Before moving to the dual task, a final consideration has to be made about the desired configuration $\mathbf{x}_d \in \mathbb{R}^{3n} \times \mathbb{S}^{3n}$. For fully-actuated formations, *any* element of $\mathbb{R}^{3n} \times \mathbb{S}^{3n}$ can be chosen as desired configuration because, by definition of fully-actuated, all the vectors in the configuration space are reachable. However, when constraints on the actuation capability of the agents are imposed, then it is no more granted that, given an initial and a desired configurations $\mathbf{x}_0, \mathbf{x}_f \in \mathbb{R}^{3n} \times \mathbb{S}^{3n}$, there exists a command function $\boldsymbol{\delta}\colon [0,\, t_f] \to \bar{\mathcal{I}}$ that drives the formation from $\mathbf{x}(t_0) = \mathbf{x}_0$ to $\mathbf{x}(t_f) = \mathbf{x}_f$ where $(\mathcal{G}, \mathbf{x}_f)$ is BC to $(\mathcal{G}, \mathbf{x}_d)$.

4.3.2 Distributed agent motion coordination

Distributed agent motion coordination is performed applying commands that lay inside the trivial variation space $\mathcal{S}_t$. It has been proven in section 3.2.1 that the trivial variation set of a mixed framework embedded into $\mathbb{R}^{6n}$ is a subset of the one of the fully-actuated twin but it is not possible to go further without specifying the types of constraints affecting the formation.

4.3.3 The response of the barycentre to the controllers

It is interesting to analyse the dynamical properties of the barycentre $\bar{\mathbf{p}} \in \mathbb{R}^3$ of a formation modeled as a mixed framework $(\mathcal{G}, \mathbf{x}, \mathcal{H})$ embedded in $\mathbb{R}^{3n} \times \mathbb{S}^{3n}$ in order, for example, to verify if the COM moves when a formation stabilization algorithm is employed. The dynamics of the barycentre is

$$\frac{d}{dt} \frac{(\mathbf{1}_n \otimes \mathbf{I}_3)^{\top}}{n} \mathbf{p} = \frac{(\mathbf{1}_n \otimes \mathbf{I}_3)^{\top}}{n} \dot{\mathbf{p}}, \tag{4.18}$$

while the control law is

$$\boldsymbol{\delta} = k_c \left(\bar{\mathbf{B}}_{\mathcal{G}}(\mathbf{x})\right)^{\top} \mathbf{b}^*_{\mathcal{G}}. \qquad \text{(4.17 revisited)}$$

Notice that in equation (4.18) the orientation of the agents are not relevant, therefore only $\boldsymbol{\delta}_p \in \mathbb{R}^{c_p}$ are to be considered. This implies that it is not necessary to embed the framework in $\mathbb{R}^{3n} \times \mathbb{S}^{3n}$ but it is sufficient to use $SE(3)^n$ and all the results form chapter 3. Consider also to represent the agent command $\boldsymbol{\delta} \in \mathbb{R}^c$ in the inertial frame, and therefore to be able to correct the values of the constraining matrix $\mathbf{S}_p \in \mathbb{R}^{3n \times c_p}$. Recalling

$$\mathbf{B}_{\mathcal{G}}(\mathbf{x}) = \begin{bmatrix} \operatorname{diag}(d_{ij}\mathbf{R}_i^{\top}\mathbf{P}(\bar{\mathbf{p}}_{ij}))\bar{\mathbf{E}}^{\top}\mathbf{S}_p & -\operatorname{diag}(\mathbf{R}_i^{\top}[\bar{\mathbf{p}}_{ij}]_{\times})\bar{\mathbf{E}}_o^{\top}\mathbf{S}_o \end{bmatrix}, \qquad \text{(3.7 revisited)}$$

and applying the control law (4.17), the agent commands $\boldsymbol{\delta}_p \in \mathbb{R}^{c_p}$ responsible to the linear velocities take expression

$$\boldsymbol{\delta}_p = k_c \, \mathbf{S}_p^{\top} \bar{\mathbf{E}} \operatorname{diag}(d_{ij}\mathbf{R}_i^{\top}\mathbf{P}(\bar{\mathbf{p}}_{ij}))^{\top} \mathbf{b}^*_{\mathcal{G}}. \qquad (4.19)$$

Finally, equations (4.18) and (4.19) are linked together by $\dot{\mathbf{p}} = \mathbf{S}_p \boldsymbol{\delta}_p$, therefore, it results

$$\dot{\bar{\mathbf{p}}} = k_c \frac{(\mathbf{1}_n \otimes \mathbf{I}_3)^{\top}}{n} \mathbf{S}_p \mathbf{S}_p^{\top} \bar{\mathbf{E}} \operatorname{diag}(d_{ij}\mathbf{R}_i^{\top}\mathbf{P}(\bar{\mathbf{p}}_{ij}))^{\top} \mathbf{b}^*_{\mathcal{G}}, \qquad (4.20)$$

and the following proposition can be stated.

Proposition 4.4 (Sufficient condition for the invariance of the barycentre)**.** *Given a mixed framework $(\mathcal{G}, \mathbf{x}, \mathcal{H})$ embedded in $\mathbb{R}^{3n} \times \mathbb{S}^{3n}$ having linear constraining maps $S_i \colon \mathcal{I}_i \to \mathbb{R}^6$ such that equation (4.20) holds when the formation stabilization law (4.17) is applied; then its barycentre remains unchanged, i.e. $\dot{\bar{\mathbf{p}}} = \mathbf{0}$ if*

$$\mathbf{S}_p \mathbf{S}_p^{\top} = \mathbf{I}_{3n} \qquad (4.21)$$

Proof. If equation (4.21) holds, then

$$\dot{\bar{\mathbf{p}}} = k_c \frac{1}{n} \underbrace{(\mathbf{1}_n \otimes \mathbf{I}_3)^{\top} \bar{\mathbf{E}}}_{=\mathbf{0}} \operatorname{diag}(d_{ij}\mathbf{R}_i^{\top}\mathbf{P}(\bar{\mathbf{p}}_{ij}))^{\top} \mathbf{b}^*_{\mathcal{G}}$$

for the properties of the incidence matrix of a graph. □

Notice that $\mathbf{S}_p\mathbf{S}_p^\top = \mathrm{diag}(\mathbf{S}_{p,i}{\mathbf{S}_{p,i}}^\top)$ and under the assumption that

$$\mathbf{S}_{p,i}{\mathbf{S}_{p,i}}^\top = \begin{bmatrix} s_{x,i} & 0 & 0 \\ 0 & s_{y,i} & 0 \\ 0 & 0 & s_{z,i} \end{bmatrix},$$

which indeed happens if UGVs, 4dofs-UAVs or 6dofs-UAVs are considered, then a more specific version of proposition 4.4 can be formulated:

- if $s_{x,i} = 1$ for all $i \in \{ 1 \dots n \}$ then $\bar{\mathbf{p}} \in \mathbb{R}^3$ does not move along the axes $\mathbf{e}_1 \in \mathbb{S}^2$ of the inertial frame.
- if $s_{y,i} = 1$ for all $i \in \{ 1 \dots n \}$ then $\bar{\mathbf{p}} \in \mathbb{R}^3$ does not move along the axes $\mathbf{e}_2 \in \mathbb{S}^2$ of the inertial frame.
- if $s_{z,i} = 1$ for all $i \in \{ 1 \dots n \}$ then $\bar{\mathbf{p}} \in \mathbb{R}^3$ does not move along the axes $\mathbf{e}_3 \in \mathbb{S}^2$ of the inertial frame.

Therefore, when the two mixed formations that have been analysed in chapter 3 are considered, UGVs+6dofs-UAVs maintains the barycentre fixed along $\mathbf{e}_2$ and $\mathbf{e}_1$, namely its barycentre can only translate vertically while for 4dofs-UAVs+6dofs-UAVs proposition 4.4 directly applies and the location of its barycentre remain fixed.

4.4 Simulations

This section is dedicated to show the validity of the proposed solutions through simulations. In testing the algorithms for the formation stabilization task the same initial and desired conditions will be adopted for both fully-actuated and mixed frameworks, in order to compare the results. Distributed agent motion will be performed upon the conclusion of the stabilization procedure.

4.4.1 Common simulation parameters

Six-agents formations are considered, modeled as a (eventually mixed) framework $(\mathcal{G}, \mathbf{x}(t))$ embedded in $(\mathbb{R}^{18} \times \mathbb{S}^{18})$. Of these six agents, the first two are always fully-actuated while the other four change among UGVs, 4dofsUAVs and 6dofsUAVs depending on the three considered scenario, see table 4.2 on page 54. During the simulations the interacting graph $\mathcal{G} = (\mathcal{V}, \mathcal{E})$ is kept fixed and it has been chosen such that all the time, for all the (mixed

and non) frameworks, the infinitesimal bearing rigidity property is present. This is done in order to better compare the results between the three different kind of frameworks. Indeed the UGVs-6dofsUAVs case requires a graph with a smaller edge set than the fully-actuated case. To be possible to use the same initial condition and the same desired configuration for all the simulations, they are chosen in accordance to the most constraining case, namely the UGVs-6dofsUAVs mixed formation (case 3), and reported in table 4.3 on the next page. All the agents are initially placed on the plane $\mathbf{e}_3 = 0$ and their orientation is such that their local vertical axis is aligned to the one of the inertial frame, namely all the agents are initially rotated by an an angle α_i, $i \in \{1, \dots 6\}$ around the axis $\mathbf{e}_3$ of $\mathcal{F}_W$. The desired configuration exhibits the four (eventually) UGVs composing a square, always laying on the plane ${\mathbf{e}_3}^\top \mathbf{p} = 0$, $\mathbf{p} \in \mathbb{R}^3$, with the two fixed 6dofsUAVs inside, vertically translated. Regarding the final orientations, all the agents have their desired local frames aligned with the inertial one. The spacial displacement (position and orientation) of the agents of the initial and of the desired framework, along with a graphical representation of the measurement capabilities (the edges interconnection the agents) is reported in figure 4.1 on page 55. Notice that all the edges are associated to bi-directional measurements.

All the formation are assumed to be subjected to the kinematic law given by equation (4.15) on page 48, namely the single integrator modes are employed. Even if the most relevant control law is

$$\boldsymbol{\delta} = k_c \left(\bar{\mathbf{B}}_{\mathcal{G}}(\mathbf{x})\right)^\top \mathbf{b}^*_{\mathcal{G}}, \qquad \text{(4.17 revisited)}$$

which uses the scale-free version of the bearing rigidity matrix, it will be also analysed, for comparison purposed, the original, scaled version stated by equation (4.16) on page 49. The communication between the agents is assumed to be instantaneous and ideal, namely, no communication delays are considered and the true orientations are assumed to be known (this assumption will be removed in the next chapter). The reason such assumption are introduced, which greatly reduces the applicability of the algorithm is to test if at least under ideal conditions the proposed control laws perform well. If the results are unsatisfactory, then there is no reason to continue the study.

4.4.2 Case 1: fully-actuated formation

The first case to be studied is the one where all the agents are fully-actuated. In this situation the behaviours of the controlled system subject to the scaled and scale-free control laws are compared. To evaluate the performances the index of cost $J(t)$ is evaluated at each time

Table 4.2: Types of agent used during the simulations of the control algorithms depending on the different adopted frameworks.

agent	case 1 non mixed	case 2 4dofsUAVs-6dofsUAVs	case 3 UGV-6dofsUAVs
1-th	6dofsUAVs	6dofsUAVs	6dofsUAVs
2-th	6dofsUAVs	6dofsUAVs	6dofsUAVs
3-th	6dofsUAVs	4dofsUAVs	UGV
4-th	6dofsUAVs	4dofsUAVs	UGV
5-th	6dofsUAVs	4dofsUAVs	UGV
6-th	6dofsUAVs	4dofsUAVs	UGV

Table 4.3: Initial and desired configurations of the formations. The orientations are expressed by the pair $(\mathbf{n}_i, \alpha_i) \in \mathbb{S}^2 \times (-\pi, \pi]$ denoting a rotation around $\mathbf{n}_i$, expressed in the inertial frame, of an angle α_i.

Initial, $t = 0\,\mathrm{s}$							
agent	$\mathbf{p}_i^\top$			$\mathbf{n}_i^\top$			α_i
1-th	4	8	0	0	0	1	0
2-th	8	2	0	0	0	1	$\pi/4$
3-th	5	-4	0	0	0	1	$-\pi/4$
4-th	-1	-3	0	0	0	1	π
5-th	14	3	0	0	0	1	$2\pi/3$
6-th	15	13	0	0	0	1	$-\pi/3$
Desired							
agent	$\mathbf{p}_i^\top$			$\mathbf{n}_i^\top$			α_i
1-th	8	7	8	0	0	1	0
2-th	5	3	8	0	0	1	0
3-th	0	10	0	0	0	1	0
4-th	0	0	0	0	0	1	0
5-th	10	0	0	0	0	1	0
6-th	10	10	0	0	0	1	0

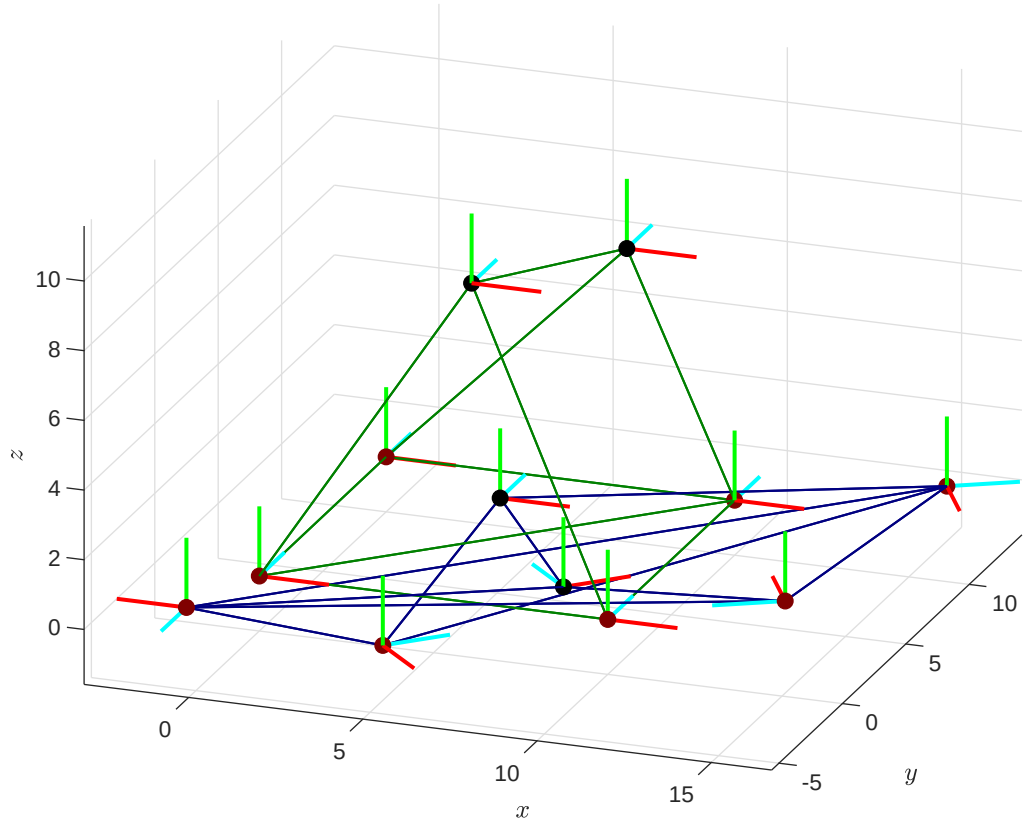

Figure 4.1: Initial and desired frameworks used during the simulations of the control algorithms. The edges of the initial framework are represented by the dark blue lines while for the ones of the desired frameworks the dark green color is used. Each edge represents a bi-directional measurement. The black dots represents the first two agents that are always fully-actuated, instead, the brown ones represents the four remaining (possibly) under-actuated agents. The local frame of each agent is reported, the red, cyan and green vectors represent the local axes $\mathbf{e}_i, i \in \{1, 2, 3\}$, respectively.

sample

$$J(t) = \frac{1}{2}\|\mathbf{b}_{\mathcal{G}}(\mathbf{x}(t)) - \mathbf{b}^*_{\mathcal{G}}\|^2.$$

$J(t)$ is (half) the square norm of the difference between the bearing vector at time t and the desired one; it provides a cumulative measure of the "bearing distance" between the formation at time t and the desired one. The trajectories of the agents and the final configurations are shown in figures 4.2a and 4.2b on the next page. For the first figure the scaled controller has been used while in the second the scale-free one has been adopted. On one hand, it is possible to observe that the scale-free controller produces smoother trajectories; on the other hand, the difference on the performances is outstanding with the scale-free control law achieving a final cost three orders of magnitude smaller than the other, see figure 4.2c. This difference in the performances may be attributed to different implicit gains factor, namely it could be said that

$$\bar{\mathbf{B}}_{\mathcal{G}}(\mathbf{x}) \approx k'_c \mathbf{B}_{\mathcal{G}}(\mathbf{x}) \tag{4.22}$$

in some sense. Indeed form the given initial conditions the inter-agents distances have order of magnitude around 10^1, therefore some terms in $\mathbf{B}_{\mathcal{G}}(\mathbf{x})$ are scaled by a factor of 10^{-1} w.r.t. the ones in $\bar{\mathbf{B}}_{\mathcal{G}}(\mathbf{x})$. Figure 4.3 on page 58 shows the behaviour of the cost functions $J(t)$ exactly as figure 4.2c but with the value of k_c used in the scale-free control law reduced by a factor of ten. The result it quite significant, because the two systems exhibit the same steady state behaviour, meaning that equation (4.22) holds in the sense that

$$\text{if } \mathbf{b}_{\mathcal{G}}(\mathbf{x}) \sim \mathbf{b}^*_{\mathcal{G}} \text{ then } \bar{\mathbf{B}}_{\mathcal{G}}(\mathbf{x})\mathbf{b}^*_{\mathcal{G}} \sim k'_c \mathbf{B}_{\mathcal{G}}(\mathbf{x})\mathbf{b}^*_{\mathcal{G}},$$

but they performs very differently during the initial transient.[2] The scaled controller reaches the steady state faster than the other solution in this setup, and considering also that its trajectories are smoother the conclusion is that

Proposition 4.5. *Based on the simulation results, when the steady state behaviours are matched then the scaled controller performs better than the scale-free one in terms of settling time and smoothness of the trajectories.*

This completely reverses the previous result. Table 4.4 on page 62 summarizes the performances of the formation stabilization controllers applied to the different formations dis-

[2] With the term *steady state* it is intended the phase of the simulation when the cost drops below a threshold value and the equilibrium can be considered reached. It must not be confused with the condition "the plot of the cost function is flat" because a logarithmic scale is used.

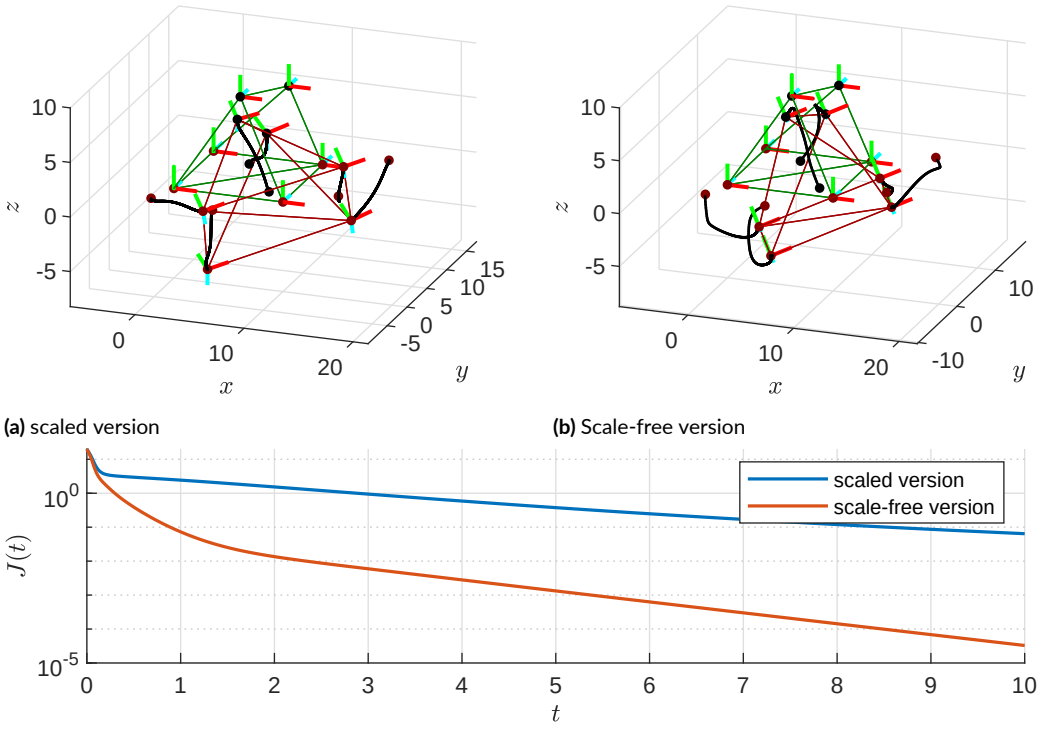

(a) scaled version

(b) Scale-free version

(c) Half square norm of the bearing error.

Figure 4.2: Comparison between the control law (4.16) and (4.17) applied to a fully-actuated IBR formation. The trajectories of the agents (the black lines) and the final configurations (brown edges) after $T = 10\,\mathrm{s}$ of simulations when the scaled (a) and the scale-free (b) control laws are applied are reported. The common desired configuration is drawn in dark green while the initial one is omitted. Logarithmic behaviour of the square norm of the bearing error $J(t) = \frac{1}{2}\|\mathbf{b}_{\mathcal{G}}(\mathbf{x}(t)) - \mathbf{b}^*_{\mathcal{G}}\|^2$ obtained in the simulations, (c).

cussed in these sections. The value of the cost function at the end of the simulation $J_{end} = J(t_{end})$ is reported, along with the angle $e_{max} \in (-\pi, \pi]$ denoting the maximum error between the desired bearing measurements and the final ones

$$e_{max} := \max_{(i,j):\ (v_i,v_j)\in\mathcal{E}} \arccos(\mathbf{b}_{ij}(t_{end})^\top \mathbf{b}^*_{ij}). \tag{4.23}$$

The controller proposed to perform the distributed agent motion coordination is tested on the final framework obtained through the scale-free formation controller. The simulation consists in applying equation (4.13) on page 46 with $\mathbf{s}^* = [1 \quad 0 \quad 0]^\top\,\mathrm{s}^{-1}$ for ten seconds in order to actuate a translation along the axis $\mathbf{e}_1$ of the inertial frame. The trajectories of the agents are reported in figure 4.4 on page 59 where it is possible to observe that the formation actually translates as desired ad it does not change its shape. Actually, the simulation shows

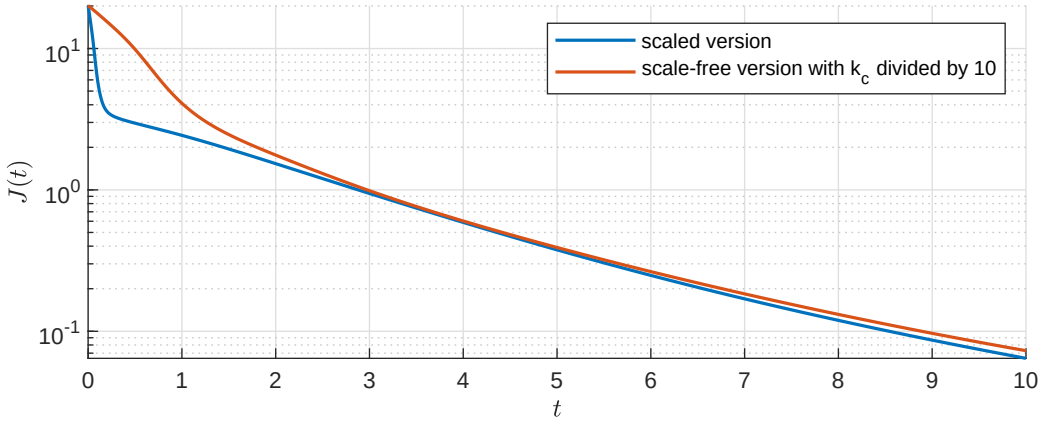

Figure 4.3: Comparison of the scaled and scale-free controllers applied to a fully-actuated formation when the adopted values of k_c are such that the convergence rate is the same. The scale of the error is logarithmic.

something more, introducing the input energy E associated to the formation input $\mathbf{u}$ as

$$E = \int_{t_1}^{t_2} \mathbf{u}(t)^\top \mathbf{u}(t)\, dt,$$

then the stabilization procedure using the scale-free control law, from $t_1 = 0\,\mathrm{s}$ to $t_2 = 10\,\mathrm{s}$ requires $E = 845.2195\,\mathrm{s}^{-1}$. Continuing the simulation from $t_2 = 10\,\mathrm{s}$ to $t_3 = 20\,\mathrm{s}$, implementing both the stabilization controller and the distributed agent motion coordination, it is required $E = 60.601\,\mathrm{s}^{-1}$ to perform the translation, and only $E = 4.7 \times 10^{-3}\,\mathrm{s}^{-1}$ to keep the formation stabilized. This confirms that the coordinated translation does not affect in any way the shape of the formation in accordance with the theory stating that this movement belongs to the trivial variation set.

4.4.3 Case 2: 4dofsUAVs-6dofsUAVs mixed formation

Migrating to the second type of formation, the one composed by two fully-actuated agents and four under-actuated agents modelling 4dofsUAVs, the evaluation of the scale-free formation controller is repeated with the same initial and desired values listed in table 4.3 on page 54 and the simulation results are reported in figure 4.5 on page 61. It has already been shown that the scaled controller should be preferred but the fact that it requires the knowledge of d_{ij} makes the the other to be adopted. The controller is able to drive the formation toward one that is BE to the desired framework, the cost $J(t)$, in fact, drops below the value 10^{-5}. Moreover, the final configuration is a roto-translated and scaled version of the desired

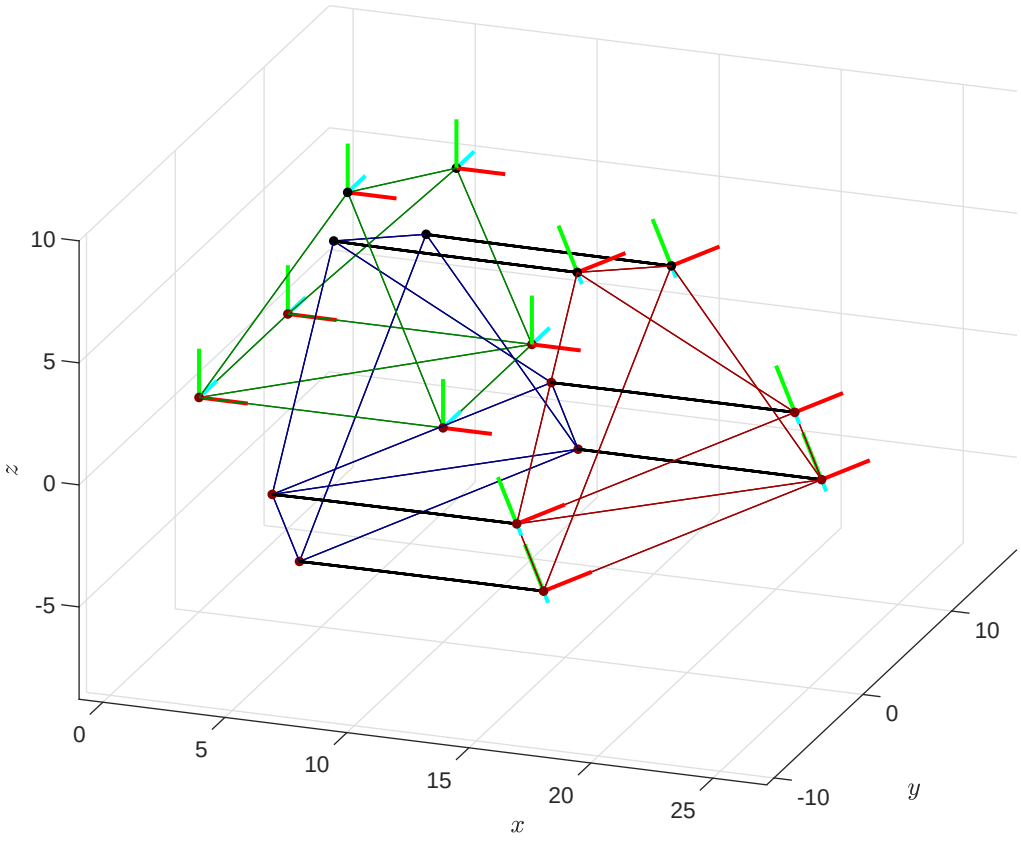

Figure 4.4: Trajectories (black lines) of the agents of a fully-actuated formation when performing a coordinated translation along the axis $\mathbf{e}_1$ of the inertial frame. In red, blue and maroon are reported the final, initial and initial desired configurations.

one with the difference from the fully-actuated case that the rotations is around the axis $\mathbf{e}_3$ of the inertial frame.

4.4.4 Case 3: UGVs-6dofsUAVs mixed formation

The last case involves a formation composed by four UGVs and two 6dofsUAVs. The scale-free controller is able to stabilize the formation, as shown in figure 4.6 on page 63. The constraints are met during the entire simulation; the trajectories of the UGVs remains all the time in the plane $z = 0$ and also the local frames are always represented by a rotation of the inertial one around the axis $\mathbf{e}_3$.

The combination of the distributed agent motion coordinator and the formation stabilizer is tested again, similarity to the analysis computed for the fully-actuated formation. However this time, to highlight the interaction of the two control laws, the UGVs are placed on a non-flat surface. If the condition of non-flatness is interpreted as a disturbance, then this simulation is also a way to test the robustness of the system. Denoting with $x, y, z \in \mathbb{R}^3$ the three components of the vector expressing the position of a point in $\mathbb{R}^3$ w.r.t. the world frame, the surface is specified by the explicit functions

$$\begin{cases} z = 0, & \text{if } x < 20, \\ z = ax^2 + bx + c & \text{if } 20 \leqslant x < 35, \\ z = mx + q & \text{if } x \geqslant 35, \end{cases} \tag{4.24}$$

where the slope $m = 0.3$ of the linear ramp is fixed and all the other parameters are computed such that the resulting surface is of class $\mathcal{C}^1$. The simulation (figure 4.7 on page 64) starts at the end of the previous ($t = 10\,\mathrm{s}$) where only the formation controller was employed and all the UGVs are in the flat region. The distributed agent motion coordinator imposes a coordinated translation with $\mathbf{s}^* = \begin{bmatrix} 1 & 0 & 0 \end{bmatrix}^\top \mathrm{s}^{-1}$ for forty seconds. Initially there is no effect on the shape of the formation and the formation stabilizer, which is always working in the background, keep decreasing the cost function. At time $t_a = 16.11\,\mathrm{s}$ the first UGV enters the parabolic ramp region. As a results, it starts rotating in order to maintain its vertical axis perpendicular to the tangent plane of the surface passing through its current position, as imposed by the constraints. The coordinated agents controllers, which do not know the analytical expression of the surface, try to keep the formation translating along the axis $\mathbf{e}_1$ that, however, is no more a trivial variation. The cost function starts increasing consistently

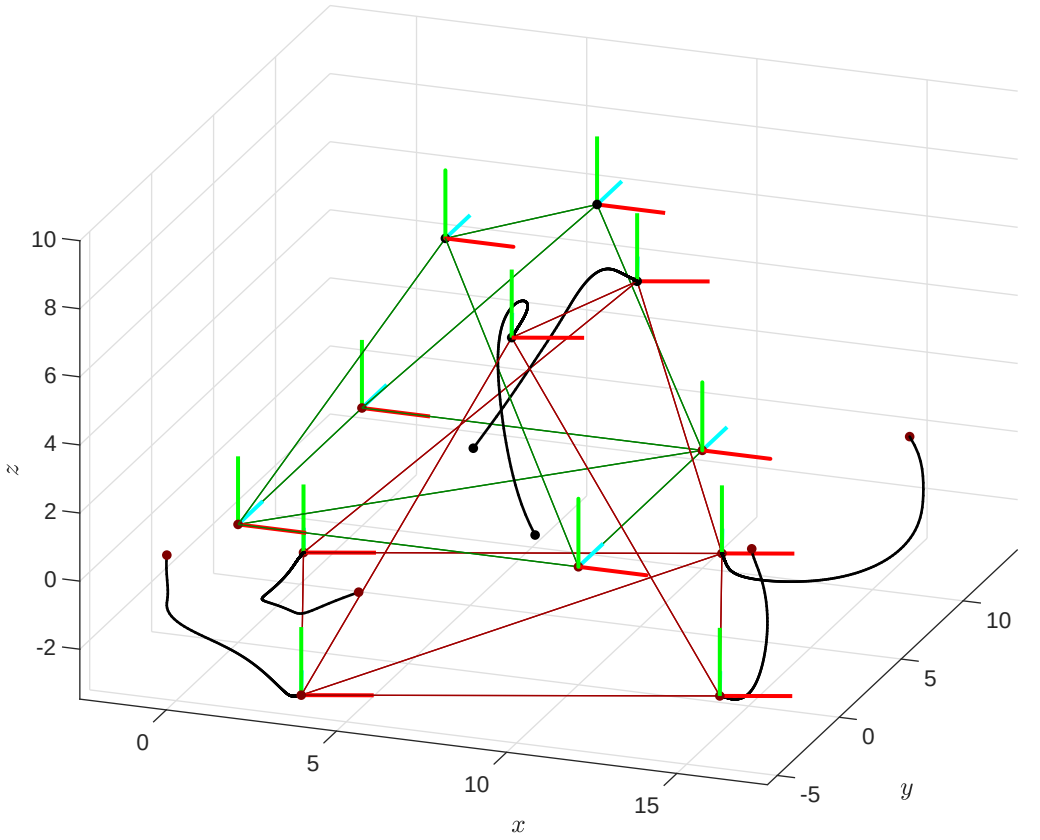

(a)

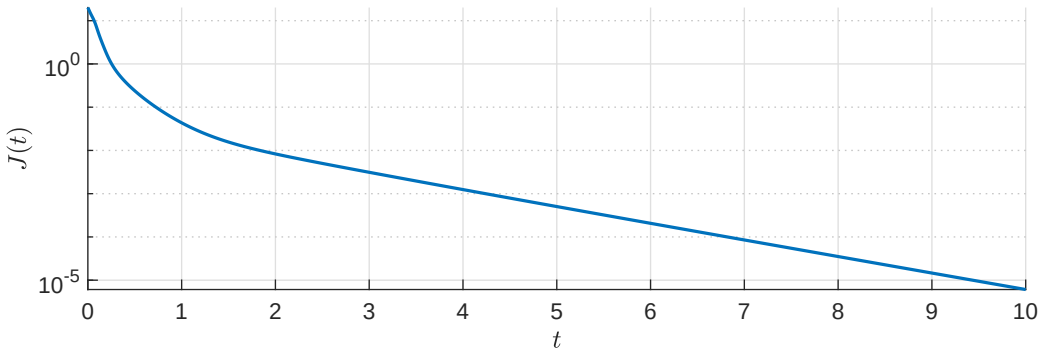

(b)

Figure 4.5: Trajectory of a mixed formation composed by 6dofsUAVs and 4dofsUAVs when the scale-free formation stabilization controller is applied (a). The green edges represent the desired framework; the black lines are the trajectories, starting from the initial framework (whose edges are not drawn) and terminating at the final framework (brown edges). Differently from figure 4.2 the final framework is only rotated around the axis $\mathbf{e}_3$ of the inertial frame as a result of having under-actuated agents. Behaviour of the cost function in logarithmic scale (b).

Table 4.4: Comparison of the simulation results for the formation stabilization task, the convergence gain is fixed to $k_c = 10$.

	J_{end}	e_{max} [degree]
case 1, scaled controller	6.43×10^{-2}	10.5885
case 1, scale-free controller	3.28×10^{-5}	0.1996
case 1, after coordinated motion	7.40×10^{-8}	0.0051
case 2	6.08×10^{-6}	0.0792
case 3	3.90×10^{-6}	0.0621
case 3, with the coordinated motion at $t_c = 50\,\mathrm{s}$	5.43×10^{-4}	0.9186
case 3, with the coordinated motion at $t_c = 60\,\mathrm{s}$	4.94×10^{-9}	0.0022

and the formation stabiliser takes actions to counter this behaviour. In particular the two UAVs begin to rotate and translate vertically. Between t_a and $t_b = 45\,\mathrm{s}$ all the UGVs enter and leave the parabolic ramp region and end up laying in the linear ramp. There the formation can be modeled as a UGVs-6dofsUAVs mixed framework where all the under-actuated agents have the same rotational axis which, however, is different from $\mathbf{e}_3$. This situation has been already studied in section 3.3.1 and there are again two independent translations belonging to the trivial variation set. Despite this, the command generated by the distributed agent motion controller is not a linear combination of them.

On one hand a controller tries to deform the formation, on the other the formation stabilizer opposes. The resulting behaviour shows a the cost function having a constant value. At $t_c = 50\,\mathrm{s}$ the distributed agent motion coordinator is deactivated and the formation stabilizer can freely drive the cost function to zero.

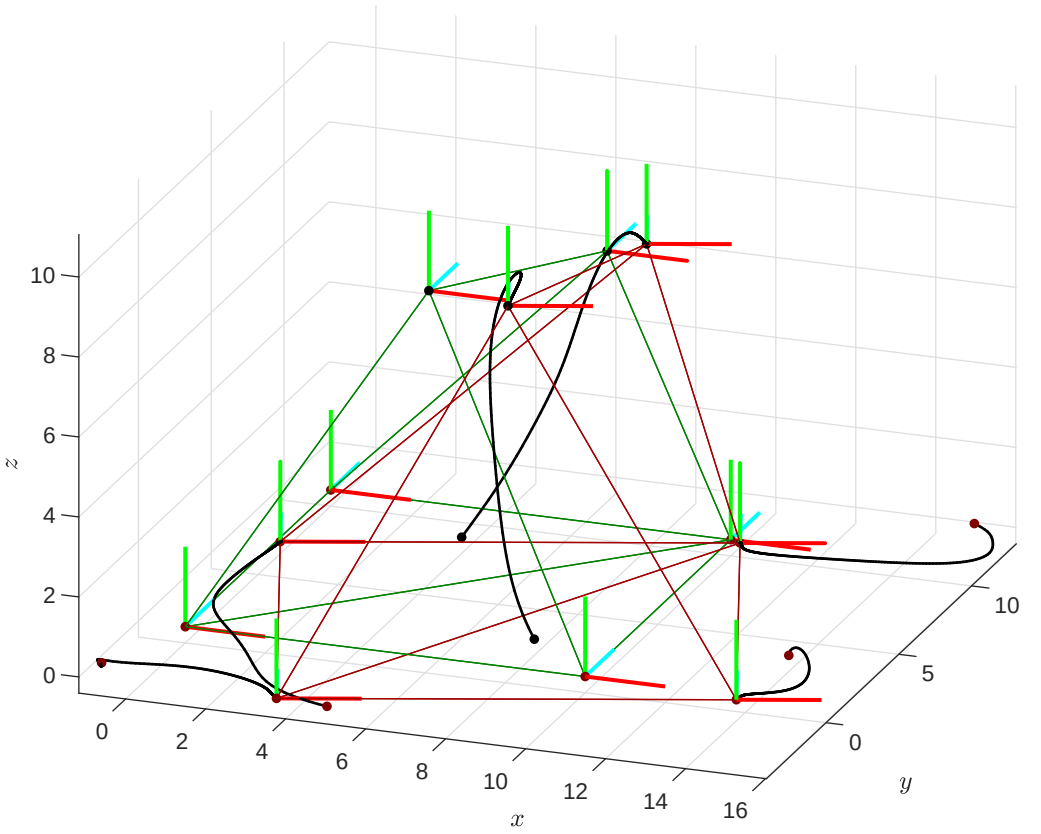

(a)

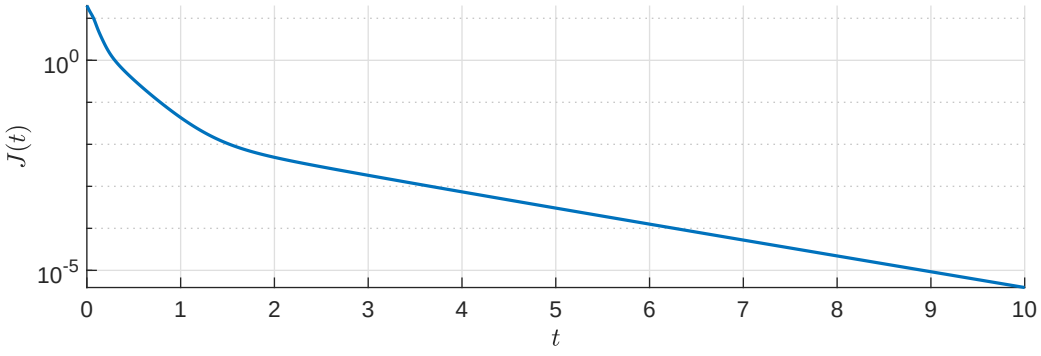

(b)

Figure 4.6: Trajectory of a mixed formation composed by 6dofsUAVs and UGVs when the scale-free formation stabilization controller is applied (a). The green edges represent the desired framework; the black lines are the trajectories, starting from the initial framework (whose edges are not drawn) and terminating at the final framework (brown edges). Differently from figure 4.5 the final framework is not only rotated around the axis $\mathbf{e}_3$ of the inertial frame but also the UGVs remain in their initial plane. Behaviour of the cost function in logarithmic scale (b).

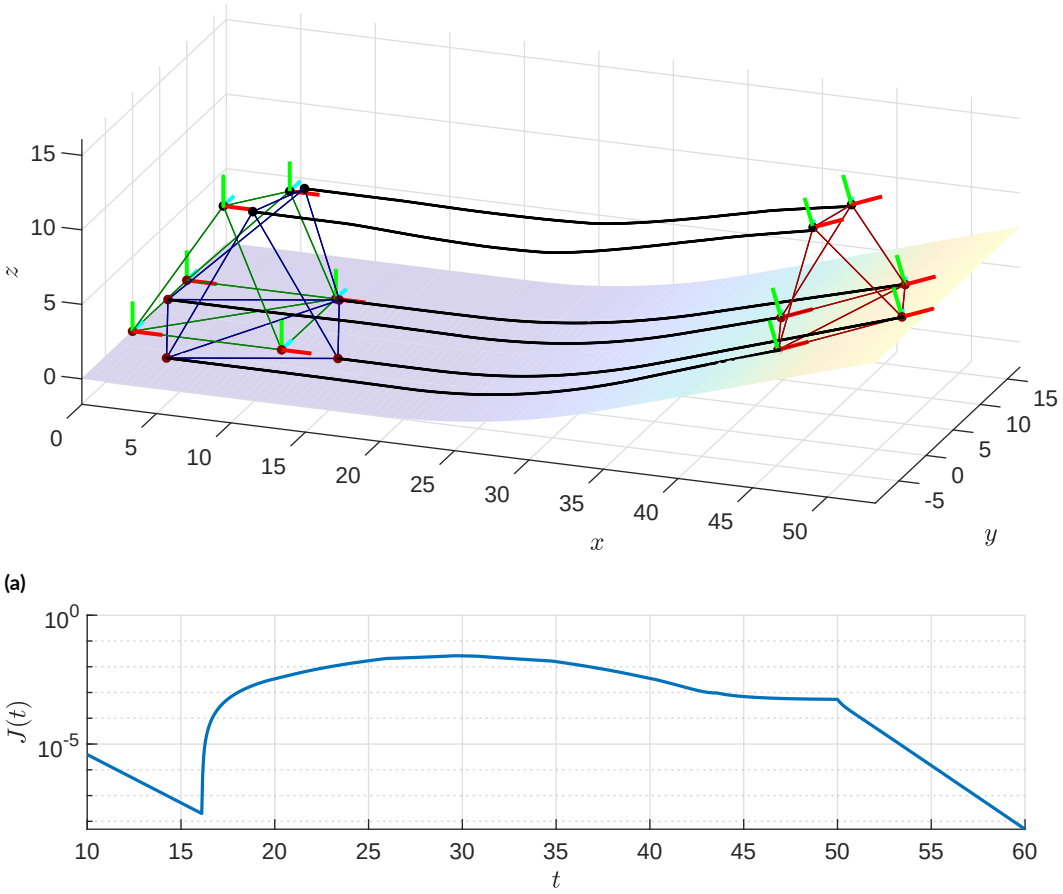

(a)

(b)

Figure 4.7: Trajectory of a mixed formation composed by 6dofsUAVs and UGVs when the both the distributed agent motion coordinator and the formation stabilized are applied (a); the UGVs lay on a non-flat surface. The green edges represent the initial desired framework; the black lines are the trajectories, starting from the initial framework (whose edges are not drawn) and terminating at the final framework (brown edges). Behaviour of the cost function in logarithmic scale (b). When the non-flat area is encountered, the cost function increased to settle to a non-zero value (at $t_c = 50\,\mathrm{s}$) due to the distributed agent motion not belonging to the trivial variation set. When that motion is removed, the formation stabilizer successes to drive to zero the cost function ($t_d = 60\,\mathrm{s}$).

5

The Localization Problem

Given a n-agents fully-actuated formation modeled as a framework $(\mathcal{G}, \mathbf{x})$ embedded in $\mathbb{R}^{3n} \times \mathbb{S}^{3n}$, it has been proven which conditions guarantee its instantaneous bearing rigidity and how it is possible to control it in a distributed way adopting bearing-based techniques. This chapter, instead, answers the question about the possibility to recover the configuration $\mathbf{x} \in \mathbb{R}^{3n} \times \mathbb{S}^{3n}$ from only the bearing measurements. A configuration estimator will be proposed, and its validity will be demonstrated through an analytical proof and simulations.

Nevertheless, should be clear that, being the common inertial frame $\mathcal{F}_W$ completely unknown to the agents and employing only inter-agents measurements, it is impossible to retrieve the true configuration. For this reason it is more accurate to say that the location estimator will make the agent build a common inertial frame $\mathcal{F}_{W'}$ which position (of its center) and orientation w.r.t $\mathcal{F}_W$ remain unknown.

5.1 Distributed bearing-based configuration estimation

In the previous chapter it has been explained how it is possible to drive a the configuration of a framework toward a new one that is BE to a fixed desired configuration exploiting only the bearing rigidity matrix and the bearing vector associated to the desired framework. The configuration estimator is developed from there applying a change of perspective. It is no more that the true configuration is driven toward the desired one, but rather that the estimated configuration is driven toward the true one. Initially, the problem of estimation the

configuration of a *fixed* framework, namely a framework such that $\dot{\mathbf{x}}(t) = \mathbf{0}$ it approached. Be $\hat{\mathbf{x}} = \begin{bmatrix}\hat{\mathbf{p}}^\top & \hat{\mathbf{q}}^\top\end{bmatrix}^\top \in \mathbb{R}^{3n} \times \mathbb{S}^{3n}$ the configuration estimated by the estimator and

$$\mathbf{e}_L(\mathbf{x}, \hat{\mathbf{x}}) \coloneqq \mathbf{b}_{\mathcal{G}}(\mathbf{x}) - \mathbf{b}_{\mathcal{G}}(\hat{\mathbf{x}}) \in \mathbb{R}^{3m}$$

the bearing estimation error. When a fixed configuration $\mathbf{x} \in \mathbb{R}^{3n} \times \mathbb{S}^{3n}$ has to be estimated, the proposed estimator is a dynamical system governed by the equations

$$\dot{\hat{\mathbf{x}}} = \mathbf{D}(\hat{\mathbf{q}})\mathbf{u}_L, \tag{5.1a}$$

$$\mathbf{u}_L = k_e \big(\mathbf{B}_{\mathcal{G}}(\hat{\mathbf{x}})\big)^\top \mathbf{b}_{\mathcal{G}}(\mathbf{x}), \tag{5.1b}$$

where $\mathbf{D}(\cdot) \in \mathbb{R}^{7n \times 6n}$ is the one introduced in equation (4.4) on page 40, $k_e > 0$ is at tunable gain and $\mathbf{u}_L = \begin{bmatrix}\mathbf{v}_L^\top & \boldsymbol{\omega}_L^\top\end{bmatrix}^\top \in \mathbb{R}^{6n}$ is the estimator input, with $\mathbf{v}_L = \begin{bmatrix}\mathbf{v}_{1,L}^\top \dots \mathbf{v}_{n,L}^\top\end{bmatrix}^\top \in \mathbb{R}^{3n}$ and $\boldsymbol{\omega}_L = \begin{bmatrix}\boldsymbol{\omega}_{1,L}^\top \dots \boldsymbol{\omega}_{n,L}^\top\end{bmatrix}^\top \in \mathbb{R}^{3n}$ the vectors stacking the estimator inputs of each agent related to the linear and angular velocities, respectively.

With this choice the dynamics of the bearing estimation error results

$$\begin{aligned}\dot{\mathbf{e}}_L(\mathbf{x}, \hat{\mathbf{x}}) &= \dot{\mathbf{b}}_{\mathcal{G}}(\mathbf{x}) - \dot{\mathbf{b}}_{\mathcal{G}}(\hat{\mathbf{x}}) \\ &= -\mathbf{B}_{\mathcal{G}}(\hat{\mathbf{x}})\mathbf{u}_L \\ &= -k_e\, \mathbf{B}_{\mathcal{G}}(\hat{\mathbf{x}})\big(\mathbf{B}_{\mathcal{G}}(\hat{\mathbf{x}})\big)^\top \mathbf{b}_{\mathcal{G}}(\mathbf{x}) \\ &= -k_e\, \mathbf{B}_{\mathcal{G}}(\hat{\mathbf{x}})\big(\mathbf{B}_{\mathcal{G}}(\hat{\mathbf{x}})\big)^\top \mathbf{e}_L(\mathbf{x}, \hat{\mathbf{x}})\end{aligned} \tag{5.2}$$

and an equivalent proposition to proposition 4.3 on page 44 can be stated.

Proposition 5.1. *Given a fixed framework $(\mathcal{G}, \mathbf{x})$ embedded in $\mathbb{R}^{3n} \times \mathbb{S}^{3n}$, the dynamical system modelling the dynamics of the bearing estimation error when the estimator* (5.1) *is employed presents an equilibrium in $\mathbf{0}_{3m}$ which is asymptotically stable.*

Proof. This proof is very similar to the one of proposition 4.3. The simple stability of the equilibrium point is shown again noticing that the Lyapunov function

$$V(\mathbf{e}_L) = \frac{1}{2k_e}\mathbf{e}_L(\mathbf{x}, \mathbf{x}_d)^\top \mathbf{e}_L(\mathbf{x}, \mathbf{x}_d),$$

which is positive definite, has time derivative that is negative semi-definite. Finally, LaSalle's invariance principle allows to conclude the asymptotic stability. □

The estimator is therefore able to converge to an estimated framework $(\mathcal{G}, \hat{\mathbf{x}})$ that is BE to $(\mathcal{G}, \mathbf{x})$. Considering the nature of the metric space $\mathbb{R}^{3n} \times \mathbb{S}^{3n}$ and its characterization performed in section 4.1 on page 38, this means that $\hat{\mathbf{x}}$ is equal to an (eventually) *modified* version of $\mathbf{x}$; where modified represents

- a translation of the COM of the formation,
- a coordinated rotation,
- a scaling.

Notice that the first two possibilities correspond to the generation of a (known) common frame $\mathcal{F}_{W'}$ while the third derive from the intrinsic absence of capability in recovering the scale of the formation using only bearing measurements. Regarding the matter of having a distributed law, the reasoning applied studying the formation stabilization controller holds, in particular it is required communication between the agents. Still, there is a major difference: the estimator does not need to employ the scale-free bearing rigidity matrix because the inter-agents distances that it needs to compute are estimates too. Each agent has therefore to employ the estimator law

$$\dot{\hat{\mathbf{x}}}_i = \begin{bmatrix} \mathbf{R}(\hat{\mathbf{q}}_i) & \mathbf{0}_{3\times 3} \\ \mathbf{0}_{4\times 3} & \bar{\mathbf{M}}(\hat{\mathbf{q}}_i) \end{bmatrix} \begin{bmatrix} \mathbf{v}_{i,L} \\ \boldsymbol{\omega}_{i,L} \end{bmatrix},$$

having input

$$\begin{cases} \mathbf{v}_{i,L} = -k_c \sum\limits_{j\colon v_j \in \mathcal{N}_i} \mathbf{P}(\hat{\mathbf{b}}_{ij})^\top \mathbf{b}_{ij} + k_c \sum\limits_{\substack{j \text{ s.t.} \\ v_i \in \mathcal{N}_j}} \mathbf{R}(\hat{\mathbf{q}}_{ij}) \mathbf{P}(\hat{\mathbf{b}}_{ji})^\top \mathbf{b}_{ji} \\ \boldsymbol{\omega}_{i,L} = k_c \sum\limits_{j\colon v_j \in \mathcal{N}_i} [\hat{\mathbf{b}}_{ij}]_\times^\top \mathbf{b}_{ij} \end{cases}.$$

However, it is not granted that the estimator is able to deal with time-varying formations. Indeed, if the formation is subjected to an input $\mathbf{u} \in \mathbb{R}^{6n}$, equation (5.2) stop holding. Anyway there is a solution if $\mathbf{u} \in \mathbb{R}^{6n}$ is known to the estimator. Indeed, in this situation, the known input $\mathbf{u} \in \mathbb{R}^{6n}$ can be use in feedforward inside the estimator dynamics providing a slightly different version of equation (5.1a),

$$\dot{\hat{\mathbf{x}}} = \mathbf{D}(\hat{\mathbf{q}})(\mathbf{u}_L + \mathbf{u}), \tag{5.3}$$

where $\mathbf{u}_L \in \mathbb{R}^{3n}$ is the same as in equation (5.1b). Equation (5.3) leads to a bearing error with dynamics

$$\dot{\mathbf{e}}_L(\mathbf{x}, \hat{\mathbf{x}}) = -k_e \, \mathbf{B}_\mathcal{G}(\hat{\mathbf{x}}) \big(\mathbf{B}_\mathcal{G}(\hat{\mathbf{x}})\big)^\top \mathbf{e}_L(\mathbf{x}, \hat{\mathbf{x}}) + \big(\mathbf{B}_\mathcal{G}(\mathbf{x}) - \mathbf{B}_\mathcal{G}(\hat{\mathbf{x}})\big)\mathbf{u} \tag{5.4}$$

that can be treated as a *perturbed* system, where the perturbation is represented by the additive term $\big(\mathbf{B}_\mathcal{G}(\mathbf{x}) - \mathbf{B}_\mathcal{G}(\hat{\mathbf{x}})\big)\mathbf{u}$. From [29], the equilibrium $\mathbf{e}_L(\mathbf{x}, \hat{\mathbf{x}}) = \mathbf{0}$ is asymptotically stable if it is so for the relative un-perturbed system (which is true by proposition 5.1) and the perturbation vanishes as $\mathbf{e}_L(\mathbf{x}, \hat{\mathbf{x}}) \to \mathbf{0}$. Desiring the second condition to hold for any input $\mathbf{u} \in \mathbb{R}^{6n}$, it is equivalent to require

$$\mathbf{B}_\mathcal{G}(\mathbf{x}) - \mathbf{B}_\mathcal{G}(\hat{\mathbf{x}}) \xrightarrow{\mathbf{e}_L(\mathbf{x},\hat{\mathbf{x}}) \to \mathbf{0}} \mathbf{0}.$$

Recalling the structure of the bearing rigidity matrix

$$\begin{cases} \begin{bmatrix} \mathbf{0}_{3\times 3(i-1)} & -d_{ij}\mathbf{P}(\mathbf{b}_{ij}) & \mathbf{0}_{3\times 3(j-i-1)} & d_{ij}\mathbf{P}(\mathbf{b}_{ij})\mathbf{R}(\mathbf{q}_i)^\top \mathbf{R}(\mathbf{q}_j) \\ \mathbf{0}_{3\times(3(n-j)+3(i-1)} & [\mathbf{b}_{ij}]_\times & \mathbf{0}_{3\times 3(n-i)} & \end{bmatrix} & \text{if } i < j, \\ \begin{bmatrix} \mathbf{0}_{3\times 3(j-1)} & d_{ij}\mathbf{P}(\mathbf{b}_{ij})\mathbf{R}(\mathbf{q}_i)^\top \mathbf{R}(\mathbf{q}_j) & \mathbf{0}_{3\times 3(i-j-1)} & -d_{ij}\mathbf{P}(\mathbf{b}_{ij}) \\ \mathbf{0}_{3\times(3(n-i)+3(i-1)} & [\mathbf{b}_{ij}]_\times & \mathbf{0}_{3\times 3(n-i)} & \end{bmatrix} & \text{if } i < j, \end{cases}$$

(4.6 revisited)

if $\mathbf{e}_L(\mathbf{x}, \hat{\mathbf{x}}) \to \mathbf{0}$ then $\mathbf{P}(\hat{\mathbf{b}}_{ij}) \to \mathbf{P}(\mathbf{b}_{ij})$. Moreover, at the equilibrium, the whole estimated formation corresponds to a (scaled) roto-translated version of the true one. This allows to relate the estimated orientations of each agent to the true ones; in particular it holds that $\hat{\mathbf{q}}_i = \mathbf{q}_{W'}\mathbf{q}_i$, where $\mathbf{q}_{W'} \in \mathbb{S}^3$ is the quaternion representing the orientation of $\mathcal{F}_W$ w.r.t. $\mathcal{F}_{W'}$. In conclusion, it results,

$$\mathbf{R}(\hat{\mathbf{q}}_i)^\top \mathbf{R}(\hat{\mathbf{q}}_j) = \mathbf{R}(\mathbf{q}_i)^\top \mathbf{R}(\mathbf{q}_{W'})^\top \mathbf{R}(\mathbf{q}_{W'})\mathbf{R}(\mathbf{q}_j) = \mathbf{R}(\mathbf{q}_i)^\top \mathbf{R}(\mathbf{q}_j).$$

The only remaining term in equation (4.6) is the (inverse) inter-agents distance $d_{ij} > 0$; therefore, the extended estimator law (5.3) leads to an asymptotically stable equilibrium point for the estimation error if it is also able to fully recover the scale of the formation. Sadly, this is not the case for the proposed estimator.

A solution for frameworks embedded in $\mathbb{R}^{2n} \times \mathbb{S}^n$ has been proposed in [24]. At the price

of partially violating the bearing-only requirement, the authors assumed to have two agents, i.e., the ι-th and the κ-th, able to directly measure their reciprocal distance $\sigma_{\iota\kappa} = \sqrt{\mathbf{p}_{\iota\kappa}^\top \mathbf{p}_{\iota\kappa}}$. In this way, it is possible to control the distance between the two agents, for example employing the following controller which moves the estimated positions of agent ι and agent κ along the line connecting them until the estimated distance reaches the true one,

$$\begin{aligned} \dot{\hat{\mathbf{p}}}_\iota &= k_d(\hat{\mathbf{p}}_{\iota\kappa}^\top \hat{\mathbf{p}}_{\iota\kappa} - \sigma_{\iota\kappa}^2)\hat{\mathbf{p}}_{\iota\kappa}, \\ \dot{\hat{\mathbf{p}}}_\kappa &= -k_d(\hat{\mathbf{p}}_{\iota\kappa}^\top \hat{\mathbf{p}}_{\iota\kappa} - \sigma_{\iota\kappa}^2)\hat{\mathbf{p}}_{\iota\kappa}. \end{aligned} \tag{5.5}$$

The validity of this solution can be verified analysing the system governing the estimated inter-agents distance square $\hat{\sigma}_{\iota\kappa}^2 = \hat{\mathbf{p}}_{\iota\kappa}^\top \hat{\mathbf{p}}_{\iota\kappa}$,

$$\frac{d}{dt}\hat{\sigma}_{\iota\kappa}^2 = -2k_d\hat{\sigma}_{\iota\kappa}^2(\hat{\sigma}_{\iota\kappa}^2 - \sigma_{\iota\kappa}^2).$$

First of all, this is a positive system, $\hat{\sigma}_{\iota\kappa}^2 > 0$, therefore the only valid equilibrium point is $\hat{\sigma}_{\iota\kappa}^2 = \sigma_{\iota\kappa}^2$. Then, the sign of the $\frac{d}{dt}\hat{\sigma}_{\iota\kappa}^2$ is controlled by

$$\begin{cases} \frac{d}{dt}\hat{\sigma}_{\iota\kappa}^2 < 0, & \text{if } \hat{\sigma}_{\iota\kappa}^2 > \sigma_{\iota\kappa}^2, \\ \frac{d}{dt}\hat{\sigma}_{\iota\kappa}^2 > 0, & \text{if } \hat{\sigma}_{\iota\kappa}^2 < \sigma_{\iota\kappa}^2, \end{cases}$$

and it is continuous in $\hat{\sigma}_{\iota\kappa}^2 = \sigma_{\iota\kappa}^2$. This is sufficient to conclude that equation (5.5) perfectly drives the estimated inter-agents distance toward the true one. Moreover, the estimated barycentre of the two agents is not affected by the controller, indeed

$$\frac{d}{dt}\left(\frac{1}{2}(\hat{\mathbf{p}}_\iota + \hat{\mathbf{p}}_\kappa)\right) = \mathbf{0}$$

and therefore no drift effect is added.

The idea is to combine the distance controller (5.5) and the estimators (5.1a) and (5.3) in order to reconstruct the configuration of the formation with the correct scale, in the fixed and non-fixed scenario, respectively. If the bearing estimation error converges to zero *and* an estimated inter-agents distance is equal to the true one, then for sure also all the other estimated inter-agents distances coincide to the true ones and the scale is successfully recovered. The new estimators are obtained summing the contributions of the two separate solutions and their interaction is regulated by the gain k_e and k_d. Their final expressions, for the fixed

and non-fixed cases, are respectively,

$$\dot{\hat{\mathbf{x}}} = \mathbf{D}(\hat{\mathbf{q}})\mathbf{u}_L + \mathbf{u}_s, \tag{5.6}$$

$$\dot{\hat{\mathbf{x}}} = \mathbf{D}(\hat{\mathbf{q}})(\mathbf{u}_L + \mathbf{u}) + \mathbf{u}_s, \tag{5.7}$$

where $\mathbf{u}_s = \begin{bmatrix}\mathbf{v}_s^\top & \boldsymbol{\omega}_s^\top\end{bmatrix}^\top \in \mathbb{R}^{6n}$ is the additive component that performs the control of the distance, with

$$\mathbf{u}_s = \begin{bmatrix} \mathbf{0}_{3(\iota-1)\times 1} \\ k_d(\hat{\mathbf{p}}_{\iota\kappa}^\top \hat{\mathbf{p}}_{\iota\kappa} - \sigma_{\iota\kappa}^2)\hat{\mathbf{p}}_{\iota\kappa} \\ \mathbf{0}_{3(\kappa-\iota-1)\times 1} \\ -k_d(\hat{\mathbf{p}}_{\iota\kappa}^\top \hat{\mathbf{p}}_{\iota\kappa} - \sigma_{\iota\kappa}^2)\hat{\mathbf{p}}_{\iota\kappa} \\ \mathbf{0}_{3(n-\kappa)\times 1} \end{bmatrix}, \text{ if } \kappa > \iota, \quad \mathbf{u}_s = \begin{bmatrix} \mathbf{0}_{3(\kappa-1)\times 1} \\ -k_d(\hat{\mathbf{p}}_{\iota\kappa}^\top \hat{\mathbf{p}}_{\iota\kappa} - \sigma_{\iota\kappa}^2)\hat{\mathbf{p}}_{\iota\kappa} \\ \mathbf{0}_{3(\iota-\kappa-1)\times 1} \\ k_d(\hat{\mathbf{p}}_{\iota\kappa}^\top \hat{\mathbf{p}}_{\iota\kappa} - \sigma_{\iota\kappa}^2)\hat{\mathbf{p}}_{\iota\kappa} \\ \mathbf{0}_{3(n-\iota)\times 1} \end{bmatrix}, \text{ if } \kappa < \iota,$$

and $\boldsymbol{\omega}_s = \mathbf{0}_{3n\times 1}$.

However, even if it is proven that the (fixed) estimator and the distance controller works separately, there is no guarantee that they will work if combined together as in (5.6). The next section is entirely dedicated to present simulation results about the application of such estimator. In particular, the effect of the gains $k_e, k_d > 0$ will be highlighted, along with the effects of the choice of the pair (ι, κ).

5.2 Simulations

To evaluate the performances of the estimators, the simulations are divided in three phases. During the former the first estimator given by equation (5.1) on page 66 is tested on a fixed framework. The scale estimator (equation (5.6)) is added in the second phase and tested again on a fixed framework. In the latter phase the complete estimator equation (5.7) is tested in combination with the scale-free control law to perform formation stabilization and distributed agent motion coordination.

5.2.1 Common simulation parameters

Analogously to the simulations performed in the previous chapter, it is considered a 6-agents fully-actuated formation modeled as a framework $(\mathcal{G}, \mathbf{x}(t))$ embedded in $\mathbb{R}^{18} \times \mathbb{S}^{18}$. During the first two phases the true framework is kept fixed and it has configuration $\mathbf{x}_0 \in \mathbb{R}^{18} \times \mathbb{S}^{18}$ which is equal to the one used for the simulations of the controllers (see table 4.3 on

page 54). For the third phase the true framework changes over time because it is subjected to the control algorithms and it is expected to be driven toward the desired configuration $\mathbf{x}_d \in \mathbb{R}^{18} \times \mathbb{S}^{18}$. The initial condition of the estimators is the same in the first two phases and it corresponds to a scaled and perturbed version of the true one

$$\hat{\mathbf{x}}_0 = c\mathbf{x}_0 + \boldsymbol{v},$$

where $c = 2$ is the scale factor and $\boldsymbol{v} \in \mathbb{R}^{42}$ is the perturbation which adds white noise to the positions and random rotations to the orientations of the agents (see figure 5.1 on the next page). However, different initial conditions are used in the third phase.

To measure the performances three cost functions are introduced:

$$J_L(t) = \frac{\|\mathbf{b}_{\mathcal{G}}(\hat{\mathbf{x}}(t)) - \mathbf{b}_{\mathcal{G}}(\mathbf{x}(t))\|^2}{\|\mathbf{b}_{\mathcal{G}}(\hat{\mathbf{x}}_0) - \mathbf{b}_{\mathcal{G}}(\mathbf{x}_0)\|^2}, \tag{5.8}$$

$$J_S(t) = \frac{\left(\hat{\sigma}_{\iota\kappa}(t)^2 - \sigma_{\iota\kappa}(t)^2\right)^2}{\left(\hat{\sigma}_{\iota\kappa}(0)^2 - \sigma_{\iota\kappa}(0)^2\right)^2}, \tag{5.9}$$

$$J_C(t) = \frac{\|\mathbf{b}_{\mathcal{G}}(\mathbf{x}(t)) - \mathbf{b}^*_{\mathcal{G}}\|^2}{\|\mathbf{b}_{\mathcal{G}}(\mathbf{x}_0) - \mathbf{b}^*_{\mathcal{G}}\|^2}. \tag{5.10}$$

Equation (5.8) is the normalized cost function associated to the estimation procedure without accounting for the scale and gives a measure about how the shape of the estimated framework is close to the true one. When the scale estimator is present and the distance $\sigma_{\iota\kappa} = \sqrt{\mathbf{p}_{\iota\kappa}^\top \mathbf{p}_{\iota\kappa}}$ between the ι-th and the κ-th agents is measured, equation (5.9) is the normalize cost function associated to its estimation $\hat{\sigma}_{\iota\kappa}$. Finally, when the formation stabilization task has to be performed, equation (5.10) is the related cost and it corresponds to the normalized version of the one used in the previous chapter.

5.2.2 Phase 1: fixed framework, without recovering the scale

In this simulation the actual frame is maintained fixed and the used estimator is the first that has been proposes which does not recover the scale: equation (5.1) on page 66. The gain k_e is fixed to $k_e = 1000\,\mathrm{s}^{-1}$ and the simulation lasts $10\,\mathrm{s}$. The trajectory of the estimated configuration is reported in figure 5.2a on page 74 while figure 5.2b shows the behaviour of the costs function $J_L(t)$ and $J_S(t)$ supposing that $\iota = 1, \kappa = 2$. The estimator is able to drive the the estimated formation to a BE version of the desired one, in fact its associated cost function has final value $J_L = 1.0956 \times 10^{-7}$. Introducing the angle $e_{L,max} \in (-\pi, \pi]$ as

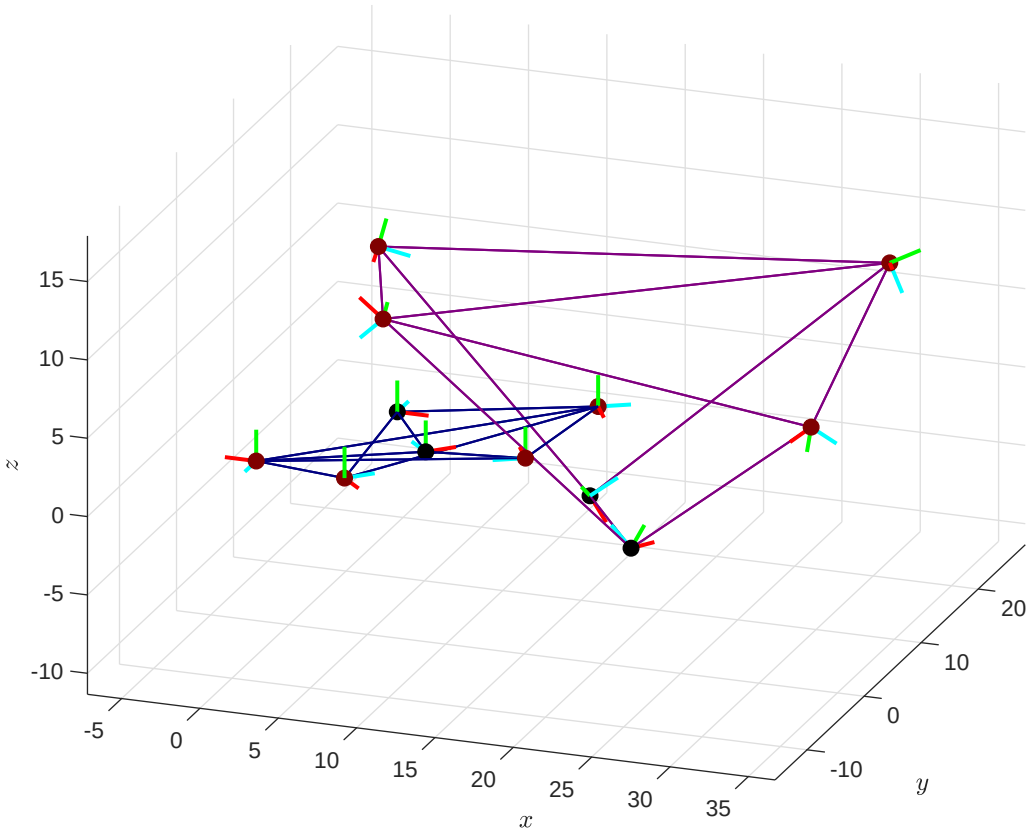

Figure 5.1: Actual and estimated initial frameworks used during the simulations of the estimation algorithms. The edges of the actual initial framework are represented by the dark blue lines while for the ones of the estimated frameworks the purple color is used. Each edge represents a bi-directional measurement. The local frame of each agent is reported, the red, cyan and green vectors represent the local axes $\mathbf{e}_i$, $i \in \{ 1, 2, 3 \}$, respectively.

the maximum error between the true bearing measurements and its final estimate

$$e_{L,max} \coloneqq \max_{(i,j)\colon (v_i,v_j)\in\mathcal{E}} \arccos(\hat{\mathbf{b}}_{ij}(t_{end})^\top \mathbf{b}_{ij}),$$

it results that $e_{L,max} = 0.0595^\circ$. Moreover, as expected, the scale is not recovered: the final cost is $J_S = 0.3504$ and, in a clearer way, $\hat{\sigma}_{\iota\kappa}/\sigma_{\iota\kappa} = 2.3757$.

5.2.3 Phase 2: fixed framework, recovering the scale

Here, the scale estimator is added and therefore, being the actual framework still fixed, the adopted estimator law is

$$\dot{\hat{\mathbf{x}}} = \mathbf{D}(\hat{\mathbf{q}})\mathbf{u}_L + \mathbf{u}_s. \qquad \text{(5.6 revisited)}$$

Ten different simulations are computed, with two pairs (ι, κ) representing the agents that are able to measure their reciprocal distance and up to 6 values of k_d. It may happen that the distance controller is able to match the estimated distance $\hat{\sigma}_{\iota\kappa}$ and the cost $J_L(t)$ is low, but the formation scale is not recovered. To detect this situation the index $s_{max} \geqslant 1$ is defined as

$$s_{max} = \max_{(i,j):(v_i,v_j)\in\mathcal{E}} \begin{cases} \hat{\sigma}_{ij}/\sigma_{ij} & \text{if } \hat{\sigma}_{ij} \geqslant \sigma_{ij} \\ \sigma_{ij}/\hat{\sigma}_{ij} & \text{otherwise} \end{cases}.$$

If $s_{max} \not\approx 1$ when $\hat{\sigma}_{\iota\kappa}/\sigma_{\iota\kappa} \approx 1$ and the cost $J_L(t)$ is low then it can be concluded that the pair (ι, κ) is not a good choice and another should be tried.

The simulation duration is equal to 20 s and final results are summarized in table 5.1 on page 75. The performances choosing $(\iota, \kappa) = (1, 2)$ are analysed first. When the gain of the distance estimator is high, $k_d = 1\,\mathrm{s}^{-1}$, the distance of the pair (ι, κ) is recovered with a relative error smaller than the $1\,\%$.[1] Nevertheless, nor the formation shape is correctly recovered, as shown by $J_L(t_{end}) = 3.9833 \times 10^{-4}$ and $e_{L,max} = 3.4055$, nor the distance of the other agent is correctly estimated ($s_{max} = 1.8038$). Decreasing the gain k_d in order to improve the shape recovering does not leads to the desired results: each time the gain is divided by ten the cost J_L almost remains unchanged but on the other hand the order of magnitude of J_S increases by one. At the and, for $k_d = 0.001$ the shape in not recovered and the same applies for the scale. This allows to conclude that $(\iota, \kappa) = (1, 2)$ is not a good choice.

[1] It may seem strange to have such different magnitude for the gain values k_e, k_d. However this is normal because $\mathbf{u}_L \propto 1/\sigma_{\iota\kappa}$, while $\mathbf{u}_s \propto \sigma^4_{\iota\kappa}$.

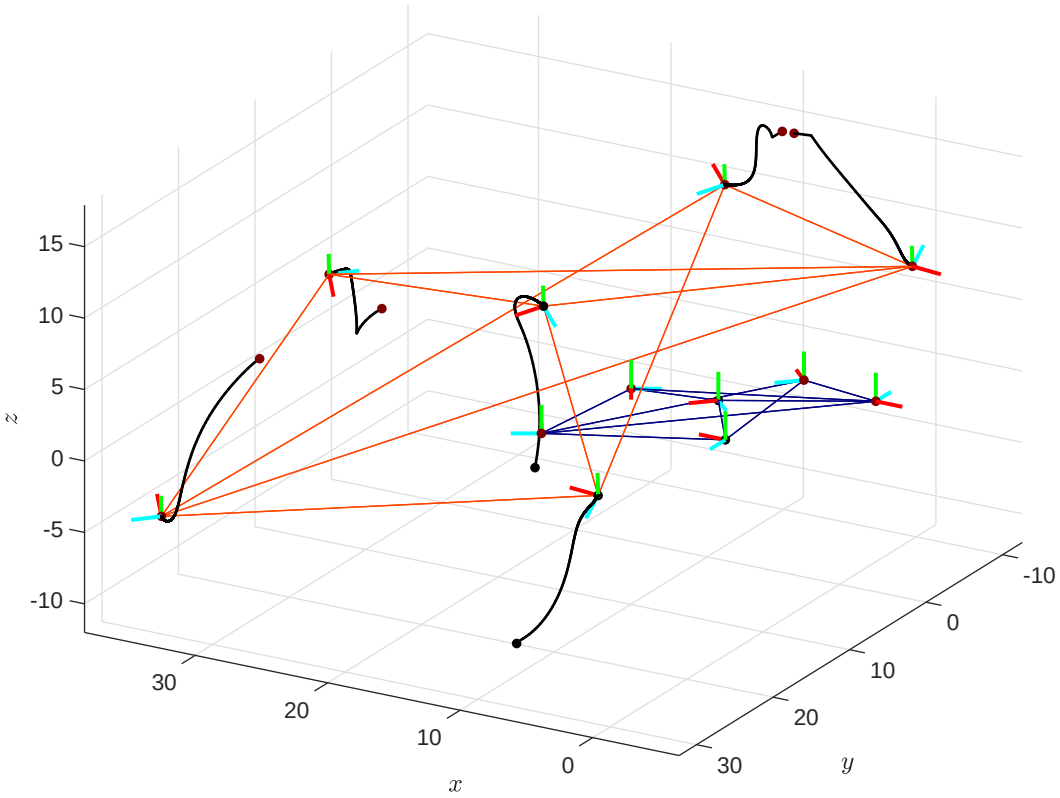

(a)

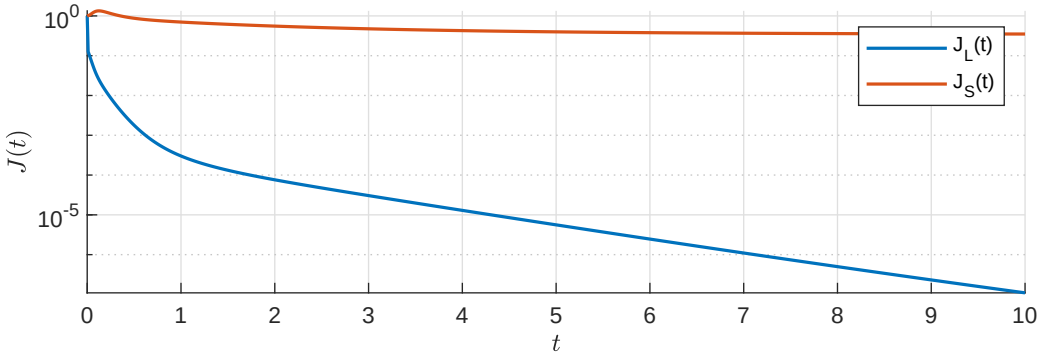

(b)

Figure 5.2: Trajectory of the estimated configuration when the estimator law equation (5.1) on page 66 is applied to a fixed fully-actuated formation (a). The blue edges represent the actual, fixed framework; the black lines are the trajectories, starting from the initial guess (whose edges are not drawn) and terminating at the final estimated framework (orange red edges). Behaviour of the cost functions in logarithmic scale (b). The estimator drives to zero the cost $J_L(t)$ but as expected it does not recover the scale.

Table 5.1: Comparison of the simulation results when the estimator recovering the scale is employed and the actual framework is fixed. The simulation has a duration of $20\,\mathrm{s}$. Two different pairs (ι, κ) of agents capable to measure their distance are tested; the formation estimator gain k_e is fixed to $1000\,\mathrm{s}^{-1}$ while the gain of the scale estimator k_d is changed.

		$(\iota, \kappa) = (1, 2)$			
$k_d\,[\mathrm{s}^{-1}]$	$J_L(t_{end})$	$e_{L,max}\,[^\circ]$	$J_S(t_{end})$	$\hat{\sigma}_{\iota\kappa}/\sigma_{\iota\kappa}$	s_{max}
10^{0}	3.9833×10^{-4}	3.4055	2.7859×10^{-6}	1.0065	1.8038
10^{-1}	3.7646×10^{-4}	3.3120	2.6706×10^{-5}	1.0201	1.7959
10^{-2}	3.2109×10^{-4}	3.0619	2.3680×10^{-4}	1.0586	1.7784
10^{-3}	2.2158×10^{-4}	2.5482	1.7733×10^{-3}	1.1534	1.7647
		$(\iota, \kappa) = (3, 5)$			
$k_d\,[\mathrm{s}^{-1}]$	$J_L(t_{end})$	$e_{L,max}\,[^\circ]$	$J_S(t_{end})$	$\hat{\sigma}_{\iota\kappa}/\sigma_{\iota\kappa}$	s_{max}
10^{1}	4.9821×10^{-14}	2.404×10^{-5}	1.0980×10^{-12}	1.0000	1.0000
10^{0}	4.2122×10^{-13}	5.135×10^{-5}	3.3743×10^{-11}	1.0000	1.0000
10^{-1}	6.7331×10^{-12}	3.754×10^{-4}	1.3994×10^{-9}	1.0001	1.0001
10^{-2}	1.6529×10^{-10}	1.869×10^{-3}	7.0862×10^{-8}	1.0007	1.0009
10^{-3}	5.0397×10^{-9}	1.035×10^{-2}	3.9326×10^{-6}	1.0055	1.0065
10^{-4}	1.2950×10^{-7}	5.245×10^{-2}	1.8851×10^{-4}	1.0373	1.0426

The system performs quite differently if $(\iota, \kappa) = (3, 5)$. In this situation it seems that it is always possible to use an arbitrary high gain k_d to obtain arbitrary high performances. Notice, however, that bigger values of k_d implies bigger magnitude of the input $\mathbf{u}_s$. Even if that is not a real input for the actual formation and it is only used by the estimator, it may leads to problems when the algorithm are discretized in order to be implemented in real world scenarios. The two pairs $(\iota, \kappa) = (3, 5)$ and $(k_e, k_d) = (10^3, 10^{-1})$ are selected to be the best choice for this kind of controller applied to this particular framework. Notice, indeed, that a framework having a different graph $\mathcal{G}$ would have probably led to an different optimal pair (ι, κ). The trajectory of the estimated configuration and the behaviour of the cost functions are reported in figure 5.3. Inspecting the two figures the estimated distance $\hat{\sigma}_{\iota\kappa}$ is driven toward the true one in the first instants of the simulation, indeed $J_S(0.5\,\mathrm{s}) = 1.7207 \times 10^{-7}$ and $\hat{\sigma}_{\iota\kappa}(0.5\,\mathrm{s})/\sigma_{\iota\kappa}(0.5\,\mathrm{s}) = 1.0011$. As the simulation proceeds, the shape is correctly estimated.

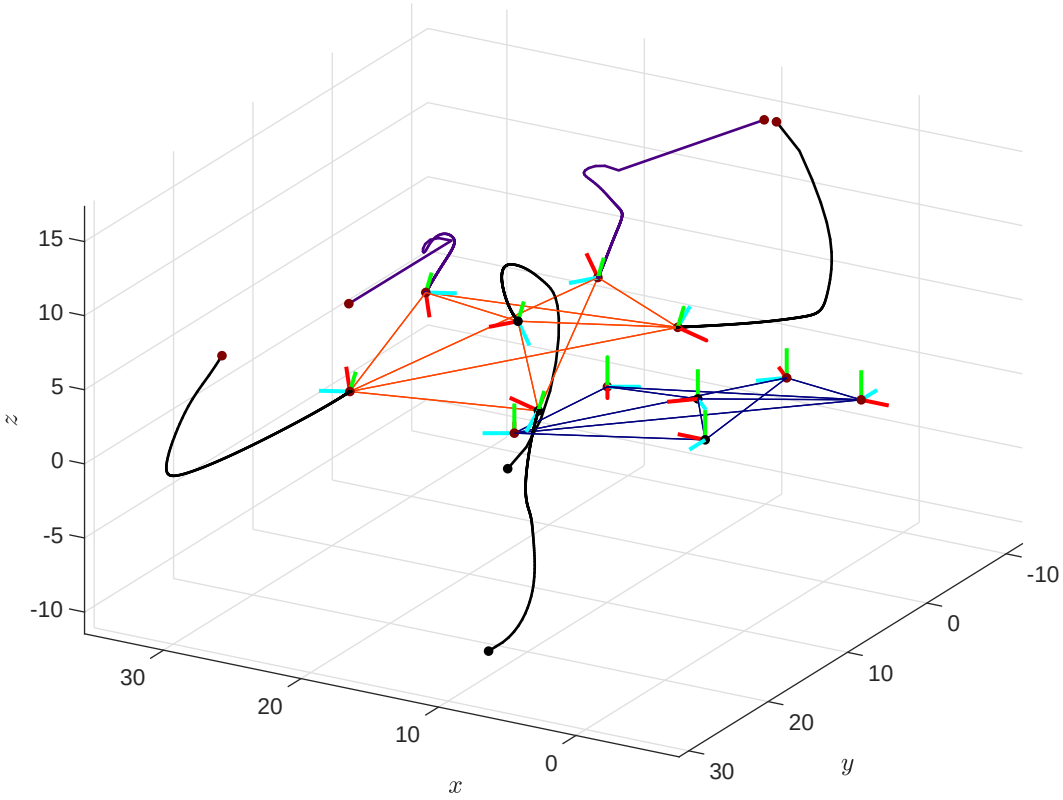

(a)

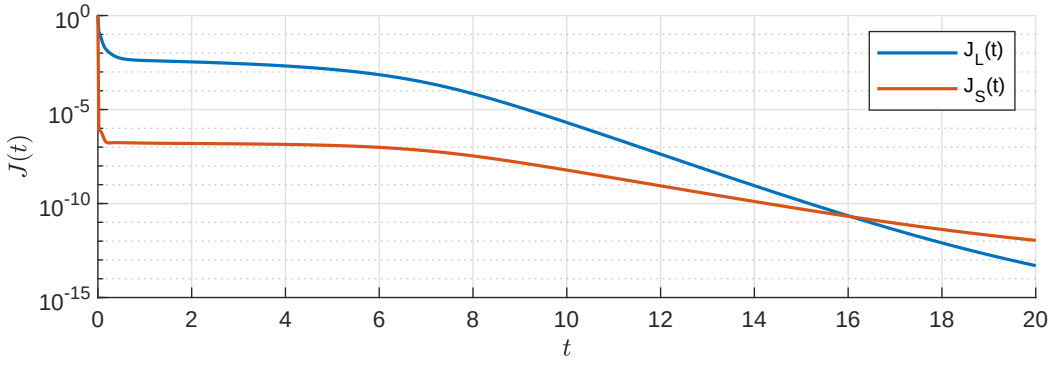

(b)

Figure 5.3: Trajectory of the estimated configuration when the estimator law equation (5.6) on page 70 is applied to a fixed fully-actuated formation (a). The blue edges represent the actual, fixed framework; The trajectories of each agent start from the initial guess (whose edges are not drawn) they terminate at the final estimated framework (orange red edges). Indigo is used for the ones associated to agents ι and κ while the ones for the other agents are in black. Behaviour of the cost functions in logarithmic scale (b). The estimator drives to zero both the cost functions.

5.2.4 Phase 3: dynamic framework

The last phase uses the previous results to perform the control of the underling fully-actuated framework. The estimated state is fed to the two control algorithms discussed in chapter 4, namely, a formation *regulator* is employed. The initial conditions are $\mathbf{x}(0) = \mathbf{x}_0$ and $\hat{\mathbf{x}}(0) = \hat{\mathbf{x}}_0$, the desired configuration is $\mathbf{x}_d$. These value have been chosen, in order to present in clearer way the results and they differ from the previous ones. For this reason, also the gain k_e, k_s, k_c are different. The equations governing the systems (the true formation and the estimator) are

$$\dot{\mathbf{x}} = \mathbf{D}(\mathbf{q})\mathbf{u}, \qquad \text{(4.4 revisited)}$$

$$\mathbf{u} = \mathbf{u}_{stab} + \mathbf{u}_{coord}, \qquad \text{(5.11a)}$$

$$\mathbf{u}_{stab} = k_c\big(\tilde{\mathbf{B}}_{\mathcal{G}}(\mathbf{x}, \hat{\mathbf{x}})\big)^{\top}\mathbf{b}^*_{\mathcal{G}} \qquad \text{(5.11b)}$$

$$\dot{\hat{\mathbf{x}}} = \mathbf{D}(\hat{\mathbf{q}})(\mathbf{u}_L + \mathbf{u}) + \mathbf{u}_s, \qquad \text{(5.7 revisited)}$$

$$\mathbf{u}_L = k_e\big(\mathbf{B}_{\mathcal{G}}(\hat{\mathbf{x}})\big)^{\top}\mathbf{b}_{\mathcal{G}}(\mathbf{x}). \qquad \text{(5.1b revisited)}$$

The first equation models the dynamics of a fully-actuated formation subjected to the input vector $\mathbf{u} \in \mathbb{R}^{6n}$. The fourth and the fifth are the most complete equations for the estimator, accounting for the recovery of the scale and for additional, known inputs. Equation (5.11a) expresses the input of the true formation as the sum of the one generated by the formation stabilizer and the one associated to the distributed agent motion coordination task. Equation (5.11b) is similar to the control law for the formation stabilization task (equation (4.11) on page 45) but at the same time is quite different. In fact, the scale-free bearing rigidity matrix is substituted by $\tilde{\mathbf{B}}_{\mathcal{G}}(\mathbf{x}, \hat{\mathbf{x}})$ which has the row block associated to the edge $(v_i, v_k) \in \mathcal{E}$ as

$$\begin{cases} \begin{bmatrix} \mathbf{0}_{3\times 3(i-1)} & -\mathbf{P}(\mathbf{b}_{ij}) & \mathbf{0}_{3\times 3(j-i-1)} & \mathbf{P}(\mathbf{b}_{ij})\mathbf{R}(\hat{\mathbf{q}}_i)^{\top}\mathbf{R}(\hat{\mathbf{q}}_j) \\ & \mathbf{0}_{3\times(3(n-j)+3(i-1)} & [\mathbf{b}_{ij}]_{\times} & \mathbf{0}_{3\times 3(n-i)} \end{bmatrix} & \text{if } i < j, \\ \begin{bmatrix} \mathbf{0}_{3\times 3(j-1)} & \mathbf{P}(\mathbf{b}_{ij})\mathbf{R}(\hat{\mathbf{q}}_i)^{\top}\mathbf{R}(\hat{\mathbf{q}}_j) & \mathbf{0}_{3\times 3(i-j-1)} & -\mathbf{P}(\mathbf{b}_{ij}) \\ & \mathbf{0}_{3\times(3(n-i)+3(i-1)} & [\mathbf{b}_{ij}]_{\times} & \mathbf{0}_{3\times 3(n-i)} \end{bmatrix} & \text{if } i < j, \end{cases}$$

namely, it is a scale-free version of a bearing rigidity matrix computed using the true bearing measurements and the estimated orientations. Finally, $\mathbf{u}_{coord} \in \mathbb{R}^{6n}$, which is responsible

for the coordinated motions of the agents, is composed by the terms

$$\begin{cases} \mathbf{v}_i = \mathbf{R}(\hat{\mathbf{q}}_i)^\top \left(\mathbf{s}^* + c^*(\hat{\mathbf{p}}_i - \hat{\bar{\mathbf{p}}}) + [\mathbf{r}^*]_\times (\hat{\mathbf{p}}_i - \hat{\bar{\mathbf{p}}}) \right) \\ \boldsymbol{\omega}_i = \mathbf{R}(\hat{\mathbf{q}}_i)^\top \mathbf{r}^* \end{cases} . \tag{5.12}$$

where once again the estimated orientations, but also the estimated position (and barycentre) are used.

The simulations is initially performed with $\mathbf{u}_{coord} = \mathbf{0}_{6n \times 1}$ in order to let the estimator and the formation stabilizer to reach their own equilibria. Then a coordinated vertical translation is performed. The behaviour of the cost function is reported in figure 5.4 on the facing page where it is made evident that the estimator is perfectly able to recover the shape and the scale of the formation. To understand the performances of the controller, it is easier to observe the index equation (4.23) on page 57 which is equal to $e_{max} = 3.4631^\circ$ which is clearly not comparable with the value reached by the estimator: $e_{L,max} = 2.7147 \times 10^{-5^\circ}$. The reason is probably related to the gain k_c being too low w.r.t. k_e, k_S. However, an higher k_c could lead to unexpected behaviour at the initial phases of the simulation, when the estimator is not at steady state. In fact, if the magnitude of the input known input $\mathbf{u}$ is high, then the perturbation $\left(\mathbf{B}_{\mathcal{G}}(\mathbf{x}) - \mathbf{B}_{\mathcal{G}}(\hat{\mathbf{x}})\right)\mathbf{u}$ affecting the dynamics of the estimation error equation (5.4) on page 68 could make the system unstable.

The trajectory of the estimated framework is shown in figure 5.5 on page 80 while the one of the actual formation are represented in figure 5.6 on page 81 along with the desired shape. The most noticeable fact is the demonstration that the estimator generates a roto-translated version of the true framework. In particular, the true orientation of the agents is recovered with a fixed and common offset. The distributed agent motion coordinator computes $\mathbf{u}_{coord}$ in equation (5.12) necessary to perform a vertical translation using the estimated orientation. A vertical translation w.r.t. the unknown inertial frame $\mathcal{F}_W$ is desired, but in the end it is obtained w.r.t. the rotated inertial frame $\mathcal{F}_{W'}$. The simulation confirm this because the estimated configuration correctly translates vertically while the true formation moves in a different direction. Nevertheless given any direction in $\mathbf{d} \in \mathbb{S}^2$, a coordinated translation along $\mathbf{d}$ is always a trivial variation for fully-actuated agents, therefore the formation stabilizer is not affected.

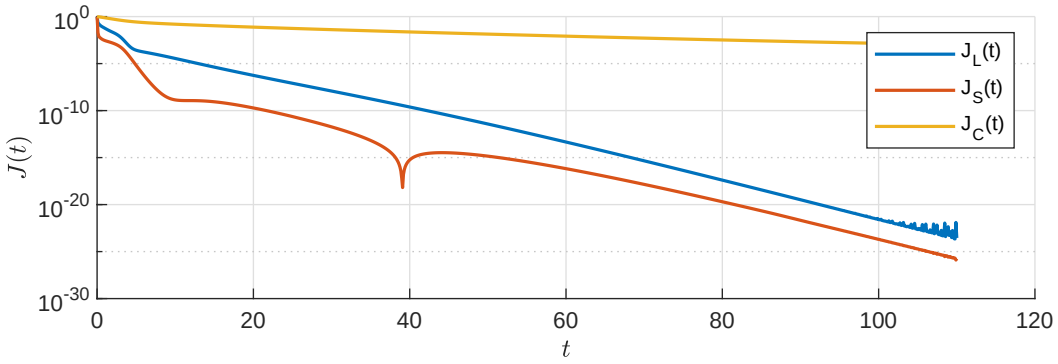

Figure 5.4: Cost functions associated to the evaluation of the regulator. It is evident that the estimator fully recover the shape of the formation with the correct scale. On the other hand the controller, has a convergence rate much slower than the ones of the others.

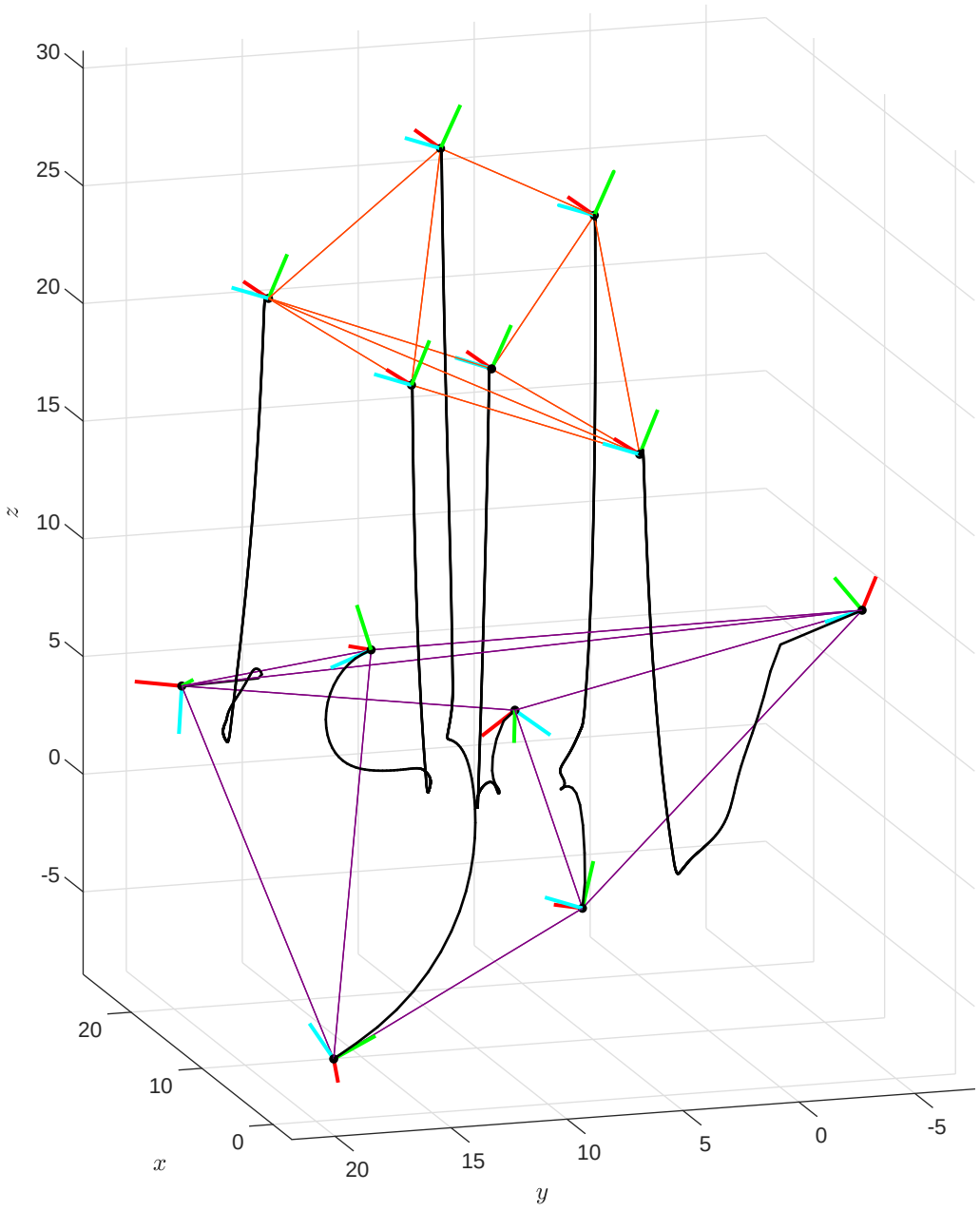

Figure 5.5: Estimated trajectories associated to the evaluation of the regulator (black lines). The initial configuration and final configuration of the estimator are drawn in purple and orange red, respectively. The effect of the distributed agent motion coordinator are made evident by the vertical translation.

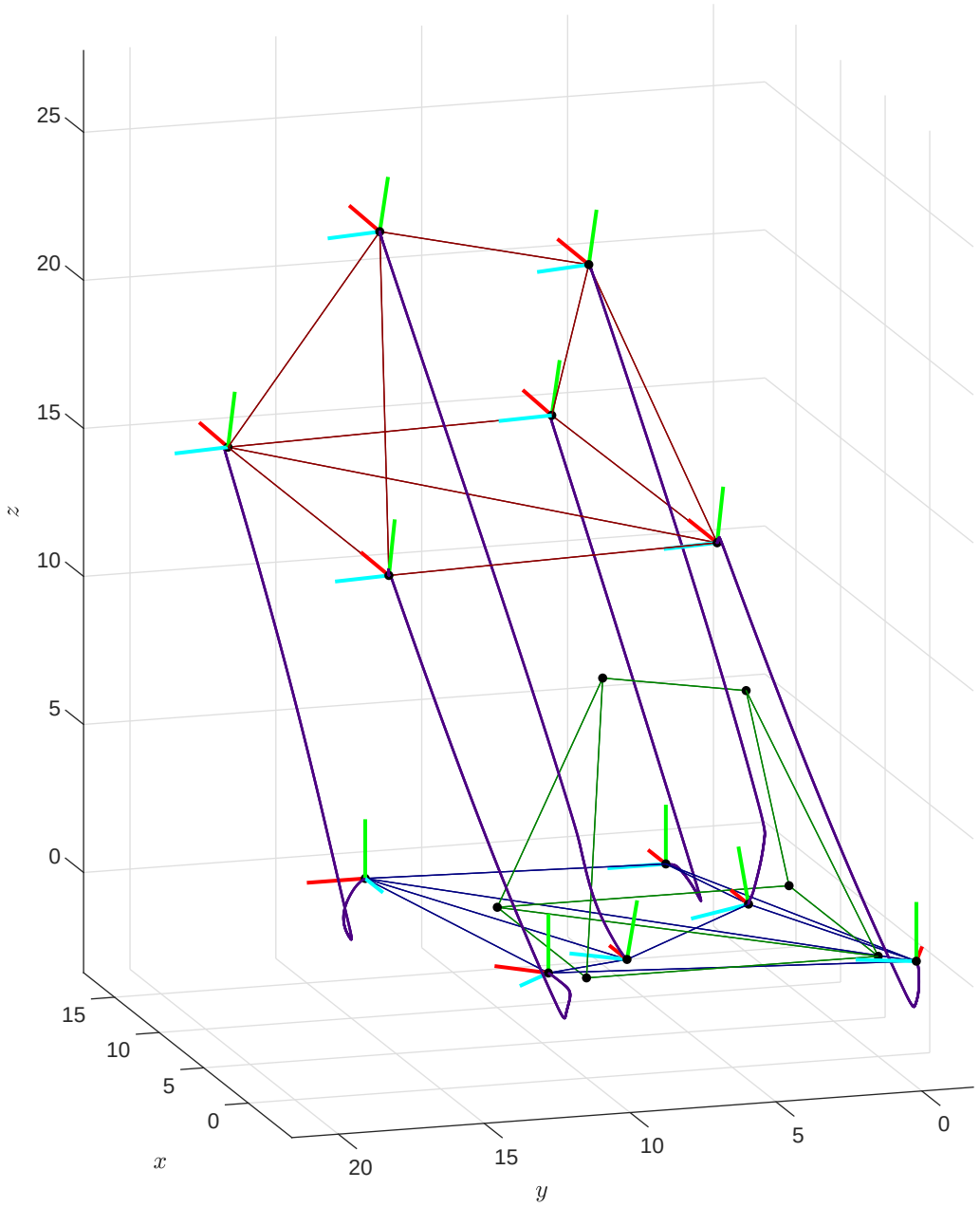

Figure 5.6: True trajectories associated to the evaluation of the regulator (indigo lines). The initial configuration and final configuration are drawn in navy blue and dark red, respectively. The desired configuration is in dark green. The effect of the distributed agent motion coordinator having a common offset applied to the orientations are made evident by the non-vertical translation.

6

Conclusion and Future Work

In this thesis the applications of the bearing rigidity theory to the control and the localization of multiagent formations operating in GPS-denied environment have been studied, starting from the work of Michieletto et al. [4]. In such situations the agents composing the formation can only rely on data coming from *inside* the formation itself, namely, inter-agents measurements. The bearing rigidity theory exploits in particular inter-agents *bearing* measurements which are nowadays easily acquired through, for example, optical cameras.

This mathematical tool models a multiagent formation as a framework, composed by the *configuration* of each agent and a graph representing the interaction of the agents; in this way it defines and characterizes the concept of *rigidity*. A frameworks is said to be rigid if every variation of the shape of the formation is detected by a variation of the measurement and vice versa. For frameworks composed by fully-actuated agents having their configuration belonging to the same metric space, meaning, for frameworks composed by agents having a reachable configuration domain, the rigidity condition is characterized by a particular matrix called bearing rigidity matrix. Inspecting the bearing rigidity matrix is not only possible to state if a formation is rigid or not, but also it is possible to identify the commands to be applied to the agents that preserve the shape of the formation. The most important configuration domains: $\mathbb{R}^2 \times \mathbb{S}^1$, $\mathbb{R}^3 \times \mathbb{S}^1$ and $SE(3)$, which are related to real world application dealing with fully-actuated unmanned ground vehicles and unmanned aerial vehicles (under actuated and fully-actuated), respectively, have been studied and their rigidity properties characterized. In particular, these three kind of formation are rigid if their bearing rigidity

matrices have null spaces with dimension 4, 5, 7, respectively. Moreover, the sets of commands that preserve the shape of the formations, the trivial variation sets, are composed (by up to three) independent coordinated translations, a scaling and (up to three) coordinated rotations.

The bearing rigidity theory can also be applied to perform distributed control of multiagent formations. Distributed control laws based on the bearing rigidity matrix, capable to drive a formation from an arbitrary initial condition to a desired shape, has been proposed and their validity has been tested analytically and through simulations.

The main contribution of this thesis is divided in three topics. The characterization of the bearing rigidity properties has been extended to formations composed by different kind of agents, namely, by agents having different configuration domains. In order to deal with such formations, a new concept of framework has been introduced, the *mixed* framework. Using mixed frameworks all the agents are embedded in the same configuration domain $SE(3)$ which is the right choice to encode the pose of rigid bodies in the real world. The differences between the agents are instead modeled accounting for different actuation capabilities and therefore considering different command domains. It has been shown that the rigidity condition is still characterized by the bearing rigidity matrix. More importantly, it has been proven that the bearing rigidity matrix of a mixed framework can be computed starting from the one of the associated fully-actuated twin and then it can be completed taking into account the different actuation capabilities of the agents. This fact allows to easily evaluate the bearing rigidity matrix for different mixed frameworks and it imposes strong relation between the trivial variation spaces. The commands that keep the shapes of the mixed formations unchanged are in fact subsets of the ones that keep the shapes of the fully-actuated twin. This general result has been specified for two types of mixed formation of interest, namely the ones composed by agents with configuration domains $\mathbb{R}^2 \times \mathbb{S}^1$ and $SE(3)$, and the ones with configuration domains $\mathbb{R}^3 \times \mathbb{S}^1$ and $SE(3)$.

The second major contribution is related to the control of mixed formations. After converting the configuration domain from $SE(3)$ to $\mathbb{R}^3 \times \mathbb{S}^3$ in order to use quaternions to represent the orientation of the agents, it has been shown that the control law proposed for non-mixed formation can be perfectly applied to mixed ones. It has also been proven that, if the convergence gains are matched such that the steady state behaviours are the same, the control law based on the bearing rigidity matrix has better performances that the scale-free one. This observation is in accordance to the fact that without removing the scale, the proposed control law is the closest to the one based on the unconstrained gradient descent, which has

the best performances but can not be applied.

Finally a solution for the distributed location estimation problem for non-mixed formation embedded in $\mathbb{R}^3 \times \mathbb{S}^3$, which was still missing, has been proposed and it validity proved analytically and through simulation. In particular it has been shown that the proposed location estimator is able to generate a common inertial frame, known by all the agents, which corresponds to a roto-translated version of the true one. In order to correctly estimate the scale of the formation, another estimator has been proposed. This latter version is different from the previous because it assume to be able to measure the distance between two agents. The validity of such estimator has been tested through simulation and the complete distributed bearing based *regulator* (controller and location estimator) has been introduced and tested.

This thesis provides a few starting points for the developing of future works.

- Regarding the characterization of mixed formations, the *static* bearing rigidity properties have been not taken into account. The reason is that the differences between the agents have been modeled though different instantaneous variation sets, which do not affect the static rigidity properties. Nevertheless it remains interesting to be able to include also these properties in the theory and to do so it is required to modify the definition of mixed framework.

- All the considered mixed frameworks are characterized by *linear* constraints that reduce the actuation capability of the agents. The characterization of more complex, specific formation is still missing.

- Even if the simulations confirm the conjecture, the analytical proof of the stability of the closed loop system when the scale-free control law is adopted has not been found yet. Moreover, at the moment, the control law itself can not be employed to real formation. Firstly, is expressed in continuous time, while the modern hardware requires it to have a discrete formulation; it is therefore required to discretize the controller (and also the location estimator). The control law requires communication between the agents. Considering that it is quite not a good idea to have wires connecting the agents, wireless communication must be used and therefore the presence of delay and the possibility of packet losses must be taken into account. Finally, it is interesting to analyse the robustness of the proposed control law against disturbances and noise.

- Migrating toward the location estimator, it has already been said that it also need to be distretized. Its robustness to noises and disturbances should be analysed too. At the moment, the location estimator can not perfectly recover the poses of the agents w.r.t. the true global inertial frame. The reason is that it is based only on inter-agents

measurements and therefore no knowledge regarding the surrounding of the formation is acquired and processed. Letting some agents to sense information from outside the formation and using this data together the one produced by the estimator could provide absolute estimated location.

- From a single bearing vector it is impossible to recover the scale of the formation. However, a *dynamic* estimator, namely an estimator exploits the dynamic behaviour of the formation could succeed in the tasks without breaking the bearing-only requirement.

A

Additional Proofs

A.1 Time derivatives of interest

A.1.1 Time derivative of rotation matrices

This section is dedicated to the expressions of the time derivative of a rotation matrix $\mathbf{R}_{W,b} \in SO(3)$ representing the orientation of the frame $\mathcal{F}_b$ attached to a rigid body w.r.t. an inertial frame $\mathcal{F}_W$ when an angular rate $\boldsymbol{\omega}$ is applied. Consider a point P in the 3D space, its coordinates, expressed in an inertial frame, are denoted with the vector $\mathbf{p} \in \mathbb{R}^3$. Assume that P possesses an angular rate $\boldsymbol{\omega} \in \mathbb{R}^3$, that has axis $\boldsymbol{\omega}/\|\boldsymbol{\omega}\| \in \mathbb{S}^2$ passing though the origin of the inertial frame and magnitude $\|\boldsymbol{\omega}\| > 0$, i.e., P moves with uniform circular motion. Under this conditions the time derivative of the position vector $\mathbf{p} \in \mathbb{R}^3$ is

$$\dot{\mathbf{p}} = \boldsymbol{\omega} \times \mathbf{p}. \tag{A.1}$$

W.l.o.g. the same equation applies if $\mathbf{p} \in \mathbb{R}^3$ is substituted by the vector representing the coordinates, expressed in the inertial frame, of the one of the axis of $\mathcal{F}_b$ and $\boldsymbol{\omega} \in \mathbb{R}^3$ is expressed too in the inertial frame. Be $\mathbf{e}_{w,i} \in \mathbb{S}^2$, $i \in \{1, 2, 3\}$ the vectors representing the canonical vectors $\mathbf{e}_i \in \mathbb{S}^2$, axes of frame $\mathcal{F}_b$, w.r.t. the inertial frame $\mathcal{F}_W$, namely $\mathbf{e}_{w,i} = \mathbf{R}_{W,b}\mathbf{e}_i$. Moreover, be $\boldsymbol{\omega}_w \in \mathbb{R}^3$ the vector stacking the coordinates of $\boldsymbol{\omega} \in \mathbb{R}^3$ expressed in

the inertial frame. Then, equation (A.1) takes form

$$\dot{\mathbf{e}}_{w,i} = \boldsymbol{\omega}_w \times \mathbf{e}_{w,i}.$$

Notice that $\mathbf{e}_{w,i} \in \mathbb{S}^2$, $i \in \{1, 2, 3\}$ are strictly related to $\mathbf{R}_{W,b} \in SO(3)$: they coincide with the i-th column of $\mathbf{R}_{W,b}$, respectively. This fact, together with the properties of the skew-symmetric matrices, allows to state the following

$$\dot{\mathbf{R}}_{W,b} = [\boldsymbol{\omega}_w]_\times \mathbf{R}_{W,b}, \tag{A.2}$$

which formulates the time derivative of a rotation matrix that represents the orientation of the frame $\mathcal{F}_b$ w.r.t the frame $\mathcal{F}_W$ when the angular rate is expressed in the frame $\mathcal{F}_W$. It is interesting to notice that the fact of $\mathcal{F}_W$ being inertial was not exploited in this reasoning, therefore equation (A.2) still holds even if both frames are not inertial.

The only case left is the one where $\boldsymbol{\omega} \in \mathbb{R}^3$ is represented in the frame $\mathcal{F}_b$, i.e., $\boldsymbol{\omega}_b = \mathbf{R}_{W,b}^\top \boldsymbol{\omega}_w$. If the roles of the frames are switched, equation (A.2) takes form

$$\dot{\mathbf{R}}_{b,W} = [\hat{\boldsymbol{\omega}}_b]_\times \mathbf{R}_{b,W},$$

where $\mathbf{R}_{b,W} = \mathbf{R}_{W,b}^\top \in SO(3)$ is the rotation matrix representing the orientation of $\mathcal{F}_W$ w.r.t. $\mathcal{F}_b$ and $\hat{\boldsymbol{\omega}}_b \in \mathbb{R}^3$ is an angular rate expressed in $\mathcal{F}_b$. However, in order to have equation (A.2) and section A.1.1 representing the *same* rotation, it must be

$$\hat{\boldsymbol{\omega}}_b = -\boldsymbol{\omega}_b = \mathbf{R}_{W,b}^\top \boldsymbol{\omega}_w$$

and thus, it holds that

$$\dot{\mathbf{R}}_{W,b} = \left(\dot{\mathbf{R}}_{b,W}\right)^\top = \mathbf{R}_{b,W}^\top [-\boldsymbol{\omega}_b]_\times^\top = \mathbf{R}_{W,b} [\boldsymbol{\omega}_b]_\times. \tag{A.3}$$

From equations (A.2) and (A.3) some other interesting equalities result

$$\begin{aligned}
[\boldsymbol{\omega}_w]_\times \mathbf{R}_{W,b} &= \mathbf{R}_{W,b} [\boldsymbol{\omega}_b]_\times \\
[\boldsymbol{\omega}_w]_\times &= \mathbf{R}_{W,b} [\boldsymbol{\omega}_b]_\times \mathbf{R}_{W,b}^\top \\
[\mathbf{R}_{W,b} \boldsymbol{\omega}_b]_\times &= \mathbf{R}_{W,b} [\boldsymbol{\omega}_b]_\times \mathbf{R}_{W,b}^\top \\
\mathbf{R}_{W,b}^\top [\boldsymbol{\omega}_w]_\times \mathbf{R}_{W,b} &= [\boldsymbol{\omega}_b]_\times
\end{aligned}$$

A.1.2 Time derivative of unit quaternions

Proposition A.1. *Given the unit quaternion* $\mathbf{q}_i \in \mathbb{S}^3$ *representing the orientation of* $\mathcal{F}_i$ *w.r.t.* $\mathcal{F}_W$*, its time derivative has expression*

$$\dot{\mathbf{q}}_i = \frac{1}{2}\boldsymbol{\omega}_w^+ \circ \mathbf{q}_i,$$

where $\boldsymbol{\omega}_w^+ = \begin{bmatrix} 0 & \boldsymbol{\omega}_w^\top \end{bmatrix}^\top \in \mathbb{R}^4$*, with* $\boldsymbol{\omega}_w \in \mathbb{R}^3$ *an angular rate expressed in* $\mathcal{F}_W$*.*

Proof. Let $\mathbf{x}_0^+ \in \mathbb{R}^4$ be any given vector (quaternion with zero scalar part) *fixed* at time t_0 and $\mathbf{x}_t^+ \in \mathbb{R}^4$ the same vector at time t. The two can be related trough the unit quaternion $\mathbf{q}_t$,

$$\mathbf{x}_t^+ = \mathbf{q}_t \circ \mathbf{x}_o^+ \circ \mathbf{q}_t^{-1}. \tag{A.4}$$

Differentiating (A.4), it results

$$\dot{\mathbf{x}}_t^+ = \dot{\mathbf{q}}_t \circ \mathbf{x}_o^+ \circ \mathbf{q}_o^{-1} + \mathbf{q}_t \circ \mathbf{x}_o^+ \circ \dot{(\mathbf{q}_t^{-1})}. \tag{A.5}$$

From equations (A.4) and (A.5) it holds

$$\dot{\mathbf{x}}_t^+ = \dot{\mathbf{q}}_t \circ \mathbf{q}_t^{-1} \circ \mathbf{x}_t^+ + \mathbf{x}_t^+ \circ \mathbf{q}_t \circ \dot{(\mathbf{q}_t^{-1})}. \tag{A.6}$$

The norm of quaternion is unit and $\mathbf{q}_t \circ \mathbf{q}_t^{-1} = 1$, therefore

$$\frac{d}{dt}\mathbf{q}_t \circ \mathbf{q}_t^{-1} = \dot{\mathbf{q}}_t \circ \mathbf{q}_t^{-1} + \mathbf{q}_t \circ \dot{(\mathbf{q}_t^{-1})} = 0. \tag{A.7}$$

It follows from equations (A.6) and (A.7) that

$$\dot{\mathbf{x}}_t^+ = \dot{\mathbf{q}}_t \circ \mathbf{q}_t^{-1} \circ \mathbf{x}_t^+ - \mathbf{x}_t^+ \circ \dot{\mathbf{q}}_t \circ \mathbf{q}_t^{-1}.$$

Let

$$\mathbf{p}_t^+ = \dot{\mathbf{q}}_t \circ \mathbf{q}_t^{-1} \in \mathbb{R}^4,$$

then, denoting with $\eta(\mathbf{q})$ and $\boldsymbol{\varepsilon}(\mathbf{q})$ the scalar and imaginary parts of the quaternion $\mathbf{q} \in \mathbb{S}^3$, $\eta(\mathbf{p}_t^+)$ is equal to

$$\eta(\mathbf{p}_t^+) = \eta(\dot{\mathbf{q}}_t)\eta(\mathbf{q}_t^{-1}) - \boldsymbol{\varepsilon}(\dot{\mathbf{q}}_t)^\top \boldsymbol{\varepsilon}(\mathbf{q}_t^{-1}) = \eta(\dot{\mathbf{q}}_t)\eta(\mathbf{q}_t) + \boldsymbol{\varepsilon}(\dot{\mathbf{q}}_t)^\top \boldsymbol{\varepsilon}(\mathbf{q}_t) = 0,$$

because the norm of $\mathbf{q}_t$ is unit and $\eta(\mathbf{p}_t^+)$ is half of its derivative, $\eta(\mathbf{p}_t^+) = \frac{1}{2}\frac{d}{dt}\|\mathbf{q}_t\|$. Then, $\eta(\mathbf{p}_t^+)$ is a pure quaternion, and being also $\mathbf{x}_t^+$ a pure quaternion, it holds that

$$\dot{\mathbf{x}}_t^+ = \mathbf{p}_t^+ \circ \mathbf{x}_t^+ - \mathbf{x}_t^+ \circ \mathbf{p}_t^+ = \begin{bmatrix} 0 \\ 2(\mathbf{p}_t \times \mathbf{x}_t) \end{bmatrix}. \tag{A.8}$$

On the other and, $\dot{\mathbf{x}}_t \in \mathbb{R}^3$ has expression

$$\dot{\mathbf{x}}_t = \boldsymbol{\omega} \times \mathbf{x}_t. \tag{A.9}$$

being the time derivative of a vector with fixed length. Putting together equations (A.8) and (A.9) it follows that

$$\boldsymbol{\omega}_t^+ = 2\mathbf{p}_t^+ = 2\dot{\mathbf{q}}_t \circ \mathbf{q}_t^{-1},$$

and thus

$$\dot{\mathbf{q}}_t = \frac{1}{2}\boldsymbol{\omega}_t^+ \circ \mathbf{q}_t \qquad \square$$

A.1.3 Time derivative of the bearing vector

This section is dedicated the time derivative of the bearing vector $\mathbf{b}_{\mathcal{G}}(\mathbf{x}) \in \mathbb{S}^{2m}$ of a framework $(\mathcal{G}, \mathbf{x})$ embedded in $\mathbb{R}^{3n} \times \mathbb{S}^{3n}$.

Proposition A.2. *It hold that,*

$$\nabla_{\mathbf{x}} \mathbf{b}_{\mathcal{G}}(\mathbf{x}) \mathbf{D}(\mathbf{q}) = \mathbf{B}_{\mathcal{G}}(\mathbf{x}). \tag{A.10}$$

Proof. Trivially, from the definition of bearing rigidity matrix

$$\begin{aligned} \dot{\mathbf{b}}_{\mathcal{G}}(\mathbf{x}) = \frac{d}{dt}\mathbf{b}_{\mathcal{G}}(\mathbf{x}) = \nabla_{\mathbf{x}} \mathbf{b}_{\mathcal{G}}(\mathbf{x}) \frac{d\mathbf{x}}{dt} = \nabla_{\mathbf{x}} \mathbf{b}_{\mathcal{G}}(\mathbf{x}) \mathbf{D}(\mathbf{q}) \mathbf{u} \\ = \mathbf{B}_{\mathcal{G}}(\mathbf{x}) \mathbf{u} \end{aligned}, \tag{A.11}$$

and this equalities hold for every value $\mathbf{u} \in \mathbb{R}^{6n}$. Thus the proposition is proven.

However, notice that if

$$\dot{\mathbf{q}}_i = \frac{1}{2}\mathbf{q}_i \circ \boldsymbol{\omega}_i^+ = \mathbf{M}(\mathbf{q}_i)\boldsymbol{\omega}_i^+ \tag{4.1b revisited}$$

had been used to model the kinematic of the agents, then, after a proper redefinition of

$\mathbf{D}(\mathbf{q})$, $\mathbf{B}_{\mathcal{G}}(\mathbf{x})$ and $\mathbf{u}$, equation (A.11) would have not held for any vector $\mathbf{u} \in \mathbb{R}^{7n}$ but only the ones of the form $\mathbf{u} = \begin{bmatrix}\mathbf{v}^\top & (\boldsymbol{\omega}^+)^\top\end{bmatrix}^\top$, with $\mathbf{v} = \begin{bmatrix}\mathbf{v}_1^\top \dots \mathbf{v}_n^\top\end{bmatrix}^\top \in \mathbb{R}^{3n}$ and $\boldsymbol{\omega}^+ = \begin{bmatrix}(\boldsymbol{\omega}_1^+)^\top \dots (\boldsymbol{\omega}_n^+)^\top\end{bmatrix}^\top \in \mathbb{R}^{4n}$. In particular, $\boldsymbol{\omega}^+$ does not span the entire space $\mathbb{R}^{4n}$. Therefore, (A.11) would have not been a sufficient condition for (A.10). □

A.2 Proofs of chapter 2

Proof of Proposition 2.6. Consider $\mathbf{x} = \mathbf{p}_j - \mathbf{p}_i$ and recall that $\|\mathbf{x}\| = \sqrt{\mathbf{x}^\top \mathbf{x}}$, which has time derivative

$$\frac{d}{dt}\|\mathbf{x}(t)\| = \frac{d}{dt}\sqrt{\mathbf{x}(t)^\top \mathbf{x}(t)} = \frac{1}{2}\big(\mathbf{x}(t)^\top \mathbf{x}(t)\big)^{-\frac{1}{2}} \frac{d}{dt}\big(\mathbf{x}(t)^\top \mathbf{x}(t)\big) = \frac{\mathbf{x}(t)^\top \dot{\mathbf{x}}(t)}{\|\mathbf{x}(t)\|}.$$

Therefore,

$$\begin{aligned}
\frac{d}{dt}\frac{\mathbf{x}(t)}{\|\mathbf{x}(t)\|} &= \frac{\dot{\mathbf{x}}(t)\|\mathbf{x}(t)\| - \mathbf{x}(t)\frac{d}{dt}\|\mathbf{x}(t)\|}{\|\mathbf{x}(t)\|^2} \\
&= \frac{1}{\|\mathbf{x}(t)\|^2}\left(\|\mathbf{x}(t)\|\dot{\mathbf{x}}(t) - \frac{1}{\|\mathbf{x}(t)\|}\mathbf{x}(t)\mathbf{x}(t)^\top \dot{\mathbf{x}}(t)\right) \\
&= \underbrace{\frac{1}{\|\mathbf{x}(t)\|}}_{=d_{ij}} \underbrace{\left(\mathbf{I}_d - \frac{\mathbf{x}(t)\mathbf{x}(t)^\top}{\|\mathbf{x}(t)\|^2}\right)}_{=\mathbf{P}(\bar{\mathbf{p}}_{ij})} \underbrace{\dot{\mathbf{x}}(t)}_{=\dot{\mathbf{p}}_j - \dot{\mathbf{p}}_i}
\end{aligned}$$

□

Proof of Proposition 2.7. Here it is reported the proof of theorem VII.1 in [4], which requires the following two lemmas.

Lemma A.3 (Lemma 3 in [20]). *A framework $(\mathcal{G}, \mathbf{x})$ in $\mathbb{R}^{nd}$ always satisfies*

$$\operatorname{span}\{\mathbf{1}_n \otimes \mathbf{I}_d, \mathbf{p}\} \subseteq \ker\big(\mathbf{B}_{\mathcal{G}}(\mathbf{x})\big)$$

and $\operatorname{rk}\big(\mathbf{B}_{\mathcal{G}}(\mathbf{x})\big) \leqslant dn - d - 1$.

Lemma A.4 (Lemma 4 in [20]). *A framework $(\mathcal{G}, \mathbf{x})$ in $\mathbb{R}^{nd}$ always satisfies*

$$\operatorname{span}\{\mathbf{1}_n \otimes \mathbf{I}_d, \mathbf{p}\} \subseteq \ker\big(\mathbf{B}_{\mathcal{K}}(\mathbf{x})\big) \subseteq \ker\big(\mathbf{B}_{\mathcal{G}}(\mathbf{x})\big)$$

and $dn - d - 1 \geqslant \operatorname{rk}\big(\mathbf{B}_{\mathcal{K}}(\mathbf{x})\big) \geqslant \operatorname{rk}\big(\mathbf{B}_{\mathcal{G}}(\mathbf{x})\big)$.

The bearing rigidity matrix associated to $(\mathcal{K}, \mathbf{x})$ is so that the k-th row block, corresponding to the edge $e_k = (v_i, v_j) \in \mathcal{E}_\mathcal{K}$ with $i < j$ has the following form where $\mathbf{B}_{ij} = d_{ij}\mathbf{P}(\bar{\mathbf{p}}_{ij}) \in \mathbb{R}^{d\times d}$

$$\begin{bmatrix} \mathbf{0}_{d\times d(i-1)} & -\mathbf{B}_{ij} & \mathbf{0}_{d\times d(j-i-1)} & \mathbf{B}_{ij} & \mathbf{0}_{d\times d(n-j)} \end{bmatrix} \tag{A.12}$$

For $d = 2$, $\mathbf{B}_{ij} = {d_{ij}}^3 \mathbf{r}_{ij}\mathbf{r}_{ij}^\top$, with $\mathbf{r}_{ij} = \begin{bmatrix} \mathrm{p}_{ij}^y & -\mathrm{p}_{ij}^x \end{bmatrix}^\top \in \mathbb{R}^2$, where $\mathrm{p}_{ij}^x, \mathrm{p}_{ij}^y \in \mathbb{R}$ are the scalar components of vector $\mathbf{p}_{ij} \in \mathbb{R}^2$ along the x-axis and y-axis of the global inertial frame, respectively. Note that $\mathbf{B}_{ij}$ is neither zero nor full-rank, hence the k-row block (A.12) of the bearing rigidity matrix $\mathbf{B}_\mathcal{K}(\mathbf{x})$ has unitary rank. For this reason, for each edge $e_k = (v_i, v_j) \in \mathcal{E}_\mathcal{K}$ with $i < j$, it is considered the next opportunely scaled version of (A.12),

$$\begin{bmatrix} \mathbf{0}_{1\times 2(i-1)} & -\mathbf{r}_{ij}^\top & \mathbf{0}_{1\times 2(j-i-1)} & \mathbf{r}_{ij}^\top & \mathbf{0}_{1\times 2(n-j)} \end{bmatrix}$$

obtaining the matrix $\mathbf{B}(n) \in \mathbb{R}^{((n-1)n/2)\times 2n}$. This has the same rank of $\mathbf{B}_\mathcal{K}(\mathbf{x})$ but lower dimensions, so hereafter $\mathbf{B}(n)$ is considered instead of $\mathbf{B}_\mathcal{K}(\mathbf{x})$ and the thesis is proven by induction on the number n of agents in the formation.

Base case: $n = 3$

The aim is to prove that $\mathrm{rk}\left(\mathbf{B}(3)\right) = 3$. To do so, observe that

$$\mathbf{B}(3) = \begin{bmatrix} -{\mathbf{r}_{12}}^\top & \mathbf{r}_{12}^\top & \mathbf{0}_{1\times 2} \\ -{\mathbf{r}_{13}}^\top & \mathbf{0}_{1\times 2} & \mathbf{r}_{13}^\top \\ \mathbf{0}_{1\times 2} & -{\mathbf{r}_{23}}^\top & \mathbf{r}_{23}^\top \end{bmatrix} \in \mathbb{R}^{3\times 6}$$

is full-rank whether the agents are not all collinear. Because of the non-degenerate formation hypotheses the thesis is proven.

Inductive step: $n = \bar{n}$

Note that, given a set of $\bar{n}$ agents, for each subset containing $\bar{n} - 1$ elements, it is possible to

partition $\mathbf{B}(\bar{n})$ so that

$$\mathbf{B}(\bar{n}) = \left[\begin{array}{cccc|c} & & & & \mathbf{0}_{1\times 2} \\ & \mathbf{B}(\bar{n}-1) & & & \vdots \\ & & & & \mathbf{0}_{1\times 2} \\ \hline \mathbf{r}_{1\bar{n}}^\top & \mathbf{0}_{1\times 2} & \dots & \mathbf{0}_{1\times 2} & -\mathbf{r}_{1\bar{n}}^\top \\ \mathbf{0}_{1\times 2} & \ddots & & \vdots & \vdots \\ \vdots & & \ddots & \mathbf{0}_{1\times 2} & \vdots \\ \mathbf{0}_{1\times 2} & \dots & \mathbf{0}_{1\times 2} & \mathbf{r}_{(\bar{n}-1)\bar{n}}^\top & -\mathbf{r}_{(\bar{n}-1)\bar{n}}^\top \end{array}\right] \tag{A.13}$$

where the first block has $(\bar{n}-1)(\bar{n}-2)/2$ rows related to the edges incident to the first $\bar{n}-1$ agents, while the second block has $\bar{n}-1$ rows related to the edges connecting the $\bar{n}$-th agent with the first $\bar{n}-1$ agents. For inductive hypothesis the thesis holds for $n = \bar{n}-1 \geqslant 3$, i.e. $\operatorname{rk}\big(\mathbf{B}(\bar{n}-1)\big) = 2\bar{n}-5$. Exploiting this fact it will be proven that for $n=\bar{n}$ $\operatorname{rk}\big(\mathbf{B}(\bar{n})\big) = 2\bar{n}-3$. For the inductive hypothesis, the first block of $\mathbf{B}(\bar{n})$ in (A.13) has $2\bar{n}-5$ linearly independent rows. Moreover, there are at least two agents, for instance the i-th and the j-th, that are not aligned with the $\bar{n}$-th agent, hence it does not exist $c\in\mathbb{R}$ such that $\mathbf{r}_{i\bar{n}} = c\mathbf{r}_{j\bar{n}}$ and the rows related to the edges $(v_i, v_{\bar{n}})$ and $(v_j, v_{\bar{n}})$ are linearly independent w.r.t. the rows of the first block. $\mathbf{B}(\bar{n})$ has thus $2\bar{n}-3$ linearly independent rows, and since $\operatorname{rk}\big(\mathbf{B}(\bar{n})\big) \leqslant 2n-3$ for lemma A.4, then it must be $\operatorname{rk}\big(\mathbf{B}(\bar{n})\big) = 2n-3$.

For $d=3$, the matrix $\mathbf{B}_{ij}$ in (A.12) turn out to be

$$\mathbf{B}_{ij} = {d_{ij}}^3 \begin{bmatrix} (\mathrm{p}_{ij}^y)^2 + (\mathrm{p}_{ij}^z)^2 & -\mathrm{p}_{ij}^x\mathrm{p}_{ij}^y & -\mathrm{p}_{ij}^x\mathrm{p}_{ij}^z \\ -\mathrm{p}_{ij}^y\mathrm{p}_{ij}^x & (\mathrm{p}_{ij}^x)^2 + (\mathrm{p}_{ij}^z)^2 & -\mathrm{p}_{ij}^y\mathrm{p}_{ij}^z \\ -\mathrm{p}_{ij}^z\mathrm{p}_{ij}^x & -\mathrm{p}_{ij}^z\mathrm{p}_{ij}^y & (\mathrm{p}_{ij}^x)^2 + (\mathrm{p}_{ij}^y)^2 \end{bmatrix}$$

where $\mathrm{p}_{ij}^x, \mathrm{p}_{ij}^y, \mathrm{p}_{ij}^z \in \mathbb{R}$ are the (scalar) components of vector $\mathbf{p}_{ij} \in \mathbb{R}^3$ along the x, y, z-axis of $\mathcal{F}_W$, respectively. The proof of this case thus follows the same inductive reasoning performed for $d=2$.

□

Proof of Proposition 2.9. Using the chain rule for the derivative, it holds that

$$\dot{\mathbf{b}}_{ij} = \frac{d\mathbf{R}_i^\top \bar{\mathbf{p}}_{ij}}{dt} = \frac{\partial \mathbf{R}_i^\top \bar{\mathbf{p}}_{ij}}{\partial \bar{\mathbf{p}}_{ij}} \frac{d\bar{\mathbf{p}}_{ij}}{dt} + \frac{\partial \mathbf{R}_i^\top \bar{\mathbf{p}}_{ij}}{\partial \alpha_i} \frac{d\alpha_i}{dt}. \tag{A.14}$$

Now, the two addend in equation (A.14) are analysed separately. The former is quite straightforward, in fact, recalling equation (2.6) on page 15, it results

$$\frac{\partial \mathbf{R}_i^\top \bar{\mathbf{p}}_{ij}}{\partial \bar{\mathbf{p}}_{ij}} \frac{d\bar{\mathbf{p}}_{ij}}{dt} = \mathbf{R}_i^\top \frac{d\bar{\mathbf{p}}_{ij}}{dt} = d_{ij} \mathbf{R}_i^\top \mathbf{P}(\bar{\mathbf{p}}_{ij})(\dot{\mathbf{p}}_j - \dot{\mathbf{p}}_i).$$

The latter, instead, requires more computations.
case 1, $d = 2$.
Writing the rotation matrix $\mathbf{R}_i \in SO(2)$ as a function of $\alpha_i \in [0, 2\pi)$ and noticing that $\frac{\partial \bar{\mathbf{p}}_{ij}}{\partial \alpha_i} = \mathbf{0}$, it holds that

$$\begin{aligned}
\frac{\partial \mathbf{R}_i^\top \bar{\mathbf{p}}_{ij}}{\partial \alpha_i} \frac{d\alpha_i}{dt} &= \frac{\partial \mathbf{R}_i^\top}{\partial \alpha_i} \bar{\mathbf{p}}_{ij} \dot{\alpha}_i \\
&= \frac{\partial}{\partial \alpha_i} \begin{bmatrix} \cos\alpha_i & \sin\alpha_i \\ -\sin\alpha_i & \cos\alpha_i \end{bmatrix} \bar{\mathbf{p}}_{ij} \dot{\alpha}_i = \begin{bmatrix} -\sin\alpha_i & \cos\alpha_i \\ -\cos\alpha_i & -\sin\alpha_i \end{bmatrix} \bar{\mathbf{p}}_{ij} \dot{\alpha}_i \\
&= \begin{bmatrix} \cos\alpha_i & \sin\alpha_i \\ -\sin\alpha_i & \cos\alpha_i \end{bmatrix} \begin{bmatrix} 0 & 1 \\ -1 & 0 \end{bmatrix} \bar{\mathbf{p}}_{ij} \dot{\alpha}_i \\
&= \mathbf{R}_i^\top \mathbf{R} \left(-\frac{\pi}{2} \right) \bar{\mathbf{p}}_{ij} \dot{\alpha}_i = \mathbf{R}_i^\top \bar{\mathbf{p}}_{ij}^\perp \dot{\alpha}_i.
\end{aligned}$$

case 2, $d = 3$.
In this case, $\mathbf{R}_i \in SO(3)$ and to compute its time derivative it has to be remarked that the rotation axis is fixed to be $\mathbf{n} \in \mathbb{S}^2$. Exploiting the works reported in section A.1.1 on page 87, it holds that $\frac{d}{dt}\mathbf{R}_i^\top = -\mathbf{R}_i^\top [\mathbf{n}]_\times \dot{\alpha}_i$; therefore, it results

$$\frac{\partial \mathbf{R}_i^\top}{\partial \alpha_i} \bar{\mathbf{p}}_{ij} \dot{\alpha}_i = \frac{d\mathbf{R}_i^\top}{dt} \bar{\mathbf{p}}_{ij} = -\mathbf{R}_i^\top [\mathbf{n}]_\times \bar{\mathbf{p}}_{ij} \dot{\alpha}_i = \mathbf{R}_i^\top [\bar{\mathbf{p}}_{ij}]_\times \mathbf{n} \dot{\alpha}_i. \qquad \square$$

Proof of Proposition 2.10. **case** 1, $d = 2$.
Define $\mathbf{z} = (\mathbf{I}_n \otimes \mathbf{R}(\pi/2))\, \mathbf{p} \in \mathbb{R}^{2n}$. It is now proved that

$$\mathbf{D}_1 \bar{\mathbf{E}}^\top \mathbf{z} = -\mathbf{D}_2 \mathbf{E}_o^\top \mathbf{1}_n, \tag{A.15}$$

where $\mathbf{D}_1 \in \mathbb{R}^{2m \times 2m}$ and $\mathbf{D}_2 \in \mathbb{R}^{2m \times m}$ are the ones defined in equations (2.11) and (2.12) on page 18, respectively. The k-th row block associated to the edge $(v_i, v_j) \in \mathcal{E}$ of the left

member of the equation has expression

$$d_{ij}\mathbf{R}_i^\top \mathbf{P}\left(\bar{\mathbf{p}}_{ij}\right)\left(\mathbf{R}\left(\frac{\pi}{2}\right)\mathbf{p}_j - \mathbf{R}\left(\frac{\pi}{2}\right)\mathbf{p}_i\right) = \mathbf{R}_i^\top \mathbf{P}\left(\bar{\mathbf{p}}_{ij}\right)\mathbf{R}\left(\frac{\pi}{2}\right)\bar{\mathbf{p}}_{ij}, \tag{A.16}$$

while k-th row block of the right member has expression

$$-\mathbf{R}_i^\top \bar{\mathbf{p}}_{ij}^{\perp}. \tag{A.17}$$

Comparing (A.16) and (A.17), the thesis is proven if

$$\mathbf{P}\left(\bar{\mathbf{p}}_{ij}\right)\mathbf{R}\left(\frac{\pi}{2}\right)\bar{\mathbf{p}}_{ij} = -\bar{\mathbf{p}}_{ij}^{\perp},$$

which is indeed true, in fact

$$\mathbf{P}\left(\bar{\mathbf{p}}_{ij}\right)\mathbf{R}\left(\frac{\pi}{2}\right)\bar{\mathbf{p}}_{ij} = \mathbf{R}\left(\frac{\pi}{2}\right)\bar{\mathbf{p}}_{ij} \tag{A.18}$$

because $\mathbf{R}\left(\frac{\pi}{2}\right)\bar{\mathbf{p}}_{ij} \in \mathbb{S}^1$ belongs to the orthogonal complement of $\bar{\mathbf{p}}_{ij} \in \mathbb{S}^1$; moreover

$$-\bar{\mathbf{p}}_{ij}^{\perp} = -\mathbf{R}\left(-\frac{\pi}{2}\right)\bar{\mathbf{p}}_{ij} = \mathbf{R}\left(\frac{\pi}{2}\right)\bar{\mathbf{p}}_{ij}, \tag{A.19}$$

and (A.18) and (A.19) are equal.
case 2, $d = 3$.
When $d = 3$, define $\mathbf{z} = (\mathbf{I}_n \otimes [\mathbf{n}]_\times)\,\mathbf{p} \in \mathbb{R}^{3n}$. Thus, the left and the right row blocks in equation (A.15) result

$$\mathbf{R}_i^\top \mathbf{P}\left(\bar{\mathbf{p}}_{ij}\right)[\mathbf{n}]_\times \bar{\mathbf{p}}_{ij}, \tag{A.20}$$

$$-\mathbf{R}_i^\top [\bar{\mathbf{p}}_{ij}]_\times \mathbf{n}. \tag{A.21}$$

In particular, (A.20) can be rewritten as

$$\mathbf{R}_i^\top \mathbf{P}\left(\bar{\mathbf{p}}_{ij}\right)[\mathbf{n}]_\times \bar{\mathbf{p}}_{ij} = -\mathbf{R}_i^\top \mathbf{P}\left(\bar{\mathbf{p}}_{ij}\right)[\bar{\mathbf{p}}_{ij}]_\times \mathbf{n} = \mathbf{R}_i^\top [\bar{\mathbf{p}}_{ij}]_\times \mathbf{n}$$

which is equal to equation (A.21). □

Proof of Proposition 2.12. The same procedure applied during the proof of proposition 2.9 for $d = 3$ can be applied here. The term linked to the linear velocities is exactly the same,

while the one related to the angular velocity comes from the reasoning that the rotation of angular rate $\dot{\alpha}_i \in \mathbb{R}$ around the axis $\mathbf{n} \in \mathbb{S}^2$, namely $\mathbf{n}\dot{\alpha}_i \in \mathbb{R}^3$, is now substituted by $\boldsymbol{\omega}_{w,i} \in \mathbb{R}^3$. □

Proof of Proposition 2.13. Notice that the vector

$$\mathbf{z} := \begin{bmatrix} (\mathbf{I}_n \otimes [\mathbf{n}]_\times)\mathbf{p} \\ \mathbf{1}_n \otimes \mathbf{n} \end{bmatrix} \in \mathbb{R}^{6n} \tag{A.22}$$

solve the equation

$$\mathbf{B}_{\mathcal{G}}(\mathbf{x})\mathbf{z} = \mathbf{0},$$

and the proof follows the same procedure applied for the one of proposition 2.10, case $d = 3$. Moreover, in (A.22) $\mathbf{n} \in \mathbb{R}^3$ can be *any* three dimensional vector; therefore the coordinated rotation set has three generators that can be chosen as the ones comparing in (2.18). □

A.3 Proofs of chapter 4

Proof of Proposition 4.3. The second part of the proof uses LaSalle's Invariance Principle to prove the asymptotic stability. Notice that the required hypothesis for the theorem are satisfied by $\dot{\mathrm{V}}(\mathbf{x})$ being negative semi-definite. Then, the bearing error dynamics converges to

$$\mathcal{Z} = \left\{ \mathbf{e}(\mathbf{x}, \mathbf{x}_d) \;\middle|\; \mathbf{x} \in \mathcal{U}(\mathbf{x}_d), \dot{\mathrm{V}}(\mathbf{x}) = 0 \right\},$$

where $\mathcal{U}(\mathbf{x}_d)$ is a neighbourhood of $\mathbf{x}_d$. It is now proven that $\mathcal{Z} = \{ \mathbf{0}_{3m} \}$. Firstly,

$$\begin{aligned} \dot{\mathrm{V}}(\mathbf{x}) = 0 \quad &\Rightarrow \quad \mathbf{B}_{\mathcal{G}}(\mathbf{x})\big(\mathbf{B}_{\mathcal{G}}(\mathbf{x})\big)^\top \mathbf{e}(\mathbf{x}, \mathbf{x}_d) = \mathbf{0}_{3m}, \\ &\Rightarrow \quad \big(\mathbf{B}_{\mathcal{G}}(\mathbf{x})\big)^\top \mathbf{e}(\mathbf{x}, \mathbf{x}_d) = \mathbf{0}_{6n}. \end{aligned} \tag{A.23}$$

Then, with $\mathbf{x}$ in a neighbourhood of $\mathbf{x}_d$ it is possible to use the Taylor's expansion

$$\begin{aligned} \big(\mathbf{B}_{\mathcal{G}}(\mathbf{x})\big)^\top \mathbf{e}(\mathbf{x}, \mathbf{x}_d) &= \big(\mathbf{B}_{\mathcal{G}}(\mathbf{x})\big)^\top \big(\mathbf{b}_{\mathcal{G}}(\mathbf{x}) - \mathbf{b}_{\mathcal{G}}(\mathbf{x}_d)\big) = -\big(\mathbf{B}_{\mathcal{G}}(\mathbf{x})\big)^\top \mathbf{b}_{\mathcal{G}}(\mathbf{x}_d), \\ &= -\big(\mathbf{B}_{\mathcal{G}}(\mathbf{x})\big)^\top \mathbf{b}_{\mathcal{G}}(\mathbf{x} + d\mathbf{x}), \\ &\simeq -\big(\mathbf{B}_{\mathcal{G}}(\mathbf{x})\big)^\top \big(\mathbf{b}_{\mathcal{G}}(\mathbf{x}) + \nabla_{\mathbf{x}} \mathbf{b}_{\mathcal{G}}(\mathbf{x}) d\mathbf{x}\big), \\ &= -\big(\mathbf{B}_{\mathcal{G}}(\mathbf{x})\big)^\top \nabla_{\mathbf{x}} \mathbf{b}_{\mathcal{G}}(\mathbf{x}) d\mathbf{x}. \end{aligned} \tag{A.24}$$

$d\mathbf{x} \in \mathbb{R}^{7n}$ in equation (A.24) represents a variation of the configuration $\mathbf{x}$, therefore it should be expressed according to equation (4.4), otherwise the constraints on the quaternions would be violated again. Thus, in a neighbourhood of $\mathbf{x}_d$, there exists $\mathbf{u} \in \mathbb{R}^{6n}$ such that

$$\big(\mathbf{B}_{\mathcal{G}}(\mathbf{x})\big)^{\top}\mathbf{e}(\mathbf{x},\mathbf{x}_d) \simeq -\big(\mathbf{B}_{\mathcal{G}}(\mathbf{x})\big)^{\top}\nabla_{\mathbf{x}}\mathbf{b}_{\mathcal{G}}(\mathbf{x})\mathbf{D}(\mathbf{q})\mathbf{u}. \tag{A.25}$$

It holds that, see section A.1.3,

$$\nabla_{\mathbf{x}}\mathbf{b}_{\mathcal{G}}(\mathbf{x})\mathbf{D}(\mathbf{q}) = \mathbf{B}_{\mathcal{G}}(\mathbf{x}), \tag{A.10 revisited}$$

so, combining equations (A.10), (A.23) and (A.25) the following property of the elements $\mathbf{e}(\mathbf{x},\mathbf{x}_d) \in \mathcal{Z}$ can be stated,

$$\mathbf{e}(\mathbf{x},\mathbf{x}_d) \in \mathcal{Z} \quad \Rightarrow \quad \dot{\mathrm{V}}(\mathbf{x}) = 0 \quad \Rightarrow \quad \big(\mathbf{B}_{\mathcal{G}}(\mathbf{x})\big)^{\top}\mathbf{B}_{\mathcal{G}}(\mathbf{x})\mathbf{u} = \mathbf{0}_{6n}$$

Finally,

$$\ker\Big(\big(\mathbf{B}_{\mathcal{G}}(\mathbf{x})\big)^{\top}\mathbf{B}_{\mathcal{G}}(\mathbf{x})\Big) = \ker\left(\mathbf{B}_{\mathcal{G}}(\mathbf{x})\right)$$

which ensures that the elements $\mathbf{e}(\mathbf{x},\mathbf{x}_d)\mathcal{Z}$ are such that $\mathbf{x}$ is BE to $\mathbf{x}$, hence $\mathbf{e}(\mathbf{x},\mathbf{x}_d) = \mathbf{0}_{3m}$. □

References

[1] Y. Cao, W. Yu, W. Ren, and G. Chen, "An overview of recent progress in the study of distributed multi-agent coordination," *IEEE Transactions on Industrial Informatics*, vol. 9, no. 1, pp. 427–438, Feb 2013.

[2] K.-K. Oh, M.-C. Park, and H.-S. Ahn, "A survey of multi-agent formation control," *Automatica*, vol. 53, pp. 424 – 440, 2015. [Online]. Available: http://www.sciencedirect.com/science/article/pii/S0005109814004038

[3] B. Siciliano, L. Sciavicco, L. Villani, and G. Oriolo, *Robotics: Modelling, Planning and Control*, 1st ed. Springer Publishing Company, Incorporated, 2008.

[4] G. Michieletto, A. Cenedese, and D. Zelazo, "A unified dissertation on bearing rigidity theory," *CoRR*, vol. abs/1902.03101v3, 2019. [Online]. Available: http://arxiv.org/abs/1902.03101v3

[5] M. Thorpe and P. Duxbury, *Rigidity Theory and Applications*, ser. Fundamental Materials Research. Springer US, 1999. [Online]. Available: https://books.google.it/books?id=yeQrSLMwBXcC

[6] L. Asimow and B. Roth, "The rigidity of graphs," *Transactions of the American Mathematical Society*, vol. 245, pp. 279–289, 1978. [Online]. Available: http://www.jstor.org/stable/1998867

[7] L. Krick, M. E. Broucke, and B. A. Francis, "Stabilisation of infinitesimally rigid formations of multi-robot networks," *International Journal of Control*, vol. 82, no. 3, pp. 423–439, 2009. [Online]. Available: https://doi.org/10.1080/00207170802108441

[8] J. M. Hendrickx, B. D. O. Anderson, J.-C. Delvenne, and V. D. Blondel, "Directed graphs for the analysis of rigidity and persistence in autonomous agent systems," *International Journal of Robust and Nonlinear Control*, vol. 17, no. 10-11, pp. 960–981, 2007. [Online]. Available: https://onlinelibrary.wiley.com/doi/abs/10.1002/rnc.1145

[9] G. Zhu and J. Hu, "Stiffness matrix and quantitative measure of formation rigidity," in *Proceedings of the 48h IEEE Conference on Decision and Control (CDC) held jointly with 2009 28th Chinese Control Conference*, Dec 2009, pp. 3057–3062.

[10] Y. Kim, G. Zhu, and J. Hu, "Optimizing formation rigidity under connectivity constraints," in *49th IEEE Conference on Decision and Control (CDC)*, Dec 2010, pp. 6590–6595.

[11] D. Zelazo, A. Franchi, F. Allgöwer, H. H. Bülthoff, and P. R. Giordano, "Rigidity maintenance control for multi-robot systems," in *Robotics: Science and Systems*, 2012.

[12] D. Zelazo, A. Franchi, H. H. BÃ¼lthoff, and P. R. Giordano, "Decentralized rigidity maintenance control with range measurements for multi-robot systems," *The International Journal of Robotics Research*, vol. 34, no. 1, pp. 105–128, 2015. [Online]. Available: https://doi.org/10.1177/0278364914546173

[13] T. Eren, W. Whiteley, A. S. Morse, P. N. Belhumeur, and B. D. O. Anderson, "Sensor and network topologies of formations with direction, bearing, and angle information between agents," in *42nd IEEE International Conference on Decision and Control (IEEE Cat. No.03CH37475)*, vol. 3, Dec 2003, pp. 3064–3069 Vol.3.

[14] T. Eren, W. Whiteley, and P. N. Belhumeur, "Using angle of arrival (bearing) information in network localization," in *Proceedings of the 45th IEEE Conference on Decision and Control*, Dec 2006, pp. 4676–4681.

[15] A. N. Bishop, I. Shames, and B. D. O. Anderson, "Stabilization of rigid formations with direction-only constraints," in *2011 50th IEEE Conference on Decision and Control and European Control Conference*, Dec 2011, pp. 746–752.

[16] A. Franchi and P. R. Giordano, "Decentralized control of parallel rigid formations with direction constraints and bearing measurements," in *2012 IEEE 51st IEEE Conference on Decision and Control (CDC)*, Dec 2012, pp. 5310–5317.

[17] S. Zhao and D. Zelazo, "Localizability and distributed protocols for bearing-based network localization in arbitrary dimensions," *Automatica*, vol. 69, pp. 334 – 341, 2016. [Online]. Available: http://www.sciencedirect.com/science/article/pii/S0005109816300899

[18] S. Zhao and D. Zelazo, "Bearing rigidity theory and its applications for control and estimation of network systems: Life beyond distance rigidity," *IEEE Control Systems Magazine*, vol. 39, no. 2, pp. 66–83, April 2019.

[19] ——, "Bearing-based distributed control and estimation of multi-agent systems," in *2015 European Control Conference (ECC)*, July 2015, pp. 2202–2207.

[20] ——, "Bearing rigidity and almost global bearing-only formation stabilization," *IEEE Transactions on Automatic Control*, vol. 61, no. 5, pp. 1255–1268, May 2016.

[21] D. Zelazo, A. Franchi, and P. R. Giordano, "Rigidity theory in se(2) for unscaled relative position estimation using only bearing measurements," in *2014 European Control Conference (ECC)*, June 2014, pp. 2703–2708.

[22] D. Zelazo, P. R. Giordano, and A. Franchi, "Bearing-only formation control using an se(2) rigidity theory," in *2015 54th IEEE Conference on Decision and Control (CDC)*, Dec 2015, pp. 6121–6126.

[23] A. Franchi, C. Masone, V. Grabe, M. Ryll, H. H. Bülthoff, and P. R. Giordano, "Modeling and control of uav bearing formations with bilateral high-level steering," *The International Journal of Robotics Research*, vol. 31, no. 12, pp. 1504–1525, 2012. [Online]. Available: https://doi.org/10.1177/0278364912462493

[24] F. Schiano, A. Franchi, D. Zelazo, and P. R. Giordano, "A rigidity-based decentralized bearing formation controller for groups of quadrotor uavs," in *2016 IEEE/RSJ International Conference on Intelligent Robots and Systems (IROS)*, Oct 2016, pp. 5099–5106.

[25] R. Spica and P. R. Giordano, "Active decentralized scale estimation for bearing-based localization," in *2016 IEEE/RSJ International Conference on Intelligent Robots and Systems (IROS)*, Oct 2016, pp. 5084–5091.

[26] G. Michieletto, A. Cenedese, and A. Franchi, "Bearing rigidity theory in se(3)," in *2016 IEEE 55th Conference on Decision and Control (CDC)*, Dec 2016, pp. 5950–5955.

[27] C. Godsil and G. Royle, *Algebraic Graph Theory*. Springer, New York, NY, 01 2001, vol. 207.

[28] G. Michieletto and A. Cenedese, "Formation control for fully actuated systems: a quaternion-based bearing rigidity approach," in *2019 18th European Control Conference (ECC)*, June 2019, pp. 107–112.

[29] H. Khalil, *Nonlinear Systems*, ser. Pearson Education. Prentice Hall, 2002. [Online]. Available: https://books.google.it/books?id=t_d1QgAACAAJ